All-Optical Multihop Free-Space Optical Communication Systems

ALL-OPTICAL MULTIHOP FREE-SPACE OPTICAL COMMUNICATION SYSTEMS

BY

SHABNAM KAZEMLOU, B.Sc.

A THESIS

SUBMITTED TO THE DEPARTMENT OF ELECTRICAL & COMPUTER ENGINEERING

AND THE SCHOOL OF GRADUATE STUDIES

OF MCMASTER UNIVERSITY

IN PARTIAL FULFILMENT OF THE REQUIREMENTS

FOR THE DEGREE OF

MASTER OF APPLIED SCIENCE

Master of Applied Science (2010)
(Electrical & Computer Engineering)

McMaster University
Hamilton, Ontario, Canada

TITLE: All-Optical Multihop Free-Space Optical Communication Systems

AUTHOR: Shabnam Kazemlou
B.Sc., (Electrical Engineering)
Sharif University of Technology, Tehran, Iran

SUPERVISOR: Dr. Steve Hranilovic
Dr. Shiva Kumar

NUMBER OF PAGES: xvi, 147

To those who were always there when I needed them

Abstract

Free-Space Optical (FSO) communication systems have recently attracted considerable attention in last-mile applications. High bandwidth, unlicensed spectrum, ease of installation, and high security have made them a good candidate for high data rate transmissions. However, distance-dependent atmospheric turbulence and channel loss degrade the optical link reliability and confine FSO systems to short-haul applications. This thesis addresses innovative all-optical relaying techniques to mitigate the degrading effects of atmospheric turbulence-induced fading by relaying data from the source to the destination using intermediate terminals. The proposed techniques, optical amplify-and-forward (OAF) relaying and optical regenerate-and-forward (ORF) relaying, are deployed in multihop FSO systems to extend the maximum accessible communicating distance of high data rate wireless optical systems.

In all-optical relaying techniques, photodetection is performed once at the receiver and intermediate terminals process optical field envelopes instead of optical intensities. This major difference requires a new definition of channel model for propagation of optical waves through the atmosphere. By using the developed channel model, bit error rate (BER) performance of multihop OAF FSO systems is analyzed through Monte-Carlo simulations. The simulation results indicate that OAF relaying technique mitigates the channel impairments and enhances the BER performance. By

employing more relays, longer distances become accessible, however distance improvement decreases due to accumulating background noise at relays. In order to remove background noise effects, another optical relaying technique is developed. The ORF relaying technique eliminates the received background noise at each relay and significantly outperforms OAF systems. For example at high bit rate BR= 10 Gbps, using two equally-spaced OAF relays during a 3 km turbulence-free link increases the total communicating distance by about 1.11 km. Replacing OAF relays by ORF relays extends the total communicating distance to 4.48 km which is 1.66 km longer than the similar OAF FSO system. By deploying more ORF relays, even longer distances are achievable.

Acknowledgements

I would like to express my heartily gratitude to my supervisor, Dr. Steve Hranilovic, whose support, advice and encouragement have been key factors to accomplish this work. It is an honor for me to study and research under his supervision.

My deepest thanks also go to my co-supervisor, Dr. Shiva Kumar, whose insightful knowledge and helpful ideas involved me in an innovative and interesting topic of research. This thesis would not have been possible without his efforts.

I also extend my thanks to my lab mates, Dr. Ahmed Farid and Mr. Kasra Asadzadeh, whose endless helps have been a key factor for successfully accomplishing this work.

Last but not least, I would like to send my special thanks to my family for their unconditional love and giving me the opportunity to follow my dreams.

List of Notations

A_{eff}	Fiber effective core area
α, p	Gaussian beam wave parameters
β	Wave number inside fiber
β_2	Fiber dispersion coefficient
c	Light velocity
C_n	Refractive-index structure constant
F	Phase front radius of curvature
g	Channel loss
G	Amplifier gain
h_a	Atmospheric attenuation
h_p	Complex propagation loss
h	Complex channel gain
H_g	Conventional geometric power loss
H_p	Propagation power loss
$i(t)$	Photodetector current
$I(t)$	Optical intensity
k	Wave number in free-space
L_k	Length of k^{th} hop
L_T	Total communicating distance
M	Number of relays
n_2	Fiber nonlinear-index coefficient
$\mathcal{N}(t, \vec{s})$	Gaussian noise distribution
P_b	Average background power
P_M	Optical peak power
P_t	Average transmit power
R	Photodetector responsivity
T	Symbol duration

T_b	Bit interval
T_{FWHM}	Full pulse width at half maximum
U_{ASE}	Spontaneous emission noise of amplifier
$U(t)$	Optical field envelope
u_F	Fiber mode weight factor
W	Gaussian beam radius
$\Delta\omega_0$	Regenerator input pulsewidth
$\Delta\omega_f$	Regenerator output pulsewidth
$\Delta\omega_{\mathrm{shift}}$	Filter frequency offset
$\Delta\omega_{\mathrm{SPM}}$	SPM spectral broadening
γ	Fiber nonlinearity coefficient
λ	Wavelength
μ_χ	Mean of intensity fluctuations
ω_0	Carrier Frequency
ω_f	Optical filter center frequency
ω_{SPM}	SPM-broadened spectrum
ϕ	Phase
$\phi_{\mathrm{NL}}(z,t)$	SPM-induced phase shift
$\Phi_n(\varkappa)$	Kolmogorov spectrum
$\psi(r,\phi)$	Transverse field profile in free-space
$\psi_F(r,\phi)$	Transverse field profile inside fiber
$\Psi(r,\phi,z,t)$	Optical beam wave
σ	Atmospheric attenuation coefficient
σ_χ	Variance of intensity fluctuations
σ_S	Variance of phase fluctuations
σ_F	Fiber attenuation coefficient
τ	Atmospheric turbulence-induced fading

Contents

List of Figures

Chapter 1

Introduction

1.1 Free-Space Optical Communication Systems

A tremendous evolution has recently emerged in telecommunication systems. Various reliable and cost-effective techniques and technologies have evolved to deliver high data rate services to users. Optical fiber communications have the potential to deliver high data rate applications for long-haul and network access. Beside optical fiber communication, wireless optical communication has recently emerged as a new technology to deliver various types of services such as indoor infrared wireless communications [1, 2], visible light communications (VLC) [3], terrestrial links [4], ground to air (UAV) [5, 6], satellite to ground [7], and inter-satellite communications [8, 9].

Free-space optical (FSO) communication is one of the most prevalent applications for wireless optical systems and refers to terrestrial line-of-sight (LOS) optical transmission through the atmosphere [10]. Today's commercial FSO systems provide bit rates ranging from 100 Megabits/second (Mbps) to 10 Gigabits/second (Gbps) over distances on the order of a few kilometers, e.g. SONAbeam™1250-M by fSONA [11] and TereScope®10GE (TS 10GE) by MRV [12]. For a given system reliability, by increasing data rate, link coverage decreases. For example SONAbeam™1250-M provides 1.25 Gbps transmission over distances up to 5400 m, while MRV product TS 10GE can deliver 10 Gbps data over only distances up to 350 m. These high-speed systems are utilized in last-mile applications to connect buildings, companies, and business offices to the fiber network.

Optical fiber systems also can be used in last-mile applications. Optical fiber is one of the most reliable candidates for connecting the end user, e.g. buildings, offices, etc, to high rate fiber networks without loosing data rate. However, its deployment requires digging and a right-of-way license which makes fiber deployment expensive and even impractical in high density cities. Various communication systems exist to connect high data rate fiber networks to the end users.

Microwave access via WiMAX technology has been introduced as a promising technology deployed in point-to-multipoint broadband wireless applications. As an example, the Proxim product Tsunami™ MP-8100 exhibits speeds up to 300 Mbps over a range of up to 8 kilometers (km) [13]. Although WiMAX technology provides high data rates, it still does not reach the demanded Gbps data rates used in optical networks. As an alternative, RF communication links operating at high frequencies in the range $60-86$ GHz can be deployed to connect local sites to the fiber network, e.g. the commercial product GigaBeam - Gi-CORE G1.25 provides 1.25 Gbps link over about 1.6 km [14]. Although these systems are capable of delivering Gbps data rates, the cost and the high attenuation in rain are the main challenges for these systems [15]. Moreover, they fail to match high speed commercial optical networks working at data rates in excess of 1.25 Gbps.

Free-space optical (FSO) systems are license-free with high-bandwidth providing a cost-effective and easy-to-install alternative to fiber optics and RF systems. They also have the features of simple deployment, digging-free installation, and redeployment felxibility [16]. They further provide inherent security due to the nature of their directional and narrow beams that makes interception difficult [17]. Moreover, narrow-beam line-of-sight FSO connections preserve the average transmit power which is limited in wireless communication systems. Compared to state-of-the-art RF technologies such as GigaBeam - Gi-CORE G1.25 accommodating 1.25 Gbps data rate, commercially-produced FSO links provide higher data rates up to 10 Gbps. In addition, FSO links suffer from smaller attenuation in rain compared to RF links which operate in the $60 - 86$ GHz band [18].

FSO links can be deployed as a high-bandwidth bridge to connect local area networks (LANs) to long-haul wide-area networks (WANs) or metropolitan area networks (MANs) [19]. They are also used as wireless backhaul for WiMAX or WiFi networks [20]. Unlike WiMAX which is mainly deployed in point-to-multipoint topologies, FSO point-to-point links provides higher data rate transmissions. In addition, FSO link is an efficient alternative to a fiber system to establish high data rate transmission in populated city areas where laying fiber is too expensive or impractical. These advantages introduce FSO communications as a promising candidate for high data rate transmissions.

Beside the advantages of FSO communication links, it is important to point out the disadvantages and challenges in these systems. Since the laser beam is extremely narrow, accurate alignment is required between transmitter and receiver. The weather dependence of the optical channel is another issue so that the system performance highly depends on atmospheric conditions. In FSO systems, the propagating optical beam is attenuated over the optical channel due to absorption and scattering [18]. The optical beam is absorbed mainly by water particles and carbon dioxide molecules in the atmosphere (absorption). In addition, scattering deflects away a portion of the optical beam from the intended direct path to the receiver and is mainly caused by fog, haze, rain, snow, etc. Although rain is known as one of the most destructive atmospheric condition for $60 - 86$ GHz radio frequency (RF) links [18], FSO links mostly suffer from fog and haze. Typical atmospheric attenuation of optical beam at clear air is 0.43 dB/km, at haze is 4.3 dB/km, and at fog is 43 dB/km [21]. That is, at a foggy weather condition, FSO transmitter must send at least 43 dB more power to overcome atmospheric attenuation during a 1 km link which is not feasible from practical stand point. Other than atmospheric attenuation, optical links also suffer from atmospheric refractive index random fluctuations (atmospheric turbulence) which induce intensity and phase fluctuations of optical beam at the receiver. This fluctuations degrade the system performance (atmospheric turbulence is described in detail in Section 2.1.2.) Furthermore, due to eye-safety regulations governed by International Electrotechnical Commission (IEC) [22], the average transmit power is limited in FSO systems. Ambient illumination is another challenge of FSO systems that is a huge amount of background noise is collected along with the incident data signal at the receive aperture [10]. In Chapter 3, it will be shown that these limitations confine FSO system transmissions to short range applications. In this thesis, the degrading effects of randomly varying atmospheric conditions and background illumination noise on the performance of FSO systems are investigated and new techniques

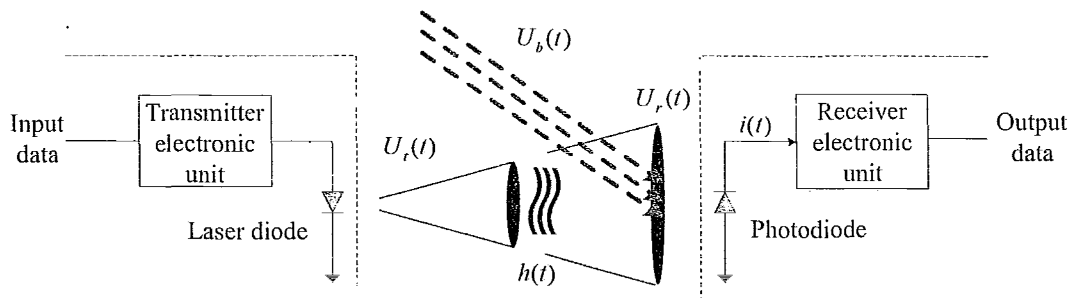

Figure 1.1: An FSO Communication system

are proposed to increase the accessible communicating distance of FSO systems. The next section presents a brief overview of FSO channels and summarizes the techniques which have been proposed so far to combat the aforementioned challenges.

1.2 FSO Systems and Channel Impairments

A point-to-point FSO communication link is shown in Fig. 1.1. In the transmitter side, a laser diode modulates data onto an optical wave. The modulated optical wave is shaped and directed through the atmosphere via an optical lens. For the sake of simplicity, in practical direct FSO systems Intensity Modulation with Direct Detection (IM/DD) is utilized in which data are modulated in the instantaneous intensity of optical waves [23]. The intensity of optical waves corresponds to the squared absolute value of optical field envelopes. The field envelope is the time-varying amplitude of an optical wave which is modulated by data. Assume a laser oscillating at angular frequency ω which is placed at $z = 0$ in the transmitter side. A forward propagating wave along the positive z-axis can be expressed as

$$\Psi(r,\phi,z,t) = \underbrace{U_t(t)}_{\text{Field envelope}} \underbrace{\psi(r,z,\phi)}_{\text{Transverse field profile}} \underbrace{\exp[-i(\omega t - kz)]}_{\text{Carrier}} \tag{1.1}$$

where $r = \sqrt{x^2 + y^2}$ is the radial distance from the beam center line, k is the propagation constant along the positive z-axis in free space, and ϕ is the phase. From (1.1), the transmit instantaneous intensity $I(t)$ is defined as

$$I(t) = |U_t(t)|^2. \tag{1.2}$$

In such systems, at the receiver, a receiving aperture followed by a lens collects and focuses the incident beam onto a photodetector. The photodetector coverts the collected optical power to an electrical current. This current is proportional to the instantaneous intensity of the received signal at the receiver scaled by the detector responsivity, R (A/W),

$$i(t) = R\,|U_r(t)|^2\,, \tag{1.3}$$

The electrical current is sampled and detected inside the receiver electronic unit. Finally, the detected data are decoded to extract the sent data stream.

In this thesis, data are modulated onto the instantaneous intensity of optical fields and at the receiver direct detection technique is performed to detect the signal (IM/DD). However, as will be discussed in Chapter 2, both intensity and phase information of optical field envelopes are required for system analyses.

An additive channel model is considered for the direct FSO system and can be expressed as [10]

$$U_r(t) = h(t)U_t(t) + U_b(t), \tag{1.4}$$

where $U_t(t)$ and $U_r(t)$ are respectively the transmitted and received optical field envelopes at the transmitter and receiver (Fig. 1.1), $h(t)$ is the temporal random fluctuations of optical channel, and $U_b(t)$ is the temporal profile of background illumination noise that are briefly overviewed in Section 1.2.1 and 1.2.2.

1.2.1 Atmospheric Channel Impairments: $h(t)$

The channel gain $h(t)$ models the random fluctuations of the propagation path. The FSO optical link is a time-varying channel whose random fluctuations arise due to variation of atmospheric conditions. Atmospheric molecules cause absorption and scattering which attenuate the power of the light traveling through the atmosphere. Furthermore, spatial and temporal variations of the air thermal inhomogeneities cause random fluctuation of the refractive index (i.e., atmospheric turbulence-induced fading) which results in fluctuation of the optical intensity at the receiving lens plane. These intensity fluctuations degrade the performance of FSO communication systems. The optical channel impairments will be discussed in more detail in Section 2.1.

The time scale at which the fading state remains approximately constant is denoted as the coherence time. If the coherence time is much smaller than the symbol duration T, many different fading states occur within the transmission, which is called fast-fading atmospheric turbulent channel. However, if the coherence time is equal or greater than T, the channel is a slow-fading atmospheric turbulent channel [24]. Typical FSO fading coherence time varies approximately between 10^{-3} and 10^{-1} sec [23] and typical symbol duration T is on the order of 10^{-9} sec, therefore FSO channels can be modeled as slow-fading channels. That is, the channel gain $h(t)$ is assumed constant over $10^6 - 10^8$ symbols. In what follows, h simply refers to the channel gain and implicitly indicates that fading is constant over many transmitted symbols. The constant channel gain h is a multiplicative factor [25] representing the amplitude and phase fluctuations which arise due to atmospheric attenuation h_a, geometric spread of optical beam h_p, and atmospheric turbulence τ, and can be formulated as

$$h(t) \approx h = h_a h_p \tau. \tag{1.5}$$

The atmospheric attenuation h_a depends on the weather condition and wavelength and includes both absorption and scattering effects (Section 2.1.1). Since the weather changes slowly on the order of minutes to hours, atmospheric attenuation can be considered constant over a long time. Geometric spread of the optical beam h_p is also constant for a given optical beam and distance (Section 2.1.3). Despite h_a and h_p, atmospheric-induced fading factor τ is a random coefficient which causes the received intensity fluctuates at the receive aperture (Section 2.1.2). Intensity fluctuations at the receiver degrades the FSO systems performance.

1.2.2 Background Illumination Noise: $U_b(t)$

The additive noise in (1.4), arises due to ambient illuminations which is the dominant source of noise in FSO communication systems. In addition to the desired signal, strong undesirable background radiation is also collected at the receive aperture. Background noise mainly originates from ambient light coming from optical sources such as sun, sky, moon, incandescent bulbs, etc, and is statistically modeled as an additive white Gaussian noise in time and space with zero mean and variance $\sigma_b^2 =$

$N_0/2$ [26]. The collected background noise is processed along with the desired signal and degrades the overall system performance.

The intensity and phase fluctuations at the receiver, that are induced by atmospheric turbulence random variations, degrade FSO system performance. Although, atmospheric turbulence mitigation techniques have been extensively investigated in literature, background illumination noise has not been separately considered as a limiting performance factor in FSO systems. Whereas, in Chapter 3, it will be shown that background illumination noise can deteriorate the error performance and limit the link distance coverage. The next section briefly denotes techniques and methods which have been proposed so far to combat atmospheric turbulence degrading effects.

1.2.3 Atmospheric Turbulence Mitigation Techniques

Atmospheric turbulence fading is one of the major impairments over FSO channels where the link range is longer than 1 km [27]. This factor limits the link rate, reliability and distance [23]. Different techniques have been proposed to mitigate fading effects such as error control coding [28, 29], maximum-likelihood sequence detection (MLSD) [30], spatial diversity [31], cooperative diversity, and multihop transmission [32].

1.2.4 Forward Error Correction

Various forward error correcting (FEC) techniques have been deployed in the literature to combat atmospheric turbulence degrading effects. Forward error correction is accomplished by adding redundancy to the transmitted data through an error correction coding algorithm such as turbo codes [33], block and convolutional codes [29], Reed-Solomon (RS) codes [34], and low-density parity-check (LDPC) codes [35]. In

[29], the performance of block codes and convolutional codes have been investigated and compared with turbo codes in the presence of weak atmospheric turbulence condition. It has been numerically shown that turbo coding can achieve better BER performance over atmospheric turbulence channel. However, turbo coding is not suitable for high-speed optical transmissions because of its high complexity and long encoding/decoding time that imposes delays on the system [36]. A promising alternative for mitigating atmospheric fluctuation is low-density parity-check (LDPC) coding scheme which greatly improves BER performance of the system even under strong atmospheric turbulence condition [35]. Although FEC is one of the best techniques to combat atmospheric turbulence-induced fading, use of them in high data rate optical transmissions imposes high delay and complexity to encoding/decoding units which may not be practical.

1.2.5 Maximum-Likelihood Sequence Detection

Based on the knowledge of the joint temporal statistics of turbulence-induced intensity fluctuations, maximum likelihood sequence detection (MLSD) has been proposed as another solution to mitigate atmospheric turbulence fading. The MLSD attempts to track the instantaneous state of intensity fluctuations and adjusts the detection threshold to the optimal value [30]. For transmitted sequences of length n, the MLSD computes the likelihood ratio of each of 2^n possible sequences which imposes complex computational costs and long delays to decoder. Various sub-optimal methods have been proposed to reduce computational complexity in MLSD method, e.g. single-step Markov chain maximum likelihood detection (SMC-ML) [30] and pilot-symbol assisted detection (PSA-ML) [30]. The sub-optimal methods provide comparable error performance with respect to the MLSD method while they reduce the computational complexity of MLSD detection method. All the proposed detection techniques provide significant performance improvements over symbol-by-symbol detection method at the cost of increased delays and computational complexity for simulating multidimensional integrals.

1.2.6 Spatial Diversity

Spatial diversity technique is another promising alternative for fading compensation that imposes less latency to encoding/decoding units. This technique takes advantage of multiple transmit/receive apertures that are placed far apart from each other so that each LOS path experiences a different fading condition [23]. Each receiver collects the received optical beam(s) from different spatial angles, this way spatial diversity provides information redundancy at the receiver and improves system performance [37]. In optical spatial diversity systems, the total average transmit power is the sum of maximum allowed transmit power of all transmit apertures, therefore, employing multiple apertures at the transmitter increases the total average transmit power of the link and allows the system to cover longer distances. Spatial diversity can significantly reduce the outage probability [38] and improve the outage capacity [39] of a multiple-input multiple-output (MIMO) link.

To maximize spatial diversity performance, the receive apertures should be placed as far apart as possible from each other, so that various receivers experience uncorrelated turbulence-induced fadings. In practice, it may not be always possible to place the receivers sufficiently far apart [23]. On the other hand, FSO systems are based on point-to-point transmission that is the transmitted signal directs to a specific receiver.

Spatial diversity requires a line-of-sight communication link between the source and destination terminals which may not be feasible in all situations. Furthermore, spatial diversity in FSO systems must involve multiple transmit and receive apertures at each terminal to create a spatial diversity. Implementing multiple transmit/receive aperture scheme and designing encoding/decoding protocols increase the complexity and implementation costs of the system. Multihop transmission is another alternative to combat the atmospheric fading effects and increasing free-space link coverage. The next section provides a brief overview of this technique.

1.3 Optical Multihop Transmission

Multihop transmission relays the data signal from the source node (transmitter) to destination node (receiver) through intermediate terminals called relays or nodes and has been introduced as a promising technique to improve FSO links coverage and reliability through mitigating atmospheric fading impairment [40, 41]. Arranging relays in a serial configuration exempts FSO relays from being equipped by multiple transmit/receive apertures. Despite spatial diversity which requires transmit/receive apertures to be positioned in a LOS configuration, in multihop systems, source and destination nodes are connected via intermediate relays and consequently LOS connectivity is not necessary. In other words, multihop techniques can support an optical connection between two buildings which do not have a line of sight. Furthermore, by subsequent deployment of smaller multiple hops (hop is the distance between two relays), more reliable FSO transmission over longer distances becomes achievable [32]. As shown in Fig. 1.3, by employing multihop links in a parallel configuration, new relaying scheme based on cooperative diversity is developed [42, 43]. In this scheme

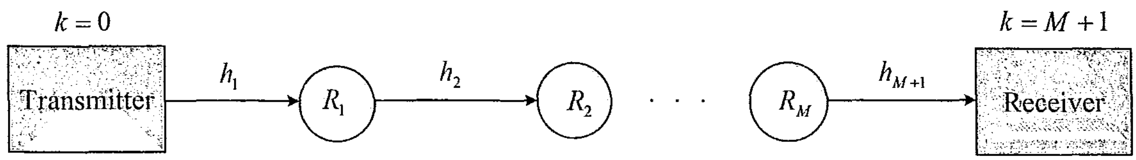

Figure 1.2: Multihop Transmission

which is a special configuration of spatial diversity, intermediate relays involve only one transmit/receive aperture and are placed far enough from each other so that each receiver suffers from a different fading condition. The diversity of received signal intensities at destination improves the link end-to-end reliability [32]. Obviously, in cooperative diversity systems, the total communicating distance is determined by the length of the shortest multihop link. Therefore, to increase the total communicating distance of the link, a huge number of relays must be placed between the communicating nodes, that in practice, may not be possible. Since the primary purpose of this study is to propose methods of increasing the total communicating distance of FSO systems, only multihop systems are of great interests.

In multihop transmission relays are employed in series. This scheme is typically illustrated in Fig. 1.2. In serial relaying scheme, the source transmits an intensity-modulated signal to the first relay. The relay (depending on relaying technique) performs optical operations on the signal and forwards it to the next relay. This continues until the transmitted signal arrives at the destination. In this thesis innovative techniques are developed for the multihop schemes to increase the total communicating distance of FSO systems while guaranteeing a reliable high data rate. The next section presents a brief overview of multihop FSO systems and summarizes their achievements and drawbacks. Also techniques which have been proposed in the literature to combat these challenges are described.

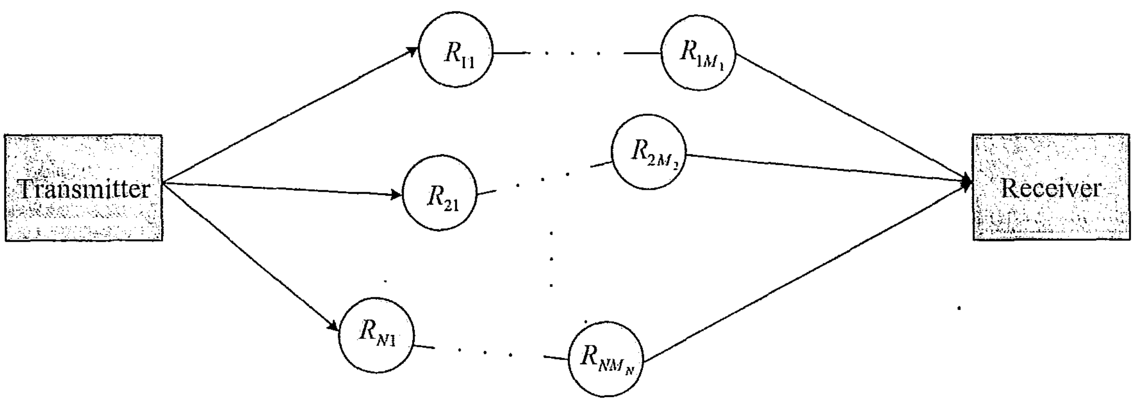

Figure 1.3: Cooperative Diversity

1.4 Multihop Communication Systems

Multihop transmission has been introduced as a powerful technique to mitigate the fading and path loss effects in FSO systems. Two processing techniques are widely used in literature to implement multihop FSO transmission; namely: decode-and-forward (DF) relaying and amplify-and-forward (AF) relaying.

1.4.1 Amplify-and-Forward relaying technique

In the previously considered AF methods, the collected optical signal at the receiving lens of each relay is converted to a photo-current via a photo detector. The electrical signal is amplified by an electrical amplifier with a gain specific to each relay. Then the amplified signal is optically modulated and retransmitted through the next hop. In all AF FSO systems proposed so far, the amplifier gain of each relay is determined based on the knowledge of the channel state of the previous hop. The channel state information-assisted (CSI-assisted) gains have been widely utilized to analytically study end-to-end performance of optical [27, 44, 45] and RF [41, 46] amplify-and-forward multihop systems. Relays using CSI-assisted gains use instantaneous CSI of previous hop to control the gain of the relay and as a result fix the instantaneous output power of the relay [47, (4)]. In the most AF multihop FSO and RF systems investigated in the literature, to make mathematical analyses tractable, an ideal model for relay gains has been considered by which relay completely compensates the channel fading effects of the last hop, regardless of the noise of that relay [47, (5)]. This approach has been widely used in analyzing the performance of RF communication systems [42, 41] and recently attracted attention in FSO system studies [27, 44, 45]. The CSI-assisted relays continuously estimates the channel fading amplitude which may not be practically feasible in all situations.

A practical alternative for CSI-assisted gain is using fixed-gain amplifiers in AF relays [47, (13)]. In [47], it has been shown that RF systems with fixed gain relays have comparable performance with systems equipped with CSI-assisted relays. However the fixed-gain method low complexity and ease of deployment make it a promising alternative for CSI-assissted AF systems. Although average BER of CSI-assisted and fixed-gain AF FSO systems over strong Gamma-Gamma atmospheric turbulence have been investigated in [45], no explicit comparison has been made between performance of these to gaining techniques. In AF FSO systems, the noise added to the signal at each relay propagates through transmission path. This accumulated noise is another limiting factor in AF FSO systems as the number of relays increases.

1.4.2 Decode-and-Forward relaying technique

Similar to AF systems, in DF FSO systems, at each intermediate relay the received optical signal is photodetected and converted to an electrical current. The electrical signal is decoded and re-encoded before retransmission. In DF technique, the noise at each relay is eliminated and does not propagate through the channel. The reconstructed signal is ideally a noiseless signal with average power equal to the transmitted power at the source. In [48] various DF techniques have been proposed for cooperative diversity systems. The primary concepts of these techniques can be applied to DF multihop systems. In bit detect-and-forward (BDF) technique the bit sequence is *detected* and the detected "0" or "1" bits are retransmitted through the next hop without applying any error correction technique.

In the normal decode-and-forward (DF) relaying technique which has been employed in all multihop FSO systems proposed in the literature [27, 32, 49], the bit stream is *decoded.* The incorrectly decoded bits are corrected before transmission via an error correcting technique. At each relay a finite error occurs due to the decoding process. This error accumulates over multiple hops for long-length hops. In [40], it is shown that for hops longer than 500m, error grows rapidly as the number of relays. In DF relaying, noise does not propagate through the channel and decoding error is less than BDF technique, therefore DF method outperforms BDF technique at a cost of higher complexity through decoding/encoding processes at each relay. Moreover, decoding and re-encoding processes at each relay inject a time delay into the system which leads to an end-to-end delay that increases by the number of relays. Although DF techniques outperform AF methods, the simplicity of AF over DF, introduce AF relaying technique a more desirable candidate for practical purposes.

1.4.3 Optical multihop relaying techniques proposed in the literature

Multihop techniques have been extensively studied for years in RF communications, however applying them to FSO systems emerged only recently. In [49], the capacity of multihop FSO systems is analyzed from a networking standpoint and channel impairments such as atmospheric fading, attenuation, and geometric loss were not considered in the analysis. The bit-error rate (BER) of a DF FSO system was studied in [40], in which atmospheric attenuation and geometric loss were the only effects included in the channel model. In [40], it was demonstrated that the mean and variance of the error rate is smaller in multihop systems rather than single hop communication systems for the same link range and launched power. In contrast to [40], a loss-free strong turbulence fading channel is considered in [27] to analyze the end-to-end outage probability of an FSO link employing OOK modulation with IM/DD scheme. Both DF and CSI-assisted AF relaying techniques have been investigated. The results indicate that the outage performance of AF multihop systems degrades with increasing number of relays. Using the same gain model, outage probability of AF multihop FSO systems has been analytically calculated for strong turbulence fading channel modeled by K-channel and Negative Exponential (NE) channel [44]. The results proposed in [44] justify that by increasing the number of relays while the hop lengths are fixed, the outage probability increases. In [32], an aggregated optical channel model including both path-loss and weak turbulence fading effects was considered and the end-to-end outage probability of FSO systems utilizing DF relaying technique was presented. A fixed spacing between the source and destination nodes has been considered in [32] and the end-to-end outage performance of the system for different number of relays is simulated. It was shown that outage probability of a fixed-length multihop system improves by increasing the number of relays because hop lengths and consequently atmospheric turbulence-induced fading decrease as the number of relays increase.

In all multihop systems proposed so far, each relay is equipped with a photodetector which converts the incident optical power into a photocurrent. Then the electrical signal is processed by electrical units performing either AF or DF relaying technique. The processed electrical current is modulated through a high bandwidth laser and retransmitted to the next relay. In fact, each relay is equipped with analog-to-digital (ADC) and digital-to-analog (DAC) convertors operating at speeds up to a few Giga samples per second (Gsps), e.g. ADX3500 – 3 Gbps XMC Digitizer produced by PMC-Sierra® provides up to 3 Gsps data rate [50]. Even if it is assumed that ADC (DAC) conserves the high data rate of the optical signal, relaying procedures, i.e. amplification or detection (decoding) process, are performed by low speed electrical processors. In other words, instead of taking advantage of wide bandwidth (high data rate) of optical systems to communicate a huge amount of information at a short time, the overall system data rate is confined to the speed of electrical processors. Although high speed electrical processors operating at Gbps rates are emerging [50], deploying them in all relays may be cost prohibitive. In addition, in DF systems, an additional encoding/decoding delay is also added to the system and increases as the number of relays. A solution for increasing the overall data rate of the multihop FSO systems and accessing wider bandwidths in a cost-effective way is utilizing all-optical processors at all relays.

Although all-optical AF relaying technique has been widely used in fiber optic communication systems [16], its application in FSO systems was tested for the first time in [51]. A dual-hop all-optical AF FSO system was implemented and its BER was obtained at different bit rates BR= 2.5 Gbps and BR= 10 Gbps. In this experiment an all-optical automatic gain controller (OAGC) is utilized to adjust the optical amplifier gain so that it compensates the power fluctuations of the received signal due to turbulence effects. The experimental results indicate that at higher bit rates the probability of error increases. In [51], dual-hop relay-assissted configuration is examined for hop lengths of 75 m over which the effects of atmospheric turbulence are negligible. Until now, no analytical investigation has been performed on the performance analysis of all-optical multihop FSO systems impaired by atmospheric turbulence in long-haul applications. This approach is the primary focus of this thesis.

1.5 Thesis Contributions

This thesis proposes novel relaying techniques for optical multihop communication systems in which all relaying processes, i.e. amplification and detection, are performed in optical domain.

In this work, an aggregated channel model is considered which takes into account atmospheric turbulence-induced fading, atmospheric attenuation due to absorption and scattering and optical beam-spread propagation loss. Although data are modulated in optical field intensity (IM/DD), instead of analyzing optical power, the magnitude and phase variations of optical fields are considered. Because all-optical components are employed in all relays and photodetection is only performed once at the receiver. To analyze the optical field characteristics, a new channel gain is proposed to completely characterize both magnitude and phase variations of optical fields propagating through the channel. The main contribution of this work in defining a new channel gain corresponds to deriving new complex propagation loss over the optical channel including beam propagation through FSO channel, beam focusing and its projection onto an optical fiber at the beginning of each relay. Although, it is optical field intensity that is finally detected at the receiver and its phase does not contribute in detection process, a complete knowledge of field distribution is required at intermediate relays. The proposed method supports more accurate description of propagation loss rather than conventional geometric loss (equation (2.16)), especially at short distances.

After completely defining the channel model, the error performance of all-optical amplify-and-forward (OAF) multihop systems are investigated. In the OAF technique, the received optical field is simply coupled into a fiber and amplified by an optical amplifier. Then the amplified signal is retransmitted through the next hop. A fixed-gain protocol is deployed for amplifier gain which only depends on the deterministic structure of the preceding hop and guarantees a constant eye-safe average power at the output of each relay. An adjustable gain optical amplifier can also be used at each relay to compensate the last hop fading effects and provides a fixed instantaneous output power at each relay. This type of OAF systems are expected to outperform the fixed-gain OAF systems, further investigations of these systems have been left for future. Regardless of the amplification method, the collected background noise is amplified along with the desired signal. The OAF technique considerably improves the BER of FSO systems over moderate distances (up to 5 km), but the amplified background noise accumulates through the channel and deteriorates OAF FSO system performance. Through Monte-Carlo simulations, it is numerically shown that by increasing data rate and/or the number of relays, error performance improves slowly because more background noise is injected into the system. This is the major drawback of OAF FSO systems that limits the maximum accessible communicating distance to a few kilometers even if a large number of relays is employed. Despite their simple structure and ease of implementation, OAF FSO systems are practically suitable for moderate-range applications, i.e. on the order of a few kilometers. To introduce FSO links as a promising candidate for long-range applications, new techniques need to be developed to eliminate background noise effects at each relay.

Also known as regenerative technique in RF communications [46], a novel all-optical regenerate-and-forward (ORF) relaying technique is proposed to combat background noise. In this technique, the optical signal is reconstructed so that the collected background noise is eliminated at each relay. Atmospheric turbulence fading effects are not considered in this study and only the effectiveness of ORF technique in removing background noise is investigated in terms of BER performance. The optimal relaying configuration is determined based on numerical simulations. It is numerically shown that ORF technique significantly outperforms OAF technique and by increasing the number of relays its performance improves steadily. Despite OAF systems whose maximum accessible distance is limited to a few kilometers, FSO systems which utilize ORF relaying are able to access extensive communicating distances, given atmospheric turbulence can be neglected. This outstanding accomplishment is achieved for the highest available data rate 10 Gbps employed in commercial FSO communication systems.

1.6 Thesis Structure

This thesis is organized as follows: In Chapter 2, a detailed description of optical wave propagation in free space is provided. An aggregated optical channel between every two relays is defined which starts from the fiber output at the transmit relay and ends at the inside of the fiber at the receive relay. It is assumed that the output laser beam at the transmitter has a Gaussian transverse profile. The paraxial approximation [52] is used to find the field distribution at the receive relay from which propagation loss due to beam spreading through the channel is obtained. The Beers-Lambert law [53] is modified to model atmospheric attenuation of optical fields instead of optical intensities. Moreover, a weak log-normal atmospheric turbulence regime is considered whose log-amplitude and phase are normally distributed and their statistical moments are mathematically described. Finally, the optical channel has been modeled as a multiplicative factor which takes into account weak log-normal atmospheric turbulence, propagation loss and atmospheric attenuation.

In Chapter 3, an optical amplify-and-forward relaying technique is introduced and applied to various FSO system configurations. The average BER is selected as an evaluating metric for analyzing the error performance of different relaying schemes. It is mathematically proved by induction that equally-spaced relaying configuration provides the best average optical SNR at the receiver side of OAF systems and the result is numerically illustrated through Matlab simulations for the systems with one and two relays. Hence, the equally-spaced relaying configuration is employed in all of the considered OAF systems. Employing this configuration, the maximum accessible communicating distance for different number of relays at two bit rates BR= 1.25 Gbps and BR= 10 Gbps is obtained through Monte-Carlo simulations. The BER results are presented for no fading and weak fading atmospheric conditions and analyzed to contrust the effects of atmospheric fading. Finally, the destructive effects of background noise in degrading BER performance of OAF systems is investigated and background noise is introduced as a major distance-limiting factor in OAF multihop FSO systems.

In Chapter 4, an optical regenerate-and-forward (ORF) relaying technique is proposed to mitigate the degrading effects of background noise. Since Monte-Carlo (MC) simulations are time-consuming, an alternative method called *Q-factor* (QF) estimation is utilized for additive white Gaussian noise (AWGN) channels to accelerate the simulation process. The performance of MC and QF methods and are compared for a nonlinear dual-hop ORF system, and it is shown that QF provides a close approximation of MC in such systems. The equally-distance relaying configuration is assumed for ORF systems based on BER simulation of a dual-hop ORF system at bit rate BR= 10 Gbps. Using equally-distance scheme, the maximum accessible distance for different number of relays is found. In this study, a very weak turbulence fading condition ($C_n^2 < 1 \times 10^{-17}\text{m}^{-2/3}$ [52]) has been considered under which the atmospheric fading effects can be neglected over distances up to 1 km. The simulation results show that ORF systems are able to remove the background noise completely at each relay when atmospheric fading is neglected. This property introduces the ORF technique as a superior method over the OAF in increasing the total communicating distance of FSO systems.

Finally, Chapter 5 presents concluding remarks and future directions.

Chapter 2

Channel Model

In the previous chapter, a typical direct FSO communication link was illustrated in Fig. 1.1 and a propagating optical beam wave was expressed by (1.1). Many lasers emit beams with a Gaussian profile, that is the laser is operating in a lowest-order mode called TEM_{00} mode. At this mode of propagation, the field profile is independent of ϕ , therefore, $\psi(r,z,\phi)$ at the transmitting aperture ($z=0$) can be described as [52]

$$\psi(r,z,\phi)\Big|_{z=0} = \psi_0(r) = A_0 \exp(-\frac{1}{2}k\alpha_0 r^2) \tag{2.1}$$

where α_0 is the complex parameter related to effective beam radius (spot size) W_0 and phase front radius of curvature F_0 at the transmitter and is given by

$$\alpha_0 = \frac{2}{kW_0^2} + i\frac{1}{F_0} \tag{2.2}$$

The factor A_0 is set to normalize the transverse field to carry unit energy at the transmitting aperture. From (2.1), it is readily shown that

$$
\begin{aligned}
1 &= \iint \psi_0(r)\psi_0^*(r) r dr d\phi \\
&= |A_0|^2 \underbrace{\int_0^{2\pi}\int_0^{\infty} \exp(-\frac{2r^2}{W_0^2}) r dr d\phi}_{\frac{1}{2}\pi W_0^2} \\
\Rightarrow & \quad |A_0| = \sqrt{\frac{2}{\pi}}\frac{1}{W_0} \qquad (2.3)
\end{aligned}
$$

For a bit stream of Gaussian pulses the transmitted optical field envelope is expressed as

$$U_t(t) = \sqrt{P_M}\sum_n a_n \exp\left(-\frac{(t-nT_b)^2}{2T_0^2}\right), \qquad (2.4)$$

here a_n is the modulating coefficient taking the values 0 and 1 randomly when on-off-keying (OOK) modulation is employed, T_0 is the half of pulse width at $1/e$-intensity, T_b is the bit interval, and P_M is the peak power of the optical signal. For Gaussian pulses, P_M is obtained as [16]

$$P_M = 2P_t\frac{T_b}{1.665T_0}, \qquad (2.5)$$

where P_t is the average transmitted power at the transmitter.

2.1 Free-Space Optical Channel

Line-of-sight FSO communication systems generally use high-power lasers that operate in eye safety Class 1M [11], [12] band to achieve a good power budget. The allowable safe laser power depends on the wavelength. According to the IEC standards [22], the 1550 nm band provides higher power budget, compared to the 850 nm band [15]. Consequently, the 1550 nm band is extensively used in long distance commercial FSO systems, while inexpensive components operating at the 850 nm band are utilized in short distance FSO systems. As mentioned, in the considered optical system, data are modulated in the optical intensity of the light, therefore the allowed power and its variations through the optical channel play a key role in overall system performance. The considered FSO channel impairments originate from the atmospheric attenuation, atmospheric turbulence, and propagation loss.

2.1.1 Atmospheric Attenuation

As the optical wave propagates through the atmosphere its power attenuates due to absorption and scattering. Both absorption and scattering phenomena are dependent on weather and wavelength. Absorption comes from the interaction between the photons and atoms or molecules that leads to the extinction of the incident photon, elevation of the temperature, and radiative emission. Scattering phenomenon redirects the incident photons into a different direction with respect to the original axis. The atmospheric optical power attenuation is determined by the exponential Beers-Lambert law [53]. Using this definition, the atmospheric attenuation for optical field, h_a, can be expressed as

$$h_a = e^{-\sigma L/2}, \tag{2.6}$$

where $\sigma(m^{-1})$ is the atmospheric attenuation coefficient. Each wavelength chosen as a central wavelength has a specific attenuation coefficient, therefore it is preferred to select the central wavelength corresponding to the least attenuation coefficient.

Table 2.1: Atmospheric attenuation coefficients for different weather conditions.

Weather Condition	Attenuation (dB/km)
Clear	0.2-0.5
Haze	2-9
Fog	21-272

Fortunately, at 850 nm, and 1550 nm the attenuation coefficient is low, i.g. for the clear weather condition $\sigma = 0.43$ dBm/km at $\lambda = 1550$ nm. The attenuation factor is also dependent on weather condition. Table 2.1 provides the attenuation coefficients for different weather conditions at wavelength $\lambda = 1550$nm. As seen from this table, the fog weather condition has the highest attenuation that limits the FSO link range to a few meters [54].

2.1.2 Atmospheric Turbulence

Optical beam traveling through the atmosphere experiences random phase and amplitude fluctuations (scintillation) due to atmospheric turbulence. Turbulence is a disordered state of the atmospheric flow which is caused by temperature variations in the atmosphere. An atmospheric turbulent media consists of many spherical regions or eddies with randomly varying diameters and different indices of refraction. The propagating optical beam experiences random spatial and temporal fluctuations in this randomly varying refractive.indexed medium with different scale sizes. Large scale inhomogeneities produce refractive effects that steer the beam in a slightly different direction, therefore, large scale effects mostly distort the phase of the propagating wave. Small scale inhomogeneities mostly produce diffractive effects and distort the amplitude of the wave through beam spreading and amplitude fluctuations [52].

According to Rytov theory which is proposed for weak turbulence conditions, the turbulent medium is assumed to consist of a series of thin slabs. Each slab modulates the optical field from the previous slab perturbation by some incremental values. The received field can be expressed in terms of the transmitted field U_t as

$$U_r = U_t \tau = U_t \prod_i e^{\zeta_i} = U_t e^{\sum_i \zeta_i}, \tag{2.7}$$

where $\tau = e^{\zeta_i} = e^{\chi + jS}$ represents the effect of turbulence-induced fading as a complex multiplicative term. According to the central limit theorem $\psi = \sum_i \psi_i$ approaches a complex Gaussian random variable and therefore, the fading log-amplitude (χ) and phase (S) are normally distributed [25].

$$f_\chi(\chi) = \frac{1}{\sqrt{2\pi\sigma_\chi^2}} \exp\left(-\frac{(\chi - \mu_\chi)^2}{2\sigma_\chi^2}\right) \tag{2.8}$$

As a result, the turbulence-induced fading amplitude ($\tau_A = |\tau| = e^\chi$) is a log-normal random variable with log-amplitude mean μ_χ and log-amplitude variance σ_χ^2.

$$f_{\tau_A}(t) = \frac{1}{t\sqrt{2\pi\sigma_\chi^2}} \exp\left(-\frac{(ln(t) - \mu_\chi)^2}{2\sigma_\chi^2}\right) \tag{2.9}$$

Considering that turbulence does not absorb optical energy, only scatters it, the energy is conserved for an infinite plane wave or a spherical wave [55]. Gaussian beam waves behave like plane waves at long distances from the source [56], therefore an energy-conserving condition can be also applied to Gaussian beam waves. As shown in [55] , to ensure that fading does not attenuate or amplify the average power ($E[|\tau_k|^2] = 1$), the log-amplitude mean μ_χ must be equal to the negative of the variance of the log-amplitude $\mu_\chi = -\sigma_\chi^2$.

The variance of log-amplitude fluctuation is a measure of the strength of the amplitude fluctuations. The principal contribution to the log-amplitude fluctuations is made by inhomogeneities whose sizes are close to Fresnel length $\sqrt{\lambda L}$ [52], where L is the thickness of the turbulent medium. The Kolmogorov spectrum is considered as a satisfactory model to calculate the log-amplitude variance [52]:

$$\Phi_n(\varkappa) = 0.033 C_n^2 \varkappa^{-11/3}, \tag{2.10}$$

where C_n^2 is the refractive index structure constant and index n indicates the refractive index dependency of turbulence. Close to ground levels, for paths that are nearly horizontal to the earth's surface, C_n^2 does not change considerably and is assumed to be constant. In (2.10), $\varkappa$ is the spatial wave number defined by $\varkappa = 2\pi/l$, where l is the scale size. The Kolmogorov model is applicable throughout the inertial interval which is defined as [57]

$$\frac{2\pi}{L_0} = \varkappa_0 \ll \varkappa \ll \varkappa_m = \frac{5.92}{l_0}, \tag{2.11}$$

where l_0 and L_0 are the internal and external turbulence scale respectively. The behavior of $\Phi_n(\varkappa)$ outside the inertial intervals is not essential. By estimating Gaussian beam waves with plane waves, the log-amplitude variance within the range of $l_0 \ll \sqrt{\lambda L} \ll L_0$ is calculated as [25]

$$\sigma_\chi^2 = 4\pi^2 k^2 L \int_0^\infty \Phi_n(\varkappa)\varkappa d\varkappa = 0.124 C_n^2 k^{7/6} L^{11/6}, \tag{2.12}$$

where $k = 2\pi/\lambda$ is the wave number.

In [58], a zero-mean normal distribution is assumed for the phase fluctuations. Despite log-amplitude fluctuations, the phase fluctuations are mainly determined by the large-scale inhomogenities (including the external scale L_0) [52]. Unfortunately the phase refractive-index power spectrum is not well defined for scale sizes equal or larger than L_0. In order to estimate the phase spectrum, certain limiting assumptions need to be imposed on the behavior of $\Phi_n(\varkappa)$ in the region of large-scale inhomogeneities. Different models for phase spectrum have been investigated [52] among which the two-parameter spectrum model proposed by Kármán is considered here

$$\Phi_n(\varkappa) = 0.033 C_n^2 (\varkappa^2 + \varkappa_0^2)^{-11/6} \exp(-\varkappa^2/\varkappa_m^2), \tag{2.13}$$

where $\varkappa_0$ and $\varkappa_m$ are given by (2.11). Under a geometrical optics approximation ($L\varkappa^2/k << 1$), the phase variance for Gaussian beam waves is obtained from [52]

$$\sigma_S^2 \approx 4\pi^2 k^2 L \int_0^\infty \Phi_n(\varkappa) \varkappa d\varkappa \tag{2.14}$$

by substituting (2.13) in (2.14) and performing mathematical simplifications, the phase fluctuation variance is expressed as

$$\sigma_S^2 \approx 0.78 C_n^2 k^2 L \varkappa_0^{-5/3}. \tag{2.15}$$

2.1.3 Propagation Loss

The third factor is the geometric power loss which results from the diffractive properties of optical wave propagating through optical media. The conventional model for geometric loss which has been widely used in IM/DD FSO systems is approximated for unbounded plane waves as [59]

$$H_g = \frac{\iint\limits_{A_{lens}} |\psi_3(r,\phi)|^2 r dr d\phi}{P_t} \approx \frac{d_r^2}{(d_t + \theta L)^2} \tag{2.16}$$

where $\psi_3(r,\phi)$ is the transverse optical field profile at the receiving lens plane (point ③), L is the propagating distance, d_t and d_r are the transmitting and receiving lens diameters in Fig. 2.1, and $\theta(rad)$ is the transmit beam divergence. In this model it is assumed that the field intensity is distributed uniformly over the receiving aperture area which is the case for plane waves. Although this model is a satisfactory estimation for modeling plane waves, in many applications the plane wave approximation is not sufficient to characterize the properties of the wave. In addition, other than power loss which is a metric for evaluating the field magnitude variations, the phase of the optical field is also of interest in many applications. In this work, since all-optical components in all relays are employed, photodetection is only performed once at the receiver. Thus, instead of analyzing optical power loss, the magnitude and phase variations of optical fields are considered. In this part, by assuming Gaussian field distribution for the propagating wave a new model for geometric loss is introduced.

The optical channel between transmitter and receiver is shown in Fig.2.1. At the transmitter, a signal is transmitted via a transmitting lens with focal length f_t. The distance between the fiber output and lens at the transmitter, L_t, is dependent upon the required beam width at the receiving lens to guarantee a reliable alignment. The receiver has a converging lens that focuses and couples the incident light into the fiber. To gain a satisfactory coupling efficiency, the fiber is placed at the focal plane of the receiving lens, i.e. $L_r = f_r$, where L_r is the distance between the lens and fiber

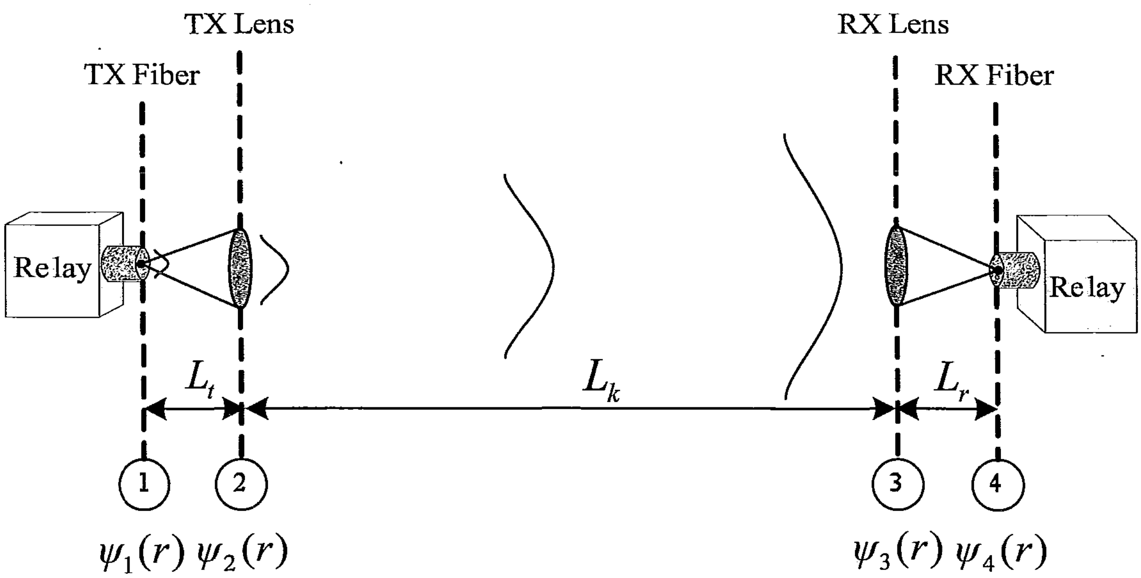

Figure 2.1: The Relay-to-Relay Channel Model

at the receiving node and f_r is the focal length of the receiving lens.

The optical channel considered here starts from the fiber output at the transmitter (point ①) to the fiber input at the receiver (point ④). The wave coming out of the fiber at point ① travels distance L_t to reach to a thin lens at point ②. After propagating thorough a free-space path with length L, it is incident on an optical lens that converges the received field and couples it onto a fiber at point ④. In order to analyze the transmitted wave characteristics after undergoing such propagation, the optical wave propagation thorough various optical media such as free-space, optical lens, and optical fiber will be discussed first.

2.1.4 Gaussian-beam wave propagation

Over distances on the order of a few kilometers, it is reasonable to consider a Gaussian model for optical wave profile propagating thorough optical media. Given the field profile at $z = 0$, the field distribution at distance z from the source must be found.

If diffraction effects on the optical wave change slowly with respect to propagation distance z, the optical wave profile at a distance z from the source can be found by solving the *paraxial wave equation* [52]

$$\frac{1}{r}\frac{\partial}{\partial r}(r\frac{\partial \psi}{\partial r}) + 2ik\frac{\partial \psi}{\partial z} = 0 \tag{2.17}$$

The paraxial approximation ($\partial^2\psi/\partial z^2 = 0$) is valid when the separation distance between optical elements is large compared with the transverse extent of the beam.

By solving (2.17) for $\psi(r, z)$, the optical wave profile at distance z from the source is obtained as [52]

$$\psi(r, z) = \frac{A_0}{1 + i\alpha_0 z} \exp\left[ikz - \frac{1}{2}k\left(\frac{\alpha_0}{1 + i\alpha_0 z}\right)r^2\right] \tag{2.18}$$

It is obvious that optical beam wave profile at distance z from the source has a complex Gaussian distribution with new complex parameters α_z and p_z

$$\psi(r, z) = \frac{A_0}{p_z} \exp(ikz) \exp(-\frac{1}{2}k\alpha_z r^2) \tag{2.19}$$

where

$$\begin{aligned} \alpha_z &= \frac{\alpha_0}{1 + i\alpha_0 z} \\ p_z &= 1 + i\alpha_0 z = \underbrace{1 - \frac{z}{F_0}}_{\Theta_0} + i\underbrace{\frac{2z}{kW_0^2}}_{\Lambda_0} \end{aligned} \tag{2.20}$$

In (2.20), Θ_0 and Λ_0 are *input plane beam parameters* and characterize, respectively, the *refractive*(focusing) and *diffractive* changes in the on-axis ($r = 0$) amplitude of the Gaussian beam [52]. The transverse field amplitude at distance z is expressed in terms of Θ_0 and Λ_0 as

$$A_z = \frac{A_0}{\sqrt{\underbrace{\Theta_0^2}_{\text{refraction}} + \underbrace{\Lambda_0^2}_{\text{diffraction}}}} \tag{2.21}$$

When a Gaussian-beam wave propagates thorough free-space, its beam waist (W) broadens due to diffractive properties of Gaussian beam waves.To find a visual intuition about this concept, a numerical example is illustrated here. Let us consider a free-space path with length $L = 1$ km. A unit-amplitude Gaussian-beam with the wavelength $\lambda = 1550$ nm, the beam radius $W_0 = 4$ cm, and the radius of curvature $F_0 = -20$ cm propagates thorough atmosphere. The intensity of the optical wave is defined as

$$I(r, z) = |\psi(r, z)|^2 \qquad [W/m^2] \tag{2.22}$$

In Figure 2.2, optical beam intensity is plotted at $z = 0$ and $z = 1$ km. As shown in this figure, the beam waist at $z = 1$ km is approximately 10 times wider than W_0.

2.1.5 *ABCD* Ray-Matrix

In Fig. 2.1, the optical channel from point ① to point ④ is composed of various optical elements placed at arbitrary positions along the propagation path i.g. free-space, optical lens, and optical fiber. In order to simplify the process of finding the Gaussian-beam wave profile after propagating thorough subsequent optical elements through the channel, 2×2 matrices called *ABCD ray matrices* have been used. More

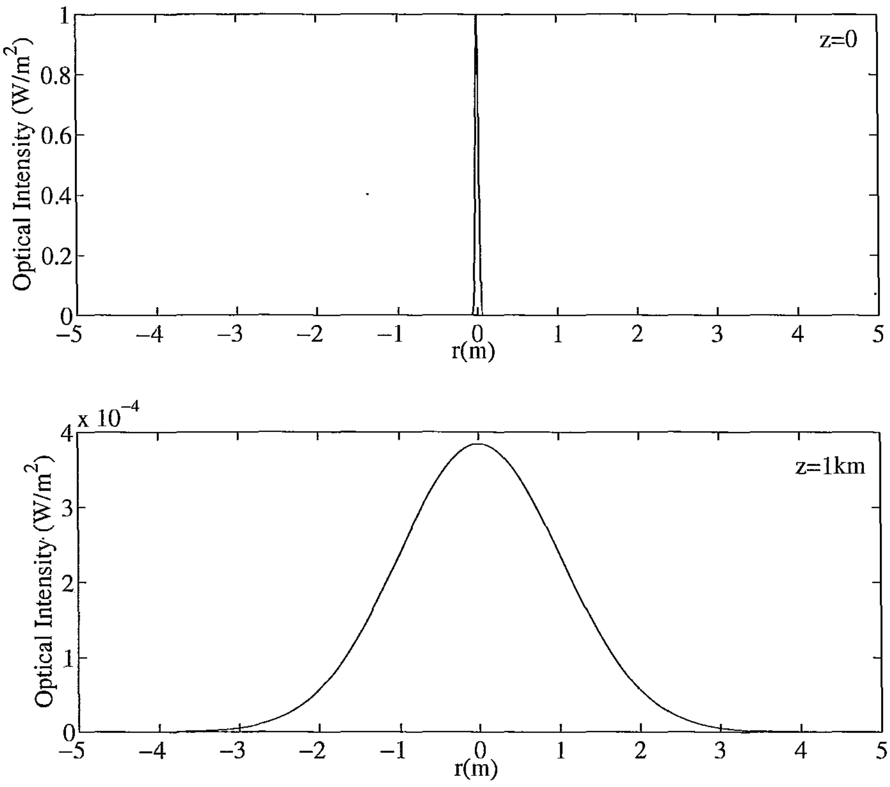

Figure 2.2: Optical intensity of Gaussian beam waves at $z = 0$ and $z = 1$ km

details of ABCD ray matrix analysis can be found in [52]. Each optical element can be represented by a matrix whose elements construct the output beam characteristics using input beam parameters. In Table 2.2, the matrix representations of a free-space path with length L and a thin lens with focal length f are listed.

The field distribution at the output of an optical element can be simply found by using its $ABCD$ ray matrix. From (2.1), the Gaussian beam profile in the input

Table 2.2: Ray matrices for various optical elements

structure	Matrix $\begin{pmatrix} A & B \\ C & D \end{pmatrix}$
Line-of-sight free-space path with length L	$\begin{pmatrix} 1 & L \\ 0 & 1 \end{pmatrix}$
Thin lens with focal length f	$\begin{pmatrix} 1 & 0 \\ -\frac{1}{f} & 1 \end{pmatrix}$

plane ($z = 0$) of an optical element is described as

$$\psi_0(r) = A_0 \exp(-\frac{1}{2}k\alpha_0 r^2) \tag{2.23}$$

As expressed in (2.19), the Gaussian-beam wave profile in the output plane ($z = L$) is defined exactly via two parameters α_L and p_L. These parameters can be chararcterized in terms of $ABCD$ matrix elements

$$\begin{aligned} \alpha_L &= \frac{\alpha_0 D - iC}{A + i\alpha_0 B} = \frac{2}{kW_L^2} + i\frac{1}{F_L} \\ p_L &= A + i\alpha_0 B \end{aligned} \tag{2.24}$$

where W_L and F_L are, respectively, the beam radius and phase front radius of curvature of the wave in the output plane. For example, for a free-space path with length

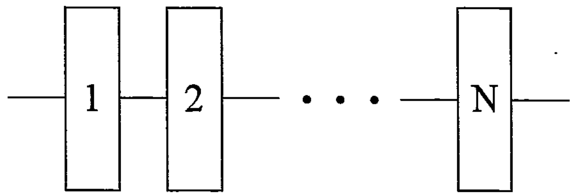

Figure 2.3: Subsequent optical elements

L, the beam characteristics at the end of the path are calculated as

$$\begin{aligned} \alpha_L &= \frac{\alpha_0}{1 + i\alpha_0 L} \\ p_L &= 1 + i\alpha_0 L \end{aligned} \tag{2.25}$$

which are consistent with those derived at (2.20).

Moreover, the received Gaussian-beam wave parameters after passing through a train of optical devices can be readily found by successively multiplying $ABCD$ matrix representations of all optical elements. In fact, an optical path including several arbitrary optical structures can be modeled by a single $ABCD$ ray matrix. Consider N arbitrary optical elements between transmitting aperture ($z = 0$) and receiving aperture ($z = L$) as shown in Fig. 2.3. Each optical element can be characterized by an $ABCD$ ray matrix. The overall $ABCD$ matrix at $z = L$ can be found by multiplying all $ABCD$ ray matrices in reverse order as

$$\begin{pmatrix} A & B \\ C & D \end{pmatrix} = \begin{pmatrix} A_N & B_N \\ C_N & D_N \end{pmatrix} \cdots \begin{pmatrix} A_2 & B_2 \\ C_2 & D_2 \end{pmatrix} \begin{pmatrix} A_1 & B_1 \\ C_1 & D_1 \end{pmatrix} \tag{2.26}$$

From (2.24), by using the overall $ABCD$ matrix, the Gaussian beam characteristics at the end of optical path can be found.

$ABCD$ ray matrices invoke the paraxial approximation to simplify the description of Gaussian wave propagation through optical media. Consequently it is valid when the separation distance between optical elements is large compared with the transverse extent of the beam. Under the assumption of lossless optical elements, $ABCD$ matrix transformation is power conservative and the power of the propagated Gaussian beam is equal to the launch power at the transmitter.

2.2 The Relay-to-Relay Channel Model

In Figure 2.1, the relay-to-relay channel refers to the optical path which starts from the fiber output at point ①. The beam is shaped and redirected to the receiving end via an optical thin lens at point ②. After propagating through a free-space path, another thin lens (at point③) collects and focuses the optical beam onto the fiber input which is placed at point ④. The channel is composed of successive optical elements, so $ABCD$ ray matrices have been used to readily characterize the transverse field distribution at each point in the channel. Using (2.1) the unit-energy transverse filed distribution at point ① is expressed as

$$\psi_1(r) = A_1 \exp(-\frac{1}{2}k\alpha_1 r^2) \tag{2.27}$$

where α_1 is the Gaussian beam parameter at point ① and A_1 is the power normalizing factor. Typically, the beam waist at point ② is considerably smaller than the transmitting lens diameter d_t, therefore $ABCD$ matrix transformation corresponding to the thin lens at the transmitter (point ②) and free space conserve the beam energy. Table 2.3 shows the corresponding $ABCD$ matrices of the optical elements used in the channel from point ① to point ④. By multiplying ray matrices of the optical ele-

Table 2.3: Ray matrices of optical elements in Figure 2.1

structure	Matrix
Line-of-sight free-space path with length L_t	$\begin{pmatrix} 1 & L_t \\ 0 & 1 \end{pmatrix}$
Thin lens with focal length f_t	$\begin{pmatrix} 1 & 0 \\ -\frac{1}{f_t} & 1 \end{pmatrix}$
Line-of-sight free-space path with length L	$\begin{pmatrix} 1 & L \\ 0 & 1 \end{pmatrix}$
Thin lens with focal length f_r	$\begin{pmatrix} 1 & 0 \\ -\frac{1}{f_r} & 1 \end{pmatrix}$
Line-of-sight free-space path with length L_r	$\begin{pmatrix} 1 & L_r \\ 0 & 1 \end{pmatrix}$

ments placed between point ① and point ③ in a reverse order, the $ABCD$ ray matrix of the beam wave at point ③ is obtained as

$$\begin{pmatrix} A_3 & B_3 \\ C_3 & D_3 \end{pmatrix} = \begin{pmatrix} 1 & L \\ 0 & 1 \end{pmatrix} \begin{pmatrix} 1 & 0 \\ -\frac{1}{f_t} & 1 \end{pmatrix} \begin{pmatrix} 1 & L_t \\ 0 & 1 \end{pmatrix} \tag{2.28}$$

therefore from (2.19), the transverse field distribution at point ③ is obtained as

$$\psi_3(r, z = L_3) = \frac{A_1}{p_3} e^{ikL_3} \exp\left(-\frac{1}{2} k\alpha_3 r^2\right) \tag{2.29}$$

where

$$L_3 = L_t + L \tag{2.30}$$

$$p_3 = A_3 + i\alpha_0 B_3 \tag{2.31}$$

$$\alpha_3 = \frac{\alpha_0 D_3 - iC_3}{A_3 + i\alpha_0 B_3} = \frac{2}{kW_3^2} + i\frac{1}{F_3} \tag{2.32}$$

W_3 and F_3 are the beam waist and phase front radius of curvature of the optical beam wave at point ③ respectively. By assuming a lossless optical lens and ignoring atmospheric absorption loss and turbulence effects (these effects have been taken into account separately), $\psi_3(r)$ retains a Gaussian profile with unit-energy, i.e.,

$$\left\langle |\psi_3(r)|^2 \right\rangle = 1. \tag{2.33}$$

Typically, in order to have a reliable alignment between the source and destination in FSO links, the optical beam waist at the receiving lens (point ③) must be sufficiently larger than the diameter of the receiving lens d_r ($W_3 \gg d_r$). The receiving lens is only able to collect the portion of the received field which is incident on the lens plane and the remaining parts of the propagating wave are discarded. This process clearly imposes a considerable power loss to the signal in line-of-sight FSO systems and is conventionally called *geometric loss* and can be calculated via (2.16).

In the new model proposed here for propgation loss, two factors are considered as the main contributors in power loss. One, η_l, is due to the finite size of the receiving lens which is considerably smaller than the received beam waist, so that a major part of the signal power is failed to be collected by the lens and dissipates in space. The other factor called *coupling efficiency*, η_c, results from the misalignment between the focused beam wave distribution at point ④ and the field distribution inside the fiber. Consequently the new model for propagation power loss is defined as

$$H_p = \eta_l \eta_c \tag{2.34}$$

In order to find η_l and η_c, first the transverse field distribution at point ④ must be determinded. The effective cross section area of the fiber is very small (on the order of micron), hence to gain a satisfactory coupling efficiency, the fiber is placed at the focal plane of the receiving lens, i.e. $L_r = f_r$, to guarantee the smallest spot size (beam waist) at point ④. Since there is no ABCD matrix which exactly models a *finite* thin lens, to find the transverse field profile in the back of focal plane of the lens, $\psi_4(r)$, the Fresnel diffraction integral is used [52],[60]

$$\psi_4(r) = \frac{\exp(i\frac{\beta}{2f_r}r^2)}{i\lambda f_r} \int_0^{\frac{d_r}{2}} \int_0^{2\pi} \psi_3(s) \exp\left(-i\frac{2\pi}{\lambda f_r} rscos\phi\right) sd\phi ds, \tag{2.35}$$

where r and s are the radial coordinates at the fiber input plane (point ④) and receiving lens plane (point ③) respectively. By substituting (2.29) in (2.35) and performing mathematical simplifications, the transverse field distribution at point ④ is obtained as

$$\psi_4(r) = \frac{-ik}{f_r}\frac{A_1}{p_3} \exp(ikL_4) \exp(\frac{ikr^2}{2f_r}) \int_0^{\frac{d_r}{2}} \exp(-\frac{1}{2}k\alpha_3 s^2) J_0(\frac{kr}{f_r}s) sds, \tag{2.36}$$

where $L_4 = L_3 + L_r = L_3 + f_r$. As shown in Fig. 2.2, in typical FSO systems, optical beam waist is on the order of a few meters which is considerably larger than the receiving lens diameter, on the order of a few centimeters. Hence, by reasonably approximating the exponential term in (2.36), $\exp(-\frac{1}{2}k\alpha_3 s^2) \approx 1$ for small s's, the beam profile at point ④ is approximated as

$$\psi_4(r) \approx \frac{-id_r}{2}\frac{A_1}{p_3}\exp(ikL_4)\exp(\frac{ikr^2}{2f_r})\frac{J_1\left(\frac{kd_r}{2f_r}r\right)}{r}, \tag{2.37}$$

where $J_1(\cdot)$ is the first order Bessel function of the first kind. For $d_r \to \infty$, $\psi_4(r)$ tends to a complete Gaussian beam profile whose characteristics can be simply found via $ABCD$ ray matrix. The thin lens transformation is power conservative that is the average power of $\psi_4(r)$ is equal to the average collected power by the receiving lens. The power loss imposed to the signal is due to the limited collecting area of the receiving lens and is defined as

$$\eta_l = \frac{\left\langle |\psi_4(r)|^2 \right\rangle}{\left\langle |\psi_3(r)|^2 \right\rangle} \tag{2.38}$$

where $\langle\cdot\rangle = \iint\limits_A \cdot\, rdrd\phi$ is the spatial average operator. From (2.33), the power loss η_l is obtained as

$$\eta_l = \left\langle |\psi_4(r)|^2 \right\rangle. \tag{2.39}$$

2.2.1 Signal projection onto Single-Mode Fiber (SMF)

In a typical application, the received optical beam must first be coupled into a single-mode fiber (SMF) to be processed by optical elements [51]. Projection of the optical field onto SMF imposes additional loss to the system. Furthermore, atmospheric turbulence degrades the spatial coherence of the propagating beam and limits the coupling efficiency [61]. However, the degrading effects of atmospheric turbulence on fiber coupling is not taken into account and the coupling efficiency arises just due to misalignment between the incident beam profile and SMF characteristic field distribution. The characteristic field distribution inside a SMF is independent of phase ϕ and is given by [16]

$$\psi_F(r) = \begin{cases} CJ_0(\gamma_1 r) & r \leq r_{co} \\ C\left(\frac{J_0(\gamma_1 r_{co})}{K_0(\gamma_2 r_{co})}\right) K_0(\gamma_2 r) & r_{co} \leq r, \end{cases} \tag{2.40}$$

where r_{co} is the radius of the fiber core, C is a constant which can be determined from the average power carried by the guided mode, and γ_1 and γ_2 are described as

$$\begin{aligned} \gamma_1 &= \sqrt{k^2 n_1^2 - \beta^2} \\ \gamma_2 &= \sqrt{\beta^2 - k^2 n_2^2} \end{aligned} \tag{2.41}$$

here n_1 and n_2 are the core and cladding refractive indices respectively ($n_1 > n_2$), and β is *propagation constant* inside the fiber which is also dependent on the mode of propagation. In single-mode fibers, n_1 and n_2 are chosen such that there is only one mode of propagation called *fundamental mode* of propagation or LP_{01} inside the fiber. In order to find the normalized field distribution corresponding to LP_{01} mode of propagation inside the SMF, the constant parameter C is determined such that the average power carried by this mode is unity, i.e.,

$$
\begin{aligned}
1 &= \iint \psi_F(r,\phi)\psi_F^*(r,\phi)rdrd\phi \\
&= 2\pi\int_0^\infty \psi_F(r)\psi_F^*(r)rdr \\
&= 2\pi C^2\left[\int_0^{r_{co}} J_0^2(\gamma_1 r)rdr + \left(\frac{J_0(\gamma_1 r_{co})}{K_0(\gamma_2 r_{co})}\right)^2\int_{r_{co}}^\infty K_0^2(\gamma_2 r)rdr\right] \\
\Rightarrow\ C &= \frac{1}{\sqrt{2\pi\left[\int_0^{r_{co}} J_0^2(\gamma_1 r)rdr + \left(\frac{J_0(\gamma_1 r_{co})}{K_0(\gamma_2 r_{co})}\right)^2\int_{r_{co}}^\infty K_0^2(\gamma_2 r)rdr\right]}}
\end{aligned}
\tag{2.42}
$$

where A_F is the fiber cross section area. The forward propagating optical field inside the fiber is described as

$$
\Psi_F(r,z,t) = \underbrace{u_F U_t(t)}_{\text{Field envelope}}\ \underbrace{\psi_F(r)}_{\text{Transverse field profile}}\ \underbrace{e^{-i(\omega t-\beta z)}}_{\text{Carrier}}
\tag{2.43}
$$

In this equation, u_F is the *mode weight factor* which is determined by the projection of received optical field onto the single-mode fiber

$$
\begin{aligned}
u_F &= \iint \psi_4(r)\psi_F^*(r,\phi)rdrd\phi \\
&= 2\pi\int_0^\infty \psi_4(r)\psi_F^*(r)rdr
\end{aligned}
\tag{2.44}
$$

By substituting $\psi_4(r)$ from (2.36) in (2.44), the mode weight is obtained as

$$u_F = \frac{-i2\pi k}{f_r}\frac{A_1}{p_3}\exp(ikL_4)\int\limits_0^{\infty}\int_0^{\frac{d_r}{2}} \exp(\frac{iks^2}{2f_r})\exp(-\frac{1}{2}k\alpha_3 r^2)J_0(\frac{krs}{f_r})\psi_F^*(s)rsdrds \tag{2.45}$$

Finally by approximating $\psi_4(r)$ with equation (2.37), the mode weight is approximated as

$$u_F \approx -i\pi d_r\frac{A_1}{p_3}\exp(ikL_4)\int\limits_0^{\infty}\exp(\frac{iks^2}{2f_r})J_1(\frac{kd_r}{2f_r}s)\psi_F^*(s)ds \tag{2.46}$$

The coupling efficiency is defined as the ratio of the average optical power coupled into the fiber to the average collected power in the receiving lens plane [61]

$$\eta_c = \frac{\langle|u_F\psi_F(r)|^2\rangle}{\langle|\psi_4(r)|^2\rangle} = \frac{\langle|u_F|^2\rangle\overbrace{\langle|\psi_F(r)|^2\rangle}^{=1}}{\langle|\psi_4(r)|^2\rangle} = \frac{|u_F|^2}{\langle|\psi_4(r)|^2\rangle} \tag{2.47}$$

by substituting (2.39) and (2.47) in (2.34), the new propagation power loss is described as

$$H_p = \eta_l\eta_c = \langle|\psi_4(r)|^2\rangle\frac{|u_F|^2}{\langle|\psi_4(r)|^2\rangle} = |u_F|^2 \tag{2.48}$$

By comparing the field envelope of the transmitted Gaussian wave, $U_t(t)$ in (1.1), with the field envelope of the propagating wave inside the fiber, $u_F U_t(t)$ in equation (2.43), the field envelope of the launch optical beam wave is multiplied by a complex constant u_F while propagating through the fiber-to-fiber optical channel. Therefore, the complex-valued geometric field loss in a fiber-to-fiber optical channel is introduced as

$$h_p = u_F \tag{2.49}$$

Table 2.4: The considered FSO system characteristics.

Parameter	Value
Transmitting lens diameter d_t	5 cm
Receiving lens diameter d_r	24 cm
Transmitting lens focal length f_t	20 cm
Receiving lens focal length f_r	58.2 cm
Distance between the fiber output plane and transmitting lens L_t	19.76 cm
Beam divergence angle θ	2.7 mrad
Beam waist at laser output W_1	4 μm
Phase front radius of curvature at laser output F_1	∞
Wavelength λ	1550 μm

Table 2.5: Single-Mode Fiber Specifications.

parameter	value
Core radius r_{co}	5 μm
Core refractive index n_1	1.5047
Cladding refractive index n_2	1.50

The comparison between the conventional and new geometric loss is illustrated via a numerical example. Table 2.4 shows typical parameters of a FSO communication system which is considered through the thesis for simulation purposes.

The distance L_t is adjusted so that the desired beamwidth ($W_3 \approx 3$ m) is achieved at the receiving lens plane. Also, the receiving lens focal length f_r is determined so that the best fiber coupling efficiency ($\eta_c \approx 82\%$) is obtained. Due to the diffractive properties of Gaussian beam wave propagation in free-space, the beamwidth broadens after propagating over long distances, hence, in order to adjust the desirable beam radius at the receiving lens plane, a converging lens is used as the transmitter side,

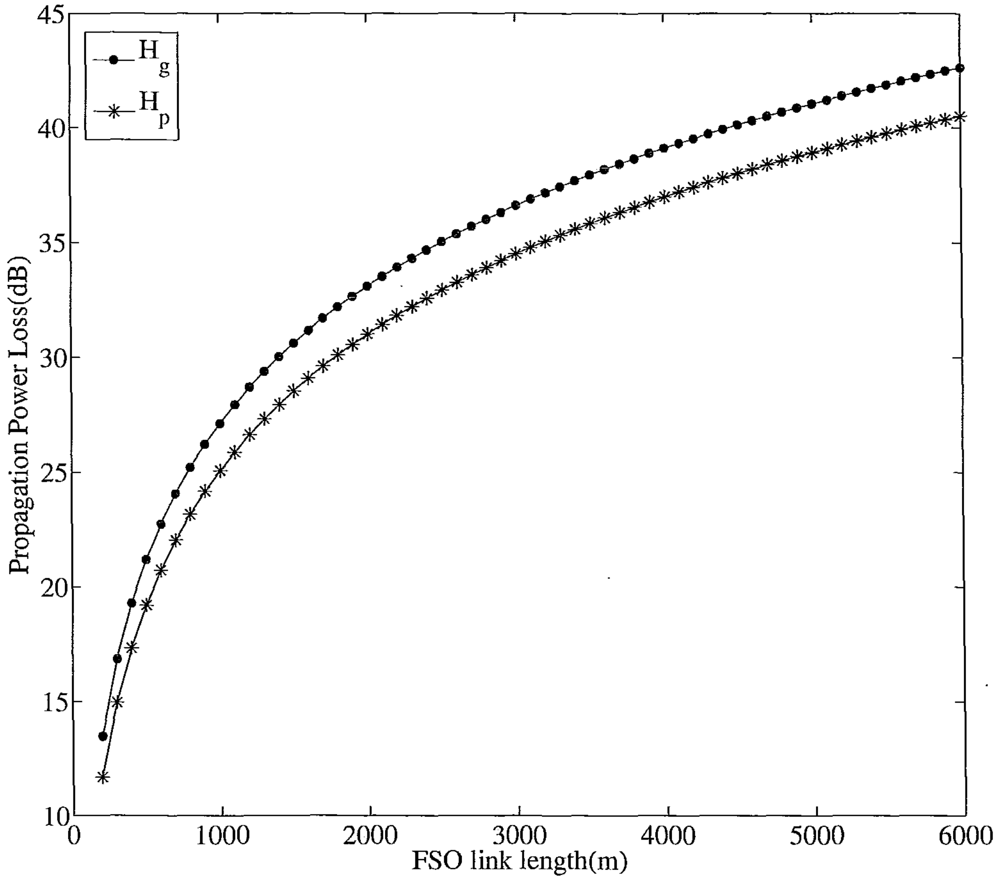

Figure 2.4: Comparison between the conventional and new geometric power loss.

point ②. Table 2.5 shows the single-mode fiber specifications which are commonly used in fiber optic systems.

In Figure 2.4, the conventional model for geometric power loss in (2.16) is compared with the new model given by (2.48). To calculate the values of u_F for different lengths (L), the approximated formula given in (2.46) is used. In Fig. 2.4, the comparison is made between these two models. For short distances where the beamwidth is a few times bigger than the receiving lens diameter, approximation of Gaussian

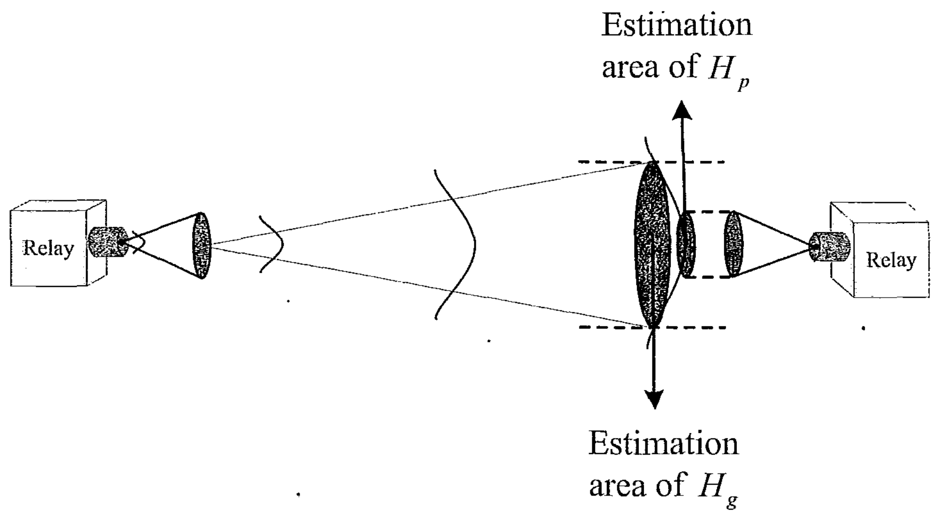

Figure 2.5: Estimation area for the conventional (H_g) and new propagation (H_p) loss.

beams by plane waves is not reliable and the beam power distribution is not uniform over the estimation area shown in Fig. 2.5. In this case, the new model for propagation loss provides more accurate approximation than the conventional model. As shown in Fig. 2.5, the area over which the Gaussian beam profile is approximated by a plane wave is much smaller for the new model than the conventional model. For long distances where the Gaussian beam profile can be approximated by a uniformly power-distributed plane wave, both the new and conventional models provide more reasonable approximations, however, the new model is more accurate. Table 2.6 provides more detailed specifications of a Gaussian wave propagating through an FSO link at two different distances from the source, $L_1 = 800$ m and $L_2 = 4000$ m.

Table 2.6: Propagating Beam Wave Specifications for Different Link Length.

Parameter	$L_1 = 800$ m	$L_2 = 4000$ m
Conventional geometric power loss H_g	3.07×10^{-3}	1.23×10^{-4}
New propagation power loss H_p	4.82×10^{-3}	1.99×10^{-4}
Propagation field loss h_p	$(-6.82 + i1.30) \times 10^{-2}$	$(-1.31 + i0.54) \times 10^{-2}$
Beamwidth at point ② W_2	2.44cm	2.44 cm
Beamwidth at point ③ W_3	1.1m	5.45 m
Coupling efficiency η_c	82.8%	82.5%

2.3 Noise Projection onto Single-Mode Fiber

Background noise is the dominant source of noise in FSO communication systems and is statistically modeled as an additive white Gaussian noise in time and space with zero mean and variance $\sigma_b^2 = N_0/2$ [26]. As expressed in (1.4), background noise is added to the signal at the receiving lens, therefore it is projected onto the fiber through the receiving lens. Let $\mathcal{N}_3(t, \vec{s})$ denote the Gaussian noise distribution at the receiving lens plane where $\vec{s}$ is the radial vector in the lens plane and t is the time scale. Since background noise distributions in time and space are independent, $\mathcal{N}_3(t, \vec{s})$ can be written as

$$\mathcal{N}_3(t, \vec{s}) = \mathcal{N}_3^t(t)\mathcal{N}_3^s(\vec{s}) \tag{2.50}$$

therefore by projection of $\mathcal{N}_3(t, \vec{s})$ onto fiber, temporal statistics of the noise remains unchanged. Based on the assumed statistical model for background light, the first moment of the noise spatial distribution at the lens plane (point ③ in Fig. 2.1) is defined as

$$\mu_{\mathcal{N}_3} = E\left[\mathcal{N}_3(t, \vec{s})\right] = E\left[\mathcal{N}_3^t(t)\right] = E\left[\mathcal{N}_3^t(\vec{s})\right] = 0 \tag{2.51}$$

where $E[\cdot]$ is the expectation operator. From definition, the correlation function can be written as

$$R_{\mathcal{N}_3}(t_1, t_2, \vec{s}_1, \vec{s}_2) = E\left[\mathcal{N}_3(t_1, \vec{s}_1)\mathcal{N}_3^*(t_2, \vec{s}_2)\right] = \frac{N_0}{2}\delta(t_2 - t_1)\delta(\vec{s}_2 - \vec{s}_1), \qquad (2.52)$$

which indicates spatially white noise distribution over the receiving lens plane. By using the Fresnel diffraction integral, the picture of the noise in the back of focal plane of the lens is obtained as

$$\mathcal{N}_4(t, \vec{r}) = \frac{-ik}{2\pi f_r} e^{ikf_r} \exp\left(\frac{ik|\vec{r}|^2}{2f_r}\right) \iint_{A_{\text{lens}}} \mathcal{N}_3(t, \vec{s}) \exp\left(-\frac{ik}{f_r}\vec{s}\cdot\vec{r}\right) d\vec{s}^{\,2}, \qquad (2.53)$$

where $\vec{s}$ and $\vec{r}$ are the radial vectors in the lens plane and fiber input plane (point ④) respectively, and dot operator $(\cdot)$ denotes the vectors inner product. The first moment of the noise picture $\mathcal{N}_4(t, \vec{r})$ is calculated as

$$\mu_{\mathcal{N}_4} = E\left[\mathcal{N}_4(t, \vec{r})\right] = \frac{-ik}{2\pi f_r} e^{ikf_r} \exp\left(\frac{ik|\vec{r}|^2}{2f_r}\right) \iint_{A_{\text{lens}}} \underbrace{E\left[\mathcal{N}_3(t, \vec{s})\right]}_{=0} \exp\left(-\frac{ik}{f_r}\vec{s}\cdot\vec{r}\right) d\vec{s}^{\,2} = 0 \qquad (2.54)$$

and spatial correlation is termed as

$$R_{\mathcal{N}_4}(t_1, t_2, \vec{r}_1, \vec{r}_2) = E\left[\mathcal{N}_4(t_1, \vec{r}_1)\mathcal{N}_4^*(t_2, \vec{r}_2)\right] = \left(\frac{k}{2\pi f_r}\right)^2 \exp\left(\frac{ik}{2f_r}(|\vec{r}_1|^2 - |\vec{r}_2|^2)\right) \qquad (2.55)$$

$$
\begin{aligned}
&\times \iint_{A_{\text{lens}}} \iint_{A_{\text{lens}}} \underbrace{E\left[\mathcal{N}_3(t_1, \vec{s}_1)\mathcal{N}_3^*(t_2, \vec{s}_2)\right]}_{\frac{N_0}{2}\delta(t_2-t_1)\delta(\vec{s}_2-\vec{s}_1)} \exp\left(-\frac{ik}{f_r}(\vec{s}_1 \cdot \vec{r}_1 - \vec{s}_2 \cdot \vec{r}_2)\right) d\vec{s}_1^{\,2} d\vec{s}_2^{\,2} \\
&= \frac{N_0}{2}\left(\frac{k}{2\pi f_r}\right)^2 \exp\left(\frac{ik}{2f_r}(|\vec{r}_1|^2 - |\vec{r}_2|^2)\right) \iint_{A_{\text{lens}}} \exp\left(-\frac{ik}{f_r}\vec{s}_1 \cdot (\vec{r}_1 - \vec{r}_2)\right) d\vec{s}_1^{\,2} \\
&= \frac{N_0}{2}\left(\frac{k}{2\pi f_r}\right)^2 \exp\left(\frac{ik}{2f_r}(|\vec{r}_1|^2 - |\vec{r}_2|^2)\right) \times (\lambda f_r)^2 \delta(\vec{r}_1 - \vec{r}_2) \\
&= \frac{N_0}{2}\delta(t_2 - t_1)\delta(\vec{r}_1 - \vec{r}_2)
\end{aligned}
$$

Therefore, the background noise after being focused in the back of focal plane of the lens has still zero mean and temporally and spatially white distribution, in other words, the thin lens conserves statistics of the incident field. Now, it must be shown that the projected noise onto the fiber has also the same statistics. From (2.44), the noise weight factor inside the fiber is defined as

$$
n_F = \iint_{A_{\text{fiber}}} \mathcal{N}_4(t, \vec{r})\psi_F^*(\vec{r}) d\vec{r}^{\,2} \tag{2.56}
$$

the mean and variance of n_F are calculated as

$$
\mu_{n_F} = E[n_F] = \iint_{A_{\text{fiber}}} \underbrace{E\left[\mathcal{N}_4(t, \vec{r})\right]}_{=0} \psi_F^*(\vec{r}) d\vec{r}^{\,2} = 0 \tag{2.57}
$$

$$
\begin{aligned}
R_{n_F} &= \sigma_{n_F}^2 = E\left[n_F n_F^*\right] = \iint_{A_{\text{fiber}}} \iint_{A_{\text{fiber}}} \underbrace{E\left[\mathcal{N}_4(t_1, \vec{r}_1)\mathcal{N}_4^*(t_2, \vec{r}_2)\right]}_{=\frac{N_0}{2}\delta(t_2-t_1)\delta(\vec{r}_2-\vec{r}_1)} \psi_F(\vec{r}_1)\psi_F^*(\vec{r}_2) d\vec{r}_1^{\,2} d\vec{r}_2^{\,2} \\
&= \frac{N_0}{2} \iint_{A_{\text{fiber}}} |\psi_F(\vec{r}_1)|^2 d\vec{r}_1^{\,2} = \frac{N_0}{2}\delta(t_2 - t_1)
\end{aligned} \tag{2.58}
$$

Equations (2.57) and (2.58) indicate that the statistics of the noise inside the single-mode fiber is the same as statistics of the background light incident on the receiving lens plane. Therefore, in the considered FSO system, the additive noise is modeled as a white Gaussian noise with zero mean and variance $\sigma_b^2 = N_0/2$.

2.4 Conclusion

In this chapter the optical channel has been modeled as an AWGN channel. Background illumination is considered as the major source of noise and is modeled as a zero-mean white Gaussian noise. Atmospheric attenuation, atmospheric turbulence induced-fading, and atmospheric propagation loss are the channel impairments considered in the channel model. In this thesis, the field envelope of the optical signal and noise are analyzed instead of optical power, therefore a complex model for atmospheric turbulence and propagation loss has been considered to completely describe the amplitude and phase variations of the propagating beam wave. A weak atmospheric turbulence condition is assumed whose log-amplitude and phase are normally distributed. Also a new method for calculating propagation loss is developed and numerically compared with the conventional model. Other than geometric spread of Gaussian beams, the coupling loss induced by the field projection onto a single-mode fiber has been considered in the new model. The proposed model provides more reliable approximation of propagation loss rather than the conventional model. This channel model is utilized to analyze performance of various FSO relaying techniques presented in the following chapters.

Chapter 3

Optical Amplify-and-Forward Relaying Technique

In this chapter, multihop FSO communications using all-optical components is studied. The distance dependence of atmospheric turbulence and path loss limits the total communicating distance in FSO systems. Using relaying techniques, FSO transmission is possible over longer distances. High-bandwidth, short-distance free-space optical tranceivers, e.g 10 Gbps TereScope TS-10GE, encourages replacement of electrical relaying processors by optical elements in all relays. In this chapter, it is shown that by using all-optical relaying techniques, longer communicating distances can be achieved in FSO systems while taking advantage of high-rate optical transmissions.

In an all-optical multihop FSO communication system at each relay data are processed in optical domain. An *optical amplify-and-forward* (OAF) relaying technique is developed and illustrated in Fig. 3.1. As shown in this figure, each relay is composed of all-optical elements such as an optical lens, optical fiber, and optical amplifier. At each relay, the background light is added to the received data field. Then the

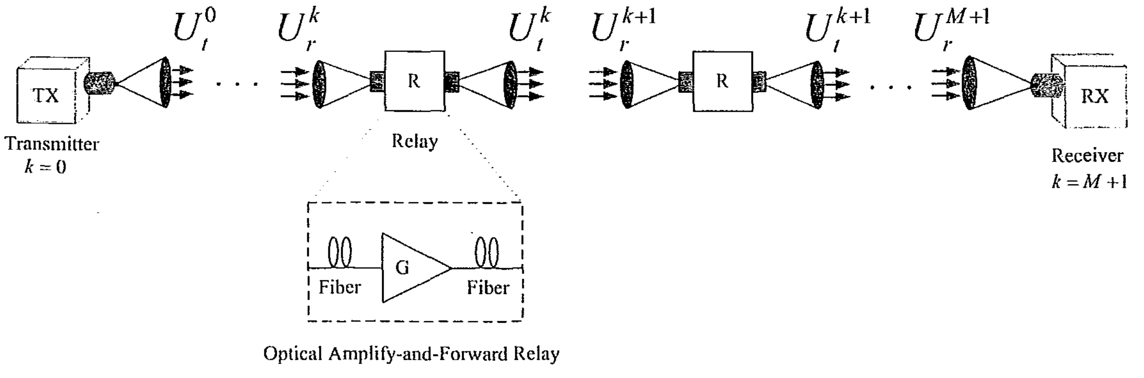

Figure 3.1: An All-Optical Multihop FSO Communication System

noisy data field is amplified by an optical amplifier and forwarded to the next relay or receiver. The optical link between each two consecutive relays is modeled as a fiber-to-fiber channel which has been completely characterized in Chapter 2.

3.1 OAF Relay Structure

In OAF relaying, there is at least one optical amplifier which amplifies the received optical field and retransmits it to the next relay. The structure of a typical OAF relay is simply shown in Fig. 3.2. As mentioned, there is a converging lens at the beginning of each relay that collects and focuses the incident light onto the back focal plane of the lens, a plane normal to the lens axis placed at distance f_{focal} behind the lens. The complex amplitude distribution of the field in the focal plane of the lens is the Fraunhofer diffraction pattern of the field incident on the lens. This field distribution is projected onto a single mode fiber (SMF). The SMF is connected to the optical

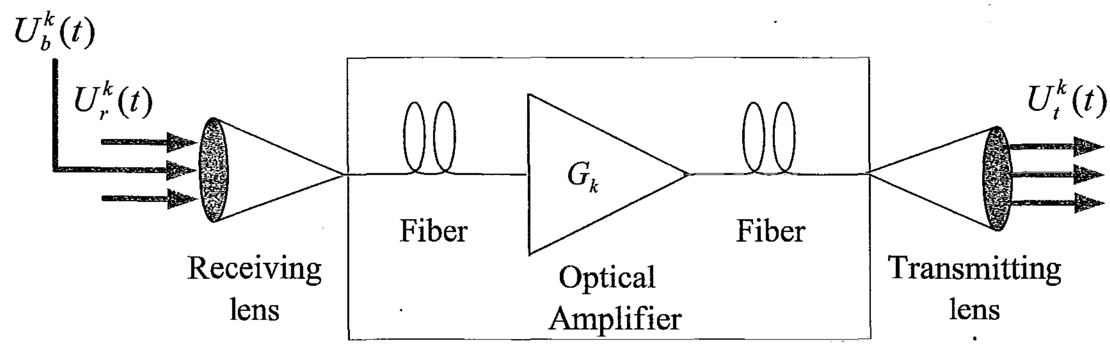

Figure 3.2: Structure of OAF Relays

amplifier that is mathematically modeled as

$$U_t^k(t) = \sqrt{G_k} U_r^k(t) + U_{ASE}^k(t), \tag{3.1}$$

where $U_r^k(t)$ and $U_t^k(t)$ are the received and transmitted signals at the k^{th} relay respectively, G_k is the k^{th} amplifier gain and $U_{ASE}^k(t)$ is the *amplified spontaneous emission* (ASE) noise of the k^{th}amplifier. The ASE noise is modeled as an additive zero-mean white Gaussian noise. The spectral density of ASE noise is given by [16]

$$N_0^k = \tilde{h} f (G_k - 1) n_{sp}, \tag{3.2}$$

where $\tilde{h}$ is Planck's constant, f is frequency, and n_{sp} is the amplifier spontaneous emission parameter. For the sake of simplicity, in what follows every field envelope $U(t)$ is referred simply by U.

As noted before, optical multihop AF systems developed so far [44, 27, 45] deployed an adjustable gain which compensates the fading effects of the preceding hop, regardless of the noise of that relay. Other than complexity in implementing adjustable gain unit at each relay, the relay output power does not satisfy eye safety limitations (IEC) on the maximum permissible average power. In this thesis a more practical model is provided for amplifier gain at each relay. The proposed model for the gain of k^{th} relay, G_k, is independent of random fading fluctuations and only compensates the propagation loss and atmospheric attenuation induced by the last hop (k^{th} hop). Also it is chosen so that the average power of the transmitted signal at the k^{th} relay $P_t^k = E\left[|U_t^k|^2\right]$ is constant and equal to the average launch power at the source $P_t = E\left[|U_t^0|^2\right]$ (U_t^0 is the transmitted field envelope at the source node), i.e.,

$$\cdots = E\left[|U_t^k|^2\right] = E\left[|U_t^{k-1}|^2\right] = \cdots = E\left[|U_t^0|^2\right] = P_t, \tag{3.3}$$

The transmitted signal at the k^{th} relay, U_t^k, can be expressed in terms of the transmitted signal at the $k-1^{th}$ relay, U_t^{k-1}, as

$$U_t^k = \sqrt{G_k}\underbrace{\left(h_k U_t^{k-1} + U_b^k\right)}_{U_r^k} + U_{ASE}^k \tag{3.4}$$

where h_k is the complex gain of the channel connecting the $k-1^{th}$ relay to the k^{th} relay, and U_b^k is the background noise collected at the receiving lens of the k^{th} relay. The data signal, atmospheric turbulence, background light and amplifier noise are all independent random processes, therefore, from (3.4)

$$E\left[|U_t^k|^2\right] = G_k E\left[|h_k|^2\right] E\left[|U_t^{k-1}|^2\right] + G_k E\left[|U_b|^2\right] + E\left[|U_{ASE}^k|^2\right] \tag{3.5}$$

As mentioned in Section 2.1.2, the lognormal fading is normalized so that the mean intensity of the propagating wave is conserved ($E[|\tau_k|^2] = 1$). Consequently, the average of the squared magnitude of the complex channel gain is

$$E\left[|h_k|^2\right] = E\left[|h_{a,k}h_{p,k}\tau_k|^2\right] = |h_{a,k}h_{p,k}|^2 = g_k \tag{3.6}$$

where $h_{a,k}$ and $h_{p,k}$ are the atmospheric attenuation and complex propagation loss of the k^{th} link respectively. Here, g_k is defined as the *channel loss* or *path loss* and includes both the effects of atmospheric attenuation and propagation loss. Using (3.3) and (3.6), Equation (3.5) can be simplified to

$$P_t = G_k g_k P_t + G_k P_b + P_{ASE}^k, \tag{3.7}$$

where $P_b = E\left[|U_b|^2\right] = \sigma_b^2$ is the average collected background light power at the receiving lens plane and assumed to be identical for all relays. $P_{ASE}^k = E\left[|U_{ASE}^k|^2\right]$ is the average ASE noise power of the k^{th} amplifier and from (3.2) is expressed as:

$$P_{ASE}^k = N_0^k \Delta f = \tilde{h} f (G_k - 1) n_{sp} \Delta f, \tag{3.8}$$

where Δf is the bandwidth of the optical amplifier. Plugging (3.8) into (3.7) and rearranging for G_k gives

$$G_k = \frac{P_t + P_A}{g_k P_t + P_b + P_A}, \tag{3.9}$$

where $P_A = \tilde{h} f n_{sp} \Delta f$. This way, it is guaranteed that the average output power of each relay satisfies the eye safety constraints. Typically, at optical frequencies, P_A is negligible with respect to P_t and P_b, so G_k can be approximated as

$$G_k \approx \frac{P_t}{g_k P_t + P_b} = \frac{1}{g_k + SNR_0^{-1}}, \tag{3.10}$$

here, $\mathrm{SNR}_0 = P_t/P_b$ is the average transmit signal-to-noise ratio (SNR) at the output of each relay. In the case of low background noise, $P_b \approx 0$, $G_k \approx g_k^{-1}$,that is , the amplifier totally compensates the effects of the channel loss. In the presence of high background noise, G_k is set to a smaller value so as to keep the average output power of each relay within the eye-safe region. Therefore, the channel power loss imposed on the data field is not compensated completely via amplification process and leads to additional degradation effects on the system performance. The amount of G_k offset from its noiseless value, g_k^{-1}, is dependent on both SNR_0 and g_k. From (3.6), it is clear that g_k is a function of the k^{th} hop distance (L_k). In the next section, by optimizing hop distances, an optimal relaying configuration is demonstrated for a given eye-safe SNR_0.

3.2 Optimal Relaying Configuration

In practice, relays are placed at fixed stations between the source and destination nodes. It is important to arrange relays such that the best system performance is achieved at the receiver. In this section, the performance of the system is analyzed in terms of the average optical signal-to-noise ratio (SNR) at the receiver. In the considered multihop system, relays are consecutively placed between the source ($k = 0$) and destination ($k = M + 1$) nodes. Figure 3.3 shows an optical Amplify-and-Forward multihop system with M relays, where OAF relays are typically shown as amplifiers.

The hop distance, L_k, which is the length of the link connecting the $(k-1)^{th}$ node to the k^{th} node varies for different relays. Let U_t^0 denotes the transmitted signal at

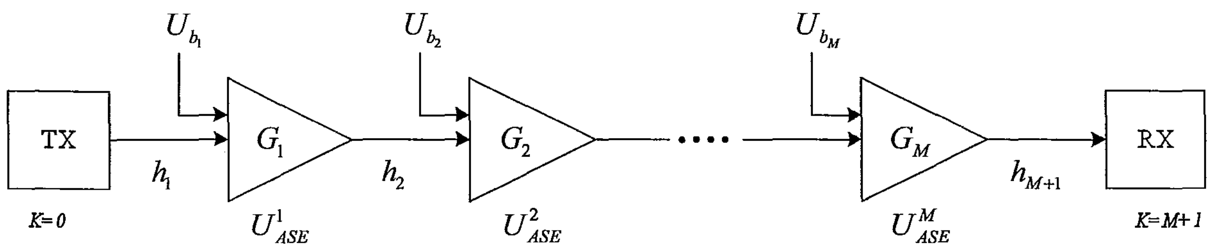

Figure 3.3: Optical Amplify-and-Foreward Multihop FSO Systems

the source, the received field at the j^{th} relay, $j = 1, 2...M+1$, is expressed as

$$\begin{aligned} U_r^j &= \left(\prod_{k=1}^{j-1} \sqrt{G_k} h_k\right) h_j U_t^0 + \left(U_b^j + \sum_{i=1}^{j-1} \prod_{k=i}^{j-1} \sqrt{G_k} h_{k+1} U_b^i\right) \\ &+ \left(h_j U_{ASE}^{j-1} + \sum_{i=1}^{j-2} \prod_{k=i+1}^{j-1} \sqrt{G_k} h_k h_j U_{ASE}^i\right) \end{aligned} \tag{3.11}$$

Assuming that the signal, background noise, ASE noise and fading are all independent, the average received power at the receiver ($j = M+1$) is

$$\begin{aligned} P_r^{M+1} &= \left(\prod_{k=1}^{M} G_k g_k\right) g_{M+1} P_t + \left(1 + \sum_{i=1}^{M} \prod_{k=i}^{M} G_k g_{k+1}\right) P_b \\ &+ \left(g_{M+1} P_{ASE}^M + \sum_{i=1}^{M-1} \prod_{k=i+1}^{M} G_k g_k g_{M+1} P_{ASE}^i\right), \end{aligned} \tag{3.12}$$

In order to analyze variations of the data signal power and noise during the channel, the average optical SNR is defined as the ratio of the average data signal power to the average total noise power. From (3.12), the average optical SNR at the receiver is obtained as

$$\mathrm{SNR}^{M+1} = \frac{\left(\prod_{k=1}^{M} G_k g_k\right) g_{M+1} P_t}{\left(1+\sum_{i=1}^{M}\prod_{k=i}^{M} G_k g_{k+1}\right) P_b + \left(g_{M+1} P_{ASE}^{M} + \sum_{i=1}^{M-1}\prod_{k=i+1}^{M} G_k g_k g_{M+1} P_{ASE}^{i}\right)}, \tag{3.13}$$

Typically amplifier spontaneous emission noise P_{ASE} is negligible with respect to data power P_t and background noise power P_b, therefore (3.13) can be approximated as

$$\mathrm{SNR}^{M+1} \approx \frac{\left(\prod_{k=1}^{M} G_k g_k\right) g_{M+1} P_t}{\left(1+\sum_{i=1}^{M}\prod_{k=i}^{M} G_k g_{k+1}\right) P_b}, \tag{3.14}$$

By substituting G_k from (3.10) into (3.14), and performing some simplifications, the average optical SNR is expressed as

$$\mathrm{SNR}^{M+1} = \frac{1}{\left[\prod_{k=1}^{M+1}(1+\mathrm{SNR}_k^{-1})\right]-1}, \tag{3.15}$$

where SNR_k is the average receive SNR at the receiver of a direct FSO link (where there is no relay between transmitter and receiver) with length L_k:

$$\mathrm{SNR_k} = g_k \mathrm{SNR_0} \tag{3.16}$$

The path loss g_k depends on the hop distance L_k. Now, SNR^{M+1} must be optimized with respect to L_k's. Consider the optimization problem

$$\begin{aligned} &\max_{L_k} \quad \mathrm{SNR^{M+1}} \\ &s.t \quad \sum_{k=1}^{M+1} L_k = L_T \end{aligned} \tag{3.17}$$

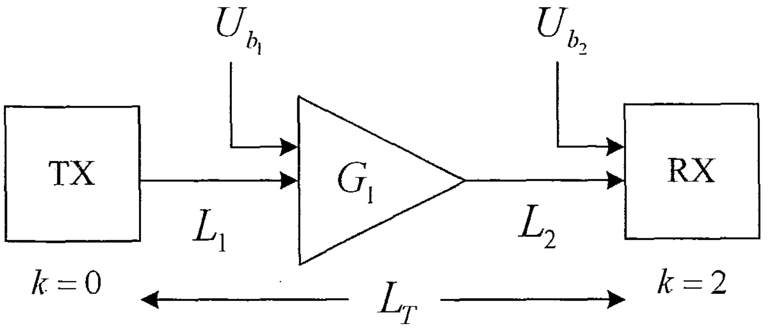

Figure 3.4: An OAF Multihop FSO System with M= 1

The above optimization problem can be converted to a simpler format. Let $h(x) = \frac{1}{f(x)}$, where $f(x) > 0$ and $f(x)$ and $h(x)$ are continuous functions whose first ($f'(x)$ and $h'(x)$) and second ($f''(x)$ and $h''(x)$) order derivatives are defined at x_0. In order to show that $h(x)$ is locally maximized at x_0, it is enough to prove $h'(x_0) = 0$ and $h''(x_0) < 0$ which is equivalent to

$$h'(x) = -\frac{f'(x)}{f^2(x)}\bigg|_{x_0} = 0 \Rightarrow f'(x_0) = 0 \tag{3.18}$$

$$h''(x) = -\frac{f''(x)}{f^2(x)}\bigg|_{x_0} < 0 \Rightarrow f''(x_0) > 0 \tag{3.19}$$

therefore, (3.17) is simplified to

$$\min_{L_k} \left[\prod_{k=1}^{M+1} (1 + g_k^{-1}\mathrm{SNR}_0^{-1})\right]$$
$$s.t \sum_{k=1}^{M+1} L_k = L_T \tag{3.20}$$

Consider an FSO system with a single OAF relay placed between the source and destination nodes as shown in Fig. 3.4.

The optimization problem in (3.20) for this system is defined as

$$\min_{L_k} \left[\prod_{k=1}^{2} (1 + g_k^{-1} \mathrm{SNR}_0^{-1}) \right] \quad s.t \quad L_1 + L_2 = L_T \tag{3.21}$$

By changing the variables $L_1 = x$ and $L_2 = L_T - x$, and some algebra, the optimization problem is simplified to

$$\min_{x} \left[g_1^{-1} + g_2^{-1} + \mathrm{SNR}_0^{-1} \mathrm{g}_1^{-1} \mathrm{g}_2^{-1} \right] \tag{3.22}$$

where g_1 and g_2 are the path loss of the first and second links. From (3.6), the path loss g_k is dependent on the hop distance L_k and is defined as

$$g_k = |h_{a,k} h_{p,k}|^2 = e^{-\sigma L_k} H_{p,k} \tag{3.23}$$

where $h_{a,k}$ and $h_{p,k}$ have been replaced by their definitions given in (2.6) and (2.48) from Chapter 2 and $H_{p,k} = |h_{p,k}|^2 = |u_F|^2$ is propagation power loss. From (2.46), propagation power loss can be approximated as

$$H_{p,k} \approx \kappa L_k^{-2}, \tag{3.24}$$

where κ is a constant. By plugging (3.24) into (3.23), the path loss is approximated as

$$g_k \approx \kappa e^{-\alpha L_k} L_k^{-2} \tag{3.25}$$

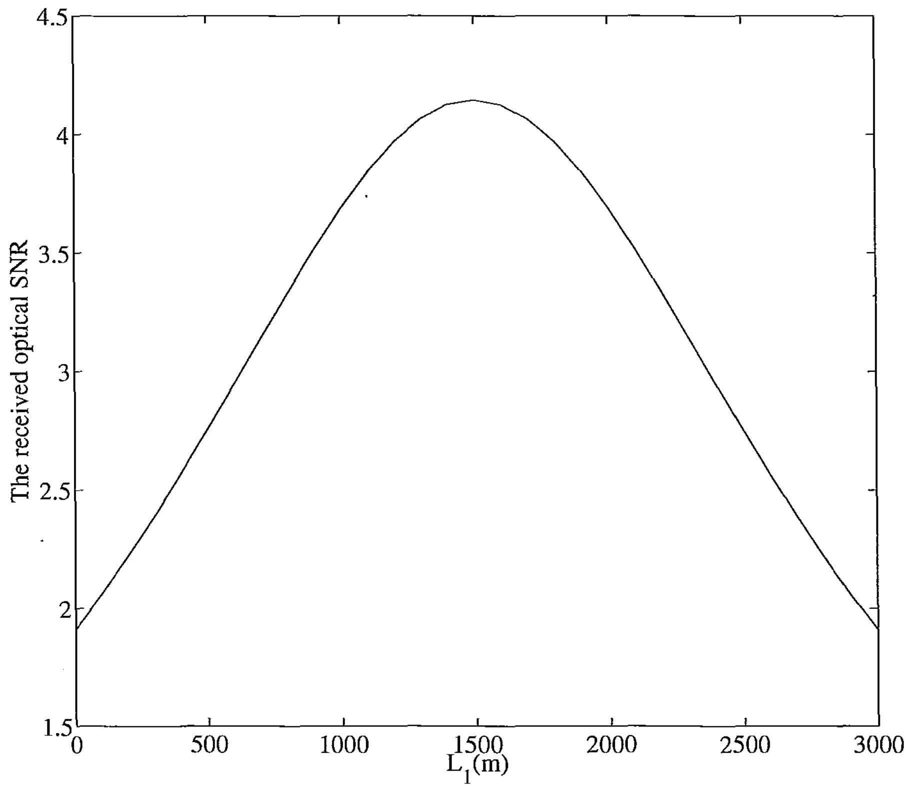

Figure 3.5: The received optical SNR of an OAF FSO system with $M = 1$ and $\mathrm{SNR}_0 = 37$ dB.

Using this approximation, (3.22) can be described in terms of L

$$\min_{x} \quad f_1(x) = \left[e^{\alpha x}x^2 + e^{\alpha(L_T - x)}(L_T - x)^2 + (\kappa \mathrm{SNR}_0)^{-1} \mathrm{e}^{\alpha \mathrm{L_T}} \mathrm{x}^2 (\mathrm{L_T} - \mathrm{x})^2\right] \tag{3.26}$$

It is shown in Appendix A that in typical FSO systems

$$\begin{aligned} f_1'(x)\Big|_{x=\frac{L_T}{2}} &= 0 \\ f_1''(x)\Big|_{x=\frac{L_T}{2}} &> 0, \end{aligned} \tag{3.27}$$

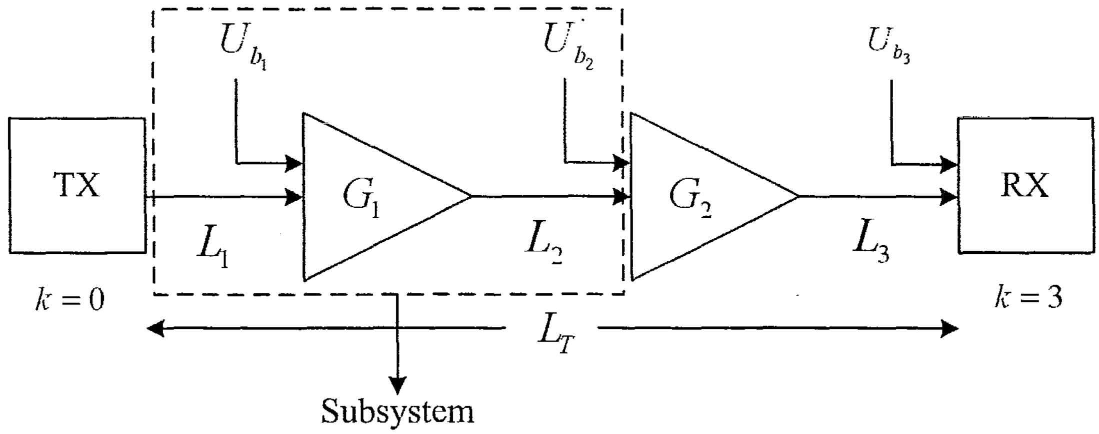

Figure 3.6: An OAF Multihop FSO System with M= 2 and $\mathrm{SNR}_0 = 37$ dB.

where $f_1'(x)$ and $f_1''(x)$ are the first and second order derivatives of function $f_1(x)$. These conditions are sufficient to prove that $f_1(x)$ has a local minimum at $L = L_T/2$ over the desired range of L_T. This range depends on α, κ, and SNR_0 and is obtained in Appendix A. In addition, it is also proved in Appendix A that $f_1''(x) > 0$, for all $0 < x < L_T$, that indicates the function $f_1(x)$ is convex for all $0 < x < L_T$ and $L = L_T/2$ is a global optimum point. Therefore, the average optical SNR received at the receiving lens of an OAF multihop system with $M = 1$, as shown in Fig. 3.4, is maximized when the OAF relay is placed at the middle of the link connecting the source and destination. Fig. 3.5 illustrates the optical SNR variations by the position of the OAF relay.

In this plot, the total communicating distance is $L_T = 3$ km which is inside the acceptable region of L_T for $\mathrm{SNR}_0 = 37$ dB. Obviously, SNR is maximized when $L_1 = L_2 = L_T/2 = 1.5$ km which means the best performance of the system is achieved for equally-spaced relaying configuration.

Similar calculations can be considered for an OAF system with $M = 2$ (Fig.3.6).

The optimization problem is defined as

$$\begin{aligned} \min_{L_k} \quad & [\textstyle\prod_{k=1}^{3}(1 + g_k^{-1}\mathrm{SNR}_0^{-1})] \\ s.t \quad & \textstyle\sum_{k=1}^{3} L_k = L_T, \end{aligned} \tag{3.28}$$

Here, L_1, L_2, and L_3 are the hop distances between the source and the first relay, the first relay and the second relay, and the second relay and the destination node respectively. By changing the variables $L_1 = x$, $L_2 = y$ and $L_3 = L_T - x - y$, the optimization problem is simplified to

$$\begin{aligned} \min_{x,y} \quad f_2(x, y) &= [(1 + (\kappa\mathrm{SNR}_0)^{-1}e^{\alpha x}x^2)(1 + (\kappa\mathrm{SNR}_0)^{-1}e^{\alpha y}y^2) \\ &\times \ (1 + (\kappa\mathrm{SNR}_0)^{-1}e^{\alpha(L_T-x-y)}(L_T - x - y)^2)] \end{aligned} \tag{3.29}$$

It can be easily shown that the Gradient vector of $f_2(x, y)$ is zero at $x = y = L_T/3$:

$$\nabla f_2(x, y) = \left.\begin{pmatrix} \frac{\partial f_2(x,y)}{\partial x} \\ \frac{\partial f_2(x,y)}{\partial y} \end{pmatrix}\right|_{x=\frac{L_T}{3}, y=\frac{L_T}{3}} = 0. \tag{3.30}$$

Proof of non-negativity of the Hessian matrix of $f_2(x, y)$ is laborious. However, the numerical simulation in Fig. 3.7 which is plotted at $\mathrm{SNR}_0 = 37$dB indicates that the maximum SNR is achieved at $L_1 = L_2 = L_3 = 1$ km.

$$H(f_2) = \begin{pmatrix} \frac{\partial^2 f_2(x,y)}{\partial x^2} & \frac{\partial^2 f_2(x,y)}{\partial x \partial y} \\ \frac{\partial^2 f_2(x,y)}{\partial y \partial x} & \frac{\partial^2 f_2(x,y)}{\partial y^2} \end{pmatrix} \succ 0. \tag{3.31}$$

For higher number of relays ($M > 1$), the mathematical induction proof is utilized

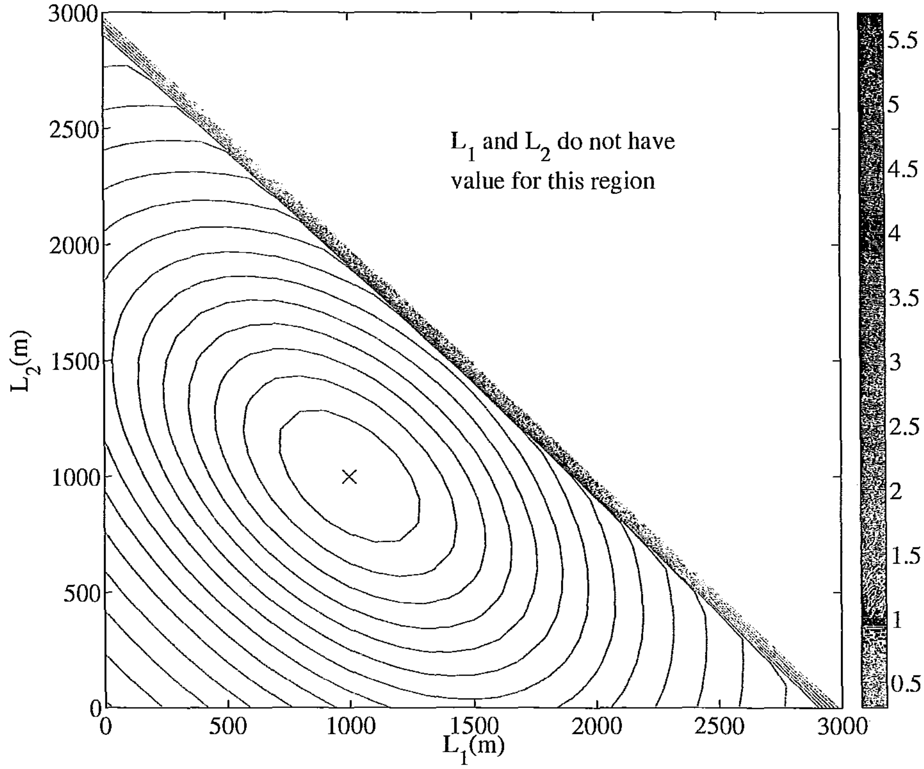

Figure 3.7: Optical SNR of an OAF FSO system with $M = 2$

to find the optimal relaying configuration. As the base case, it has been proved that for the OAF system with $M = 1$ (dual-hop system), equally-spaced relaying configuration provides the best performance at the receiver. Now, assume that for $M = p$, the equally-spaced relaying optimizes the problem (induction hypothesis). Based on induction proof, it should be proved that equidistance relaying configuration also maximizes the total average received SNR at the receiver when $M = p + 1$. In Fig. 3.8, p relays are equally spaced between the source and destination nodes with total distance of x. From (3.20), the modified optimization problem for this system is expressed as

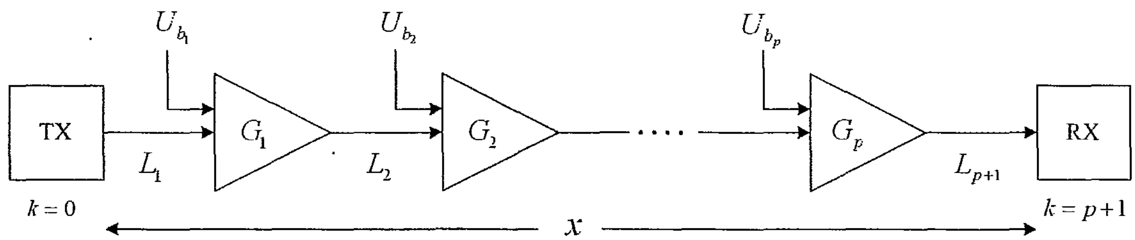

Figure 3.8: An OAF FSO system with $M = p$

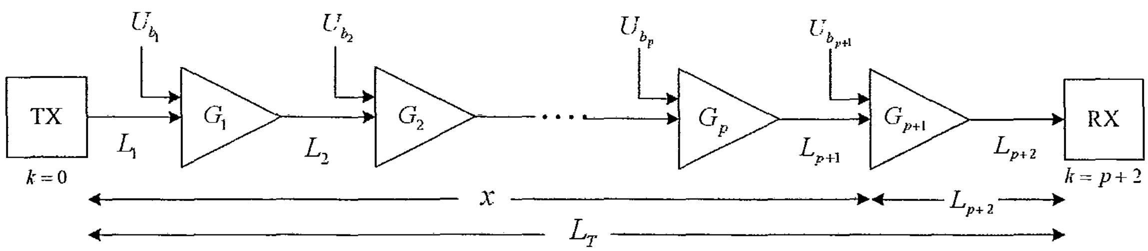

Figure 3.9: An OAF FSO system with $M = p + 1$

$$\begin{aligned} \min_{L_k} \quad & f_2(L_1, L_2, \cdots, L_{p+1}) = \left[\prod_{k=1}^{p+1}(1 + g_k^{-1}\mathrm{SNR}_0^{-1})\right] \\ s.t \quad & \textstyle\sum_{k=1}^{p+1} L_k = x. \end{aligned} \tag{3.32}$$

Based on the induction hypothesis, the function $f_p(L_1, L_2, \cdots, L_{p+1})$ is minimized for equal hop lengths, i.e. $L_1 = L_2 = \cdots = L_{p+1} = x/(p+1)$. From (3.25) and (3.32), the minimized $f_p^{min}(x)$ is obtained as

$$f_p^{min}(x) = \left[1 + (\kappa\mathrm{SNR}_0)^{-1} e^{\alpha\left(\frac{x}{p+1}\right)} \left(\frac{x}{p+1}\right)^2\right]^{p+1} \tag{3.33}$$

In Fig. 3.9, one more relay is added to the link plotted in Fig. 3.8 and provides a longer link with $p+1$ relays and total communicating distance of $L_T = x + L_{p+2}$. The optimization problem for the extended link can be expressed as

$$\begin{aligned} \min_{L_k} \quad & f_{p+1}(L_1, L_2, \cdots, L_{p+2}) = \left[\prod_{k=1}^{p+2}(1 + g_k^{-1}\mathrm{SNR}_0^{-1})\right] \\ & s.t \quad \sum_{k=1}^{p+2} L_k = L_T. \end{aligned} \tag{3.34}$$

The function $f_{p+1}(L_1, L_2, \cdots, L_{p+2})$ can be rewritten in terms of $f_p(L_1, L_2, \cdots, L_{p+1})$ as follows

$$\begin{aligned} f_{p+1}(L_1, L_2, \cdots, L_{p+2}) &= \left[\prod_{k=1}^{p+1}(1 + g_k^{-1}\mathrm{SNR}_0^{-1})\right](1 + g_{p+2}^{-1}\mathrm{SNR}_0^{-1}) \\ &= f_p(L_1, L_2, \cdots ; L_{p+1}) \times (1 + g_{p+2}^{-1}\mathrm{SNR}_0^{-1}) \end{aligned} \tag{3.35}$$

As shown in Fig. 3.9, the total communicating distance L_T is divided into x and L_{p+2}, therefore $L_{p+2} = L_T - x$. Furthermore, in order to optimize the SNR^{M+1} at the receiver of an OAF system with $M = p + 1$, the received SNR at the previous relay should maximize or equivalently $f_p(L_1, L_2, \cdots, L_{p+1})$ minimizes. By substituting $f_p^{min}(x)$ from (3.33) and utilizing (3.25), the optimization problem defined in (3.34) is simplified to

$$\begin{aligned} \min_x \quad f_{p+1}(x) &= \left[1 + (\kappa\mathrm{SNR}_0)^{-1} e^{\alpha\left(\frac{x}{p+1}\right)} \left(\frac{x}{p+1}\right)^2\right]^{p+1} \\ &\times \left[1 + (\kappa\mathrm{SNR}_0)^{-1} e^{\alpha(L_T - x)}(L_T - x)^2\right] \end{aligned} \tag{3.36}$$

In Appendix A, it is shown that for the equally-spaced relaying configuration $L_1 =$

$L_2 = \cdots = L_{p+1} = L_{p+2} = \frac{x}{(p+1)} = \frac{L_T}{(p+2)}$, the function $f_{p+1}(x)$ satisfies

$$\begin{aligned} f'_{p+1}(x) &= 0 \\ f''_{p+1}(x) &> 0. \end{aligned} \tag{3.37}$$

In other words, the equally-spaced relaying configuration provides the best performance at the receiver and all the previous relays for $M = p + 1$ and consequently the induction proof is complete. Therefore for any arbitrary number of relays M, equally-spaced relaying configuration, i.e.

$$L_1 = \cdots = L_{M+1} = \frac{L_T}{M+1}, \tag{3.38}$$

provides the maximum average SNR^{M+1} at the receiver over the desired region of L_T. This configuration is utilized in the next section to simulate various OAF systems.

3.3 Numerical Results and System Performance

In this section, the performance of different OAF multihop FSO communication systems with equally-spaced relaying configurations is analyzed. Monte-Carlo simulations are used to calculate the Bit-Error Rate (BER) of various systems. System performance is studied at two bit-rates (BR) 1.25 Gbps and 10 Gbps. The degrading effect of atmospheric turbulence on BER is analyzed at both bit-rates and compared with turbulence-free system performance.

The system under consideration operates at $\lambda = 1550$ nm in clear atmospheric conditions with attenuation coefficient of $\sigma = 0.43$ dB/km and weak turbulence with refractive index structure constant of $C_n^2 = 1 \times 10^{-14} \mathrm{m}^{-2/3}$ [52]. The background noise power spectral density is assumed to be $N_0 = 2 \times 10^{-15}$ W/Hz [1, 10, 62, 40] and the amplifier spontaneous emission parameter is $n_{sp} = 5$. The other characteristics of the system are as given in Chapter 2 via Tables 2.4 and 2.5.

3.3.1 Fixed Total Communicating Distance

Consider an FSO system where the source and destination nodes are placed at a total communicating distance of $L_T = 3$ km from each other. In this section, by placing a different number of relays (different M) between the source and destination nodes, the significant role of relaying technique in improving the performance of the system is justified. In order to simulate the FSO system in the slowly-varaying optical channel, 10^7 bits are transmitted per channel state. At both bit rates, 64 samples per bit interval are provided. In the presence of atmospheric turbulence, the BER is averaged over $N_\tau = 1000$ different fading conditions to reasonably simulate the slow-fading turbulence channel.

The overall performance of the system for different number of relays, M, placed between the source and destination is analyzed by plotting the BER versus the transmit signal-to-noise ratio $\mathrm{SNR}_0 = P_t/P_b$. Fig. 3.10 and 3.11 correspond to the systems working at bit rates BR= 1.25 Gbps and BR= 10 Gbps respectively. The turbulence fading effects are not considered in these plots. Table 3.3.1 summarizes the configuration, i.e., number of relays and hop distance, of the systems considered in these figures.

From (3.15) and (3.16), the overall performance of the system only depends on the average transmit SNR_0 and the relaying configurations, g_k. By comparing two figures,

Table 3.1: Different system configurations for $L_T = 3$ km.

Marker	hop Distance $L_k(km)$	Number of Relays M
—⊖—	3	0
—×—	1.5	1
—⊟—	1	2
—●—	0.75	3
—✳—	0.6	4
—▽—	0.5	5

it is justified that for a given SNR_0 the system performance for a specific configuration is nearly the same at both bit rates. Since the amount of background power is relative to the optical bandwidth or equivalently optical bit rate, the noise power collected at each relay (or receiver) in 10 Gbps system is more than the noise power in 1.25 Gbps system. Therefore, In order to gain relatively similar performance at both bit rates, almost 9dB more power must be transmitted by the system operating at 10 Gbps. The maximum average power transmitted by the state-of-the-art FSO transceivers is on the order of hundreds of miliwatts, SONAbeam$^{\mathrm{TM}}$ 1250-M transceiver sends 640mW power via four transmitters each sending 160 mW. By assuming $P_t = 640$ mW as the maximum available transmit power, the maximum achievable SNR_0 at BR$=$ 1.25 Gps and BR$=$ 10 Gbps is about 39 dB and 30 dB respectively.

In Fig. 3.11, the BER of the systems operating at BR$=$ 10 Gbps with $M = 0$ (direct transmission) and $M = 1$ relay have been plotted in the region $\mathrm{SNR}_0 > 30$ dB which is called *inaccessible power region.* The best performance of a FSO direct transmission inside the accessible power region is BER$= 1.26 \times 10^{-2}$. By employing one relay in the mid-way, the system achieves BER$= 7 \times 10^{-4}$ which is an order of magnitude improvement. But, in order to reduce the bit-error rate to BER$= 10^{-5}$ or

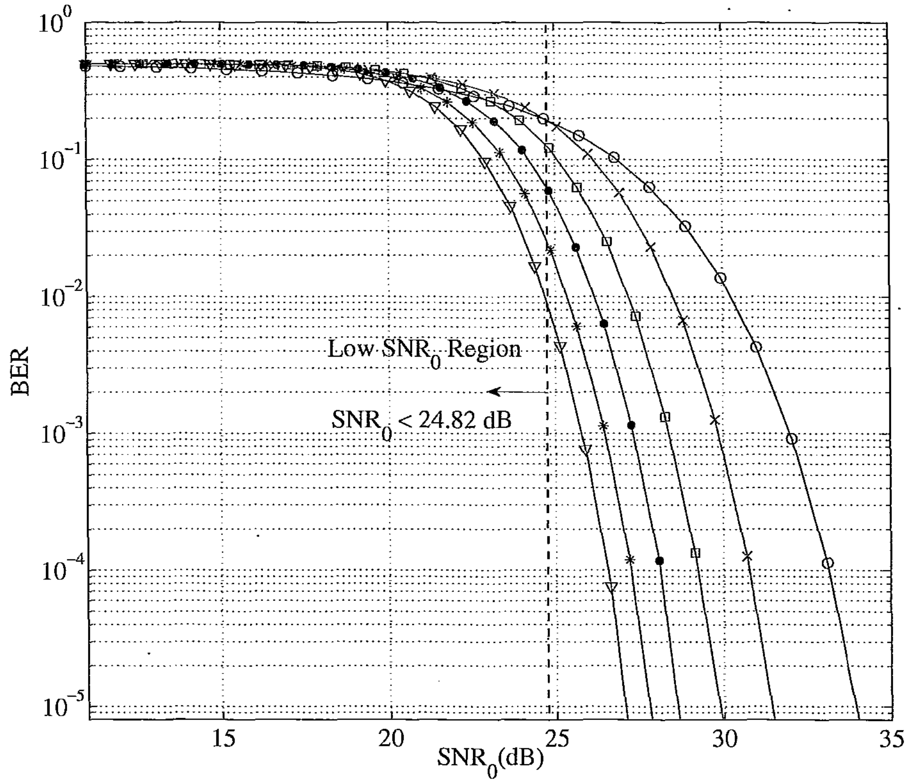

Figure 3.10: BER versus SNR_0 for a 3 km link and different number of relays M at BR= 1.25 Gbps, no fading effect is considered. (The plot descriptions are given in Table 3.1)

less, at least two relays must be placed between the transmitter and receiver ($M = 2$ or more).

At both bit rates, for a given SNR_0, by shortening the hop distances via inserting more relays between communicating nodes (increasing M), BER at the destination node decreases. As shown in Fig. 3.10 and 3.11, inserting one relay at the middle of a 3 km link gains 2.49 dB improvement at BER $= 10^{-5}$. Here the effects of atmospheric fading are not considered. Thus this gain mainly comes from the reduction in path loss achieved by shortening the hop distances.

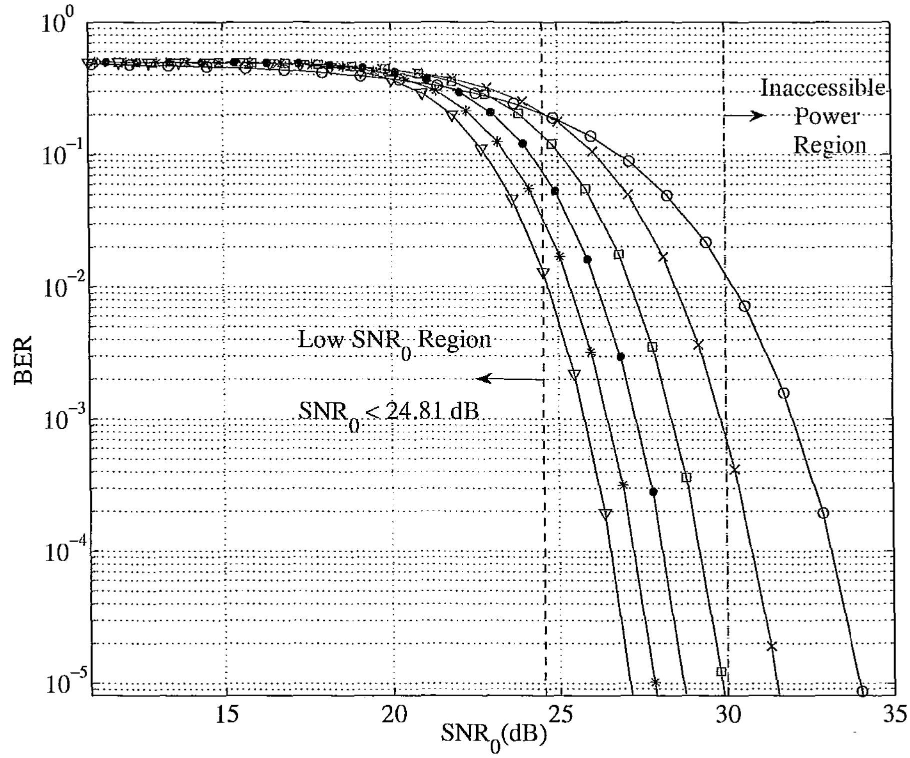

Figure 3.11: BER versus SNR_0 for a 3 km link and different number of relays M at BR= 10 Gbps, no fading effect is considered. (The plot descriptions are given in Table 3.1)

As the number of relays increases, the system performance improves slightly. Qualitatively, by increasing the number of relays from $M = 4$ to $M = 5$, at $\mathrm{BER} = 10^{-5}$, the system performance gains only 0.74 dB improvement which is considerably smaller than 2.49 dB, the gain achieved by inserting just one relay at the middle of a 3km link. This deficiency mainly occurs due to the presence of background light noise. As mentioned before, ambient illumination is collected at each relay. On the other hand, to keep the average output power of each relay inside the eye-safe region, the amplifier boosts up the signal with a relatively smaller gain. Therefore, the power

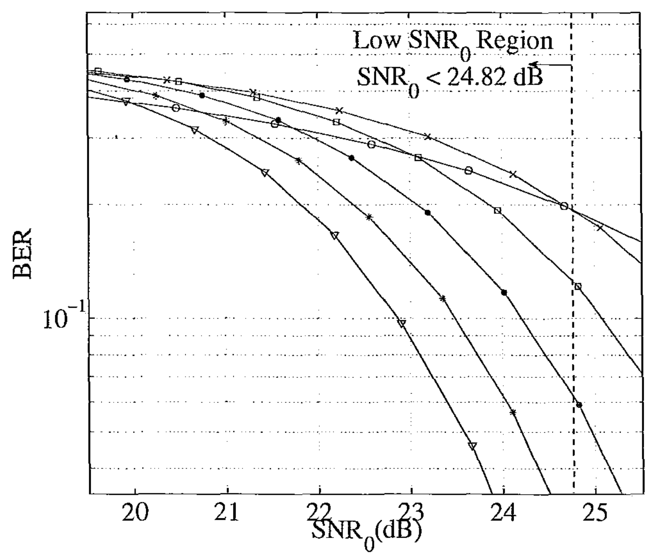

Figure 3.12: BER in low SNR$_0$ region for $L_T = 3$ km and BR= 1.25 Gbps. (The plot descriptions are given in Table 3.1)

of the attenuated signal over the previous hop can not be recovered completely via amplification process. The other reason is the small changes in hop distances and consequently smaller reductions in channel loss. As an example, by placing only one relay in the mid-way ($M = 0 \rightarrow M = 1$) the hop distance reduces by 50%, however by increasing $M = 4$ to $M = 5$, hop distances change from 0.6 km to 0.5 km which means only 16% reduction in L_k. Therefore, the path loss and therefore the system performance improvement is less than the former case.

In summary, by continuously increasing the number of relays, M, the system performance always improves but after some points the gain achieved by inserting one more relay is not significant enough to justify the additional costs of inserting the relay. Thus, depending on the required link coverage, BER, power budget, and financial feasibility, the number of relays is determined.

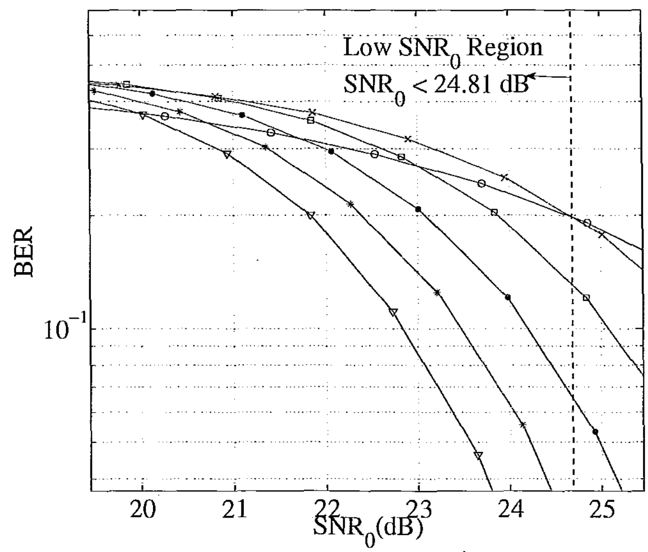

Figure 3.13: BER in low SNR_0 region for $L_T = 3$ km and BR= 10 Gbps. (The plot descriptions are given in Table 3.1)

For low SNR_0 the system performance is different. The low SNR_0 region corresponds to the region that for any SNR_0 bigger than this region, relaying technique always improves the system performance. As shown in Figs. 3.12 and 3.13, increasing the number of relays does not necessarily improve the system performance. For low SNR_0, the average transmit power is relatively small and background noise degradation effects are dominant. For this region, BER of a direct transmission (DT) FSO link, i.e. no relay is placed between the source and destination nodes $M = 0$, is less than BER of a multihop system with one relay at the middle of the link ($M = 1$). Although by dividing the link into two parts the channel loss reduces, the amount of collected background noise becomes nearly double. So, at the very low SNR_0, the system can not compensate the effects of background noise. By inserting more relays, hop distances decrease more and the channel loss reduces. Simultaneously, the amount of background noise increases. Compromising a trade off between channel loss reduction and background noise increase determines the minimum required transmit power for which relaying technique outperforms the DT transmission. The required transmit power decreases by the number of relays.

In order to understand the power variations in the low SNR_0 region, the received signal power P_r^k, the background noise power P_b^k, the ASE noise power P_{ASE}^k and SNR^k variations during the above mentioned 3 km link are analyzed. From (3.12) and (3.13), for equidistance relaying configuration, signal and noise powers received at the k^{th} relay are defined as

$$P_r^k = (gG)^{(k-1)} g P_t \tag{3.39}$$

$$P_b^k = \frac{(gG)^k - 1}{gG - 1} P_b \tag{3.40}$$

$$P_{ASE}^k = \frac{(gG)^{(k-1)} - 1}{gG - 1} g P_{ASE} \tag{3.41}$$

$$SNR^k = \frac{P_r^k}{P_b^k + P_{ASE}^k} \tag{3.42}$$

In Fig. 3.14, the signal and noise power variations during the 3 km link are illustrated for BR= 1.25Gbps. Each square denotes a relay placed during the link in an equally-spaced relaying configuration. The average transmit power is $P_t = 10$ mW ($\mathrm{SNR}_0 = 21$ dB < 24.82 dB) which is small enough to see the effects of background noise. The SNR of a DT link is denoted by a black-filled square. As expected, at this power, performance of a DT link is better than multihop systems with $M = 1$, 2, and 3 relays. In other words, in the low SNR_0 region ($\mathrm{SNR}_0 < 24.81$ dB), the relaying technique not only does not improve the system performance but degrades

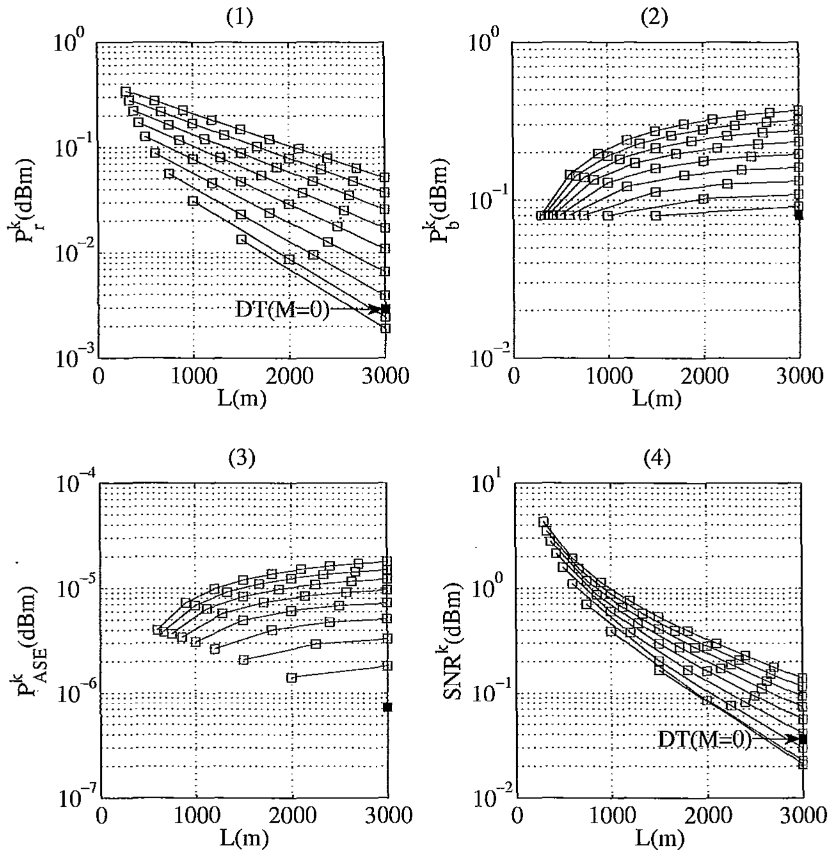

Figure 3.14: The signal and noise power variations during a 3 km link operating at BR= 1.25Gbps with different number of relays M, P_t = 10mW, and $N_0 = 2 \times 10^{-15}$W/Hz.

it. Whereas, for high SNR_0 ($\mathrm{SNR}_0 >$ 24.81 dB), the system performance always improves by employing relaying techniques. Fig. 3.15 shows the power and noise variations of the system for $P_t = 40$ mW ($\mathrm{SNR}_0 = 27$ dB> 24.81 dB) where the signal power is strong enough to combat the background noise. Obviously, by inserting more relays, SNR at the destination node increases gradually. From Figs. 3.12 and 3.13, the desired BER region ($10^{-6} - 10^{-5}$) is taken place at high SNR_0. Therefore for all desired SNR_0, relaying technique improves the system performance. The same

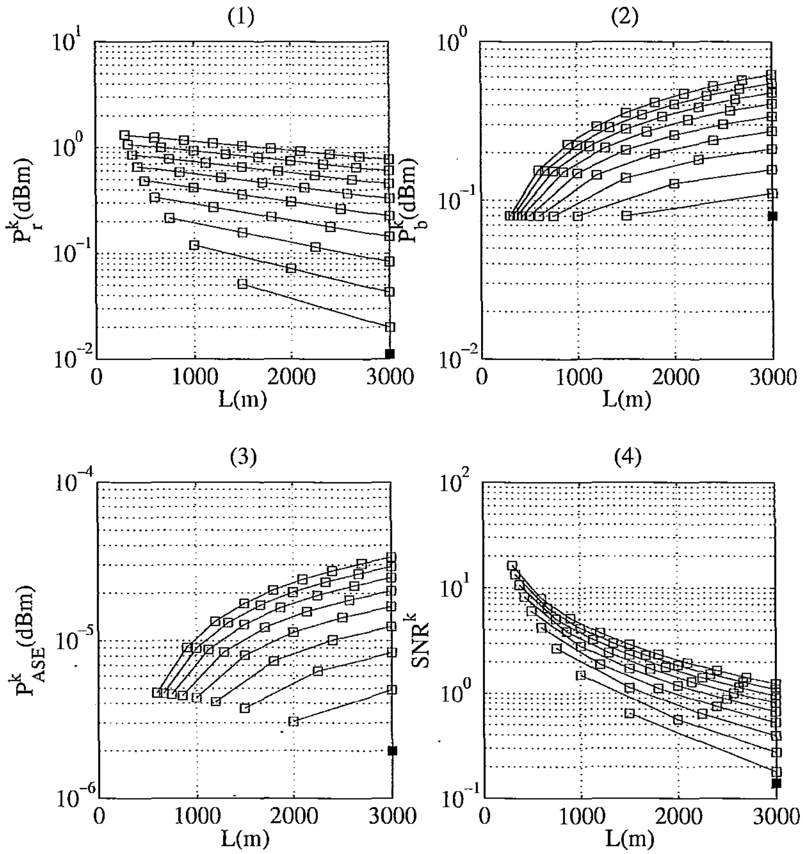

Figure 3.15: The signal and noise power variations during a 3 km link operating at BR= 1.25 Gbps with different number of relays M, $P_t = 40$ mW, and $N_0 = 2 \times 10^{-15}$ W/Hz.

senario is applied to BR= 10 Gbps systems, because its performance in terms of SNR_0 is similar to 1.25 Gbps systems.

Other than background noise, FSO systems strongly suffer from atmospheric turbulence. In order to realize the degrading effects of atmospheric fading on FSO systems performance, the BER of above mentioned systems, whose BER are plotted in Figs. 3.10 and 3.11, has been simulated in the presence of log-normal fading and shown in Figs. 3.16 and 3.17. The BER gets averaged over $N_\tau = 1000$ different fading

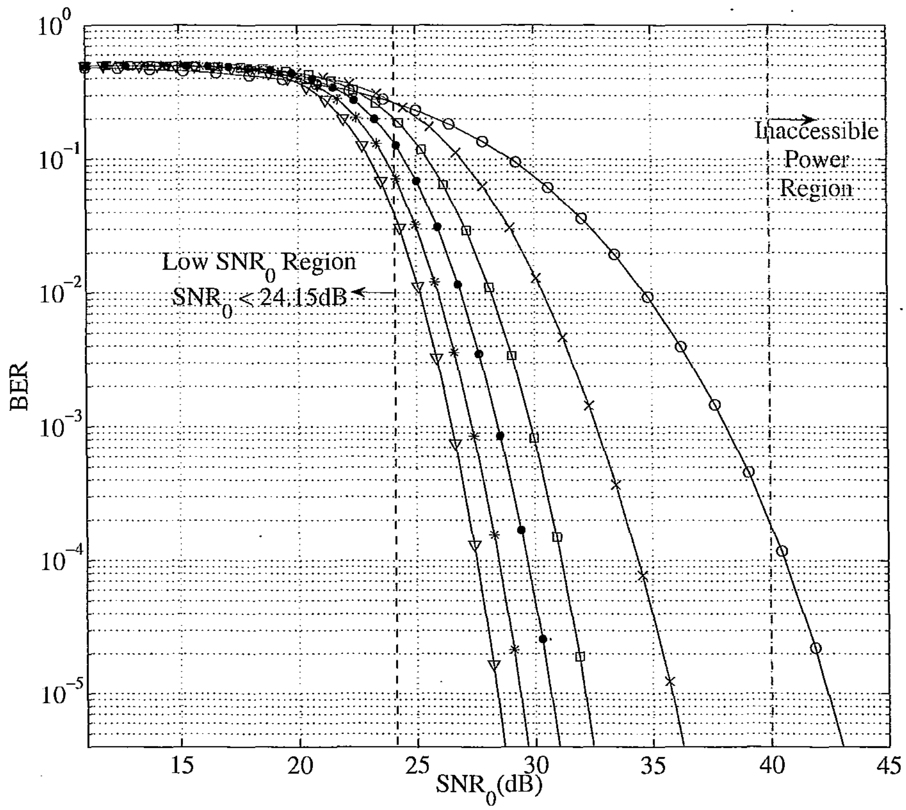

Figure 3.16: BER versus SNR_0, for $L_T = 3$ km, BR= 1.25 Gbps, and different number of relays M, with fading effects. (The plot descriptions are given in Table 3.1)

states and at each state 10^6 bits are sent.

Again, the system performance in terms of SNR_0 is similar at both bit rates. To achieve the same BER at both bit rates for a given BER= 10^{-5}, the transmitter needs to send about 9 dB more power when bit rate is 10 Gbps rather than 1.25 Gbps. By comparing Figs. 3.16 and 3.17 with Figs. 3.10 and 3.11, it turns out that to mitigate the effects of atmospheric fading on a DT link, respectively 8.45 dB and 8.49 dB more power must be transmitted at BR= 1.25 Gbps and BR= 10 Gbps. Table 3.2, summarizes the difference between the average transmit power of different systems

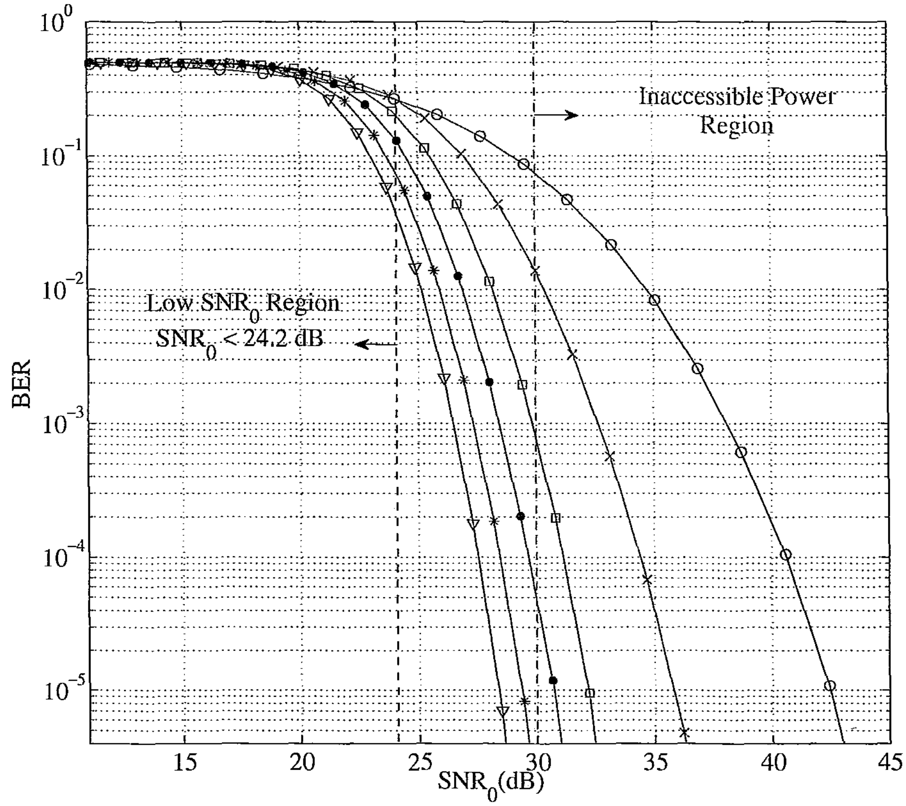

Figure 3.17: BER versus SNR_0, for $L_T = 3$ km, BR= 10 Gbps, and different number of relays M, with fading effects. (The plot descriptions are given in Table 3.1)

with and without fading effects when BER= 10^{-5}. According to Table 3.2, as M increases less average transmit power is required to mitigate the degrading effects of atmospheric turbulence. Because by increasing the number of relays the hop distances decrease and therefore the fading effects reduce. The atmospheric fading varies by weather conditions and is not dependent on the system bit rate. Therefore, for a given system configuration and weather condition, the BER performance of the system is similar for both bit rates.

The huge required average transmit power confines FSO communication systems

Table 3.2: The difference between the transmit power of different systems with and without fading when BER= 10^{-5}.

Number of relays	BER= 1.25 Gbps	BER= 10 Gbps
M	dB	dB
0	8.45	8.49
1	4.39	4.41
2	2.25	2.33
3	2.06	2.00
4	1.56	1.55
5	1.33	1.33

to short distances even at low bit rates. Illustratively, at BR= 1.25 Gbps whose corresponding plot is shown in Fig. 3.16, a direct FSO system requires 42.4 dB transmit SNR_0 to reach the 3 km distance from the source. As mentioned before, the maximum available transmit SNR_0 at BR= 1.25 Gbps is 39 dB, thus direct FSO transmission is not possible over 3 km link at BR= 1.25 Gbps. By placing only one relay in the mid-way, a 6.59 dB gain is achieved and the required transmit SNR_0 decreases to 35.8 dB which is inside the accessible power region. In other words, in order to communicate over a 3 km link at BR= 1.25 Gbps, at least one relay must be placed between the source and destination node.

For higher bit rates the situation is even worse. As noted, at BR= 10 Gbps, the maximum available SNR_0 is 30 dB. Clearly, without employing relaying techniques to guarantee BER= 10^{-5}, the direct FSO system needs to provide at least 42.4dB transmit SNR_0 which lays inside the inaccessible power region. The best performance of a direct 3 km FSO link at $\mathrm{SNR}_0 = 30$ dB is BER= 7.43×10^{-2}. In section 2.1.2, it is shown that atmospheric turbulence directly depends on the propagation distance. Therefore, the effects of atmospheric fading is considerably mitigated by reducing the hop distances. By placing one relay at the middle of the 3 km link, BER reduces to

Table 3.3: Power gains achieved by employing OAF relaying technique in a FSO communication system operating at BR= 1.25 Gbps for a particular BER= 10^{-5}.

Increasing the number of relays $M \rightarrow M+1$	Power gain without fading dB	Power gain with fading dB
$0 \rightarrow 1$	2.52	6.59
$1 \rightarrow 2$	1.55	3.68
$2 \rightarrow 3$	1.27	1.46
$3 \rightarrow 4$	0.82	1.32
$4 \rightarrow 5$	0.74	0.97

Table 3.4: Power gains achieved by employing OAF relaying technique in a FSO communication system operating at BR= 10 Gbps for a particular BER= 10^{-5}.

Increasing the number of relays $M \rightarrow M+1$	Power gain without fading dB	Power gain with fading dB
$0 \rightarrow 1$	2.49	6.63
$1 \rightarrow 2$	1.61	3.63
$2 \rightarrow 3$	1.15	1.47
$3 \rightarrow 4$	0.86	1.31
$4 \rightarrow 5$	0.74	0.96

1.39×10^{-2}. Although dividing the propagation path into two smaller parts reduces the fading effects, to achieve the particular performance BER= 10^{-5} at the receiver, the hop distances must be shortened more to overcome the degrading effects of channel loss and high background noise. From Fig. 3.17, in order to communicate over a 3 km FSO link with BER= 10^{-5} at least four equidistance OAF relays must be placed between the source and destination nodes.

Tables 3.3 and 3.4 respectively summarize the power gains achieved at a given BER= 10^{-5} by increasing the number of relays for bit rates BR= 1.25 Gbps and BR= 10 Gbps. By comparing the second and third columns of Table 3.3 or 3.4, the substantial role of relaying technique in mitigating the atmospheric fading effects is realized. When no fading is considered in the channel model, the relaying technique reduces the channel loss but increases the collected background noise. However, when fading effects are taken into account, shortening the hop distances other than the channel loss also decreases the degrading effects of fading. Therefore, in a slow fading channel , relaying technique obtains a considerable gain in the average transmit power. Illustratively, at BER= 10^{-5}, by using only one relay in the mid-way of a 3 km link operating at BR=1.25 Gbps, 6.59 dB improvement is achieved. But when fading is neglected, the system obtains only 2.52 dB gain, i.e. 4 dB less.

By increasing the number of relays, the difference between the power gains obtained in the absence and presence of atmospheric fading decreases. The reason can be simply explained via the distance dependence of atmospheric fading. At short distances (less than 1 km) fading effects are negligible so that by changing the hop distances from 0.6 km to 0.5 km, they do not change by much. Consequently, at very short hop distances relaying technique mainly decreases the channel loss to overcome the effects of background noise and its contribution in mitigating fading effects is negligible.

As shown in Figs. 3.16 and 3.17, at a given BER= 10^{-5} in order to communicate over a 3 km FSO link some of the considered OAF FSO systems require to send a huge amount of power which exceeds the maximum available average power. In other words, for some configurations it is not possible to reach the 3 km distance from the transmitter. In the following section, the maximum accessible distance from the transmitter for various relaying configurations is presented.

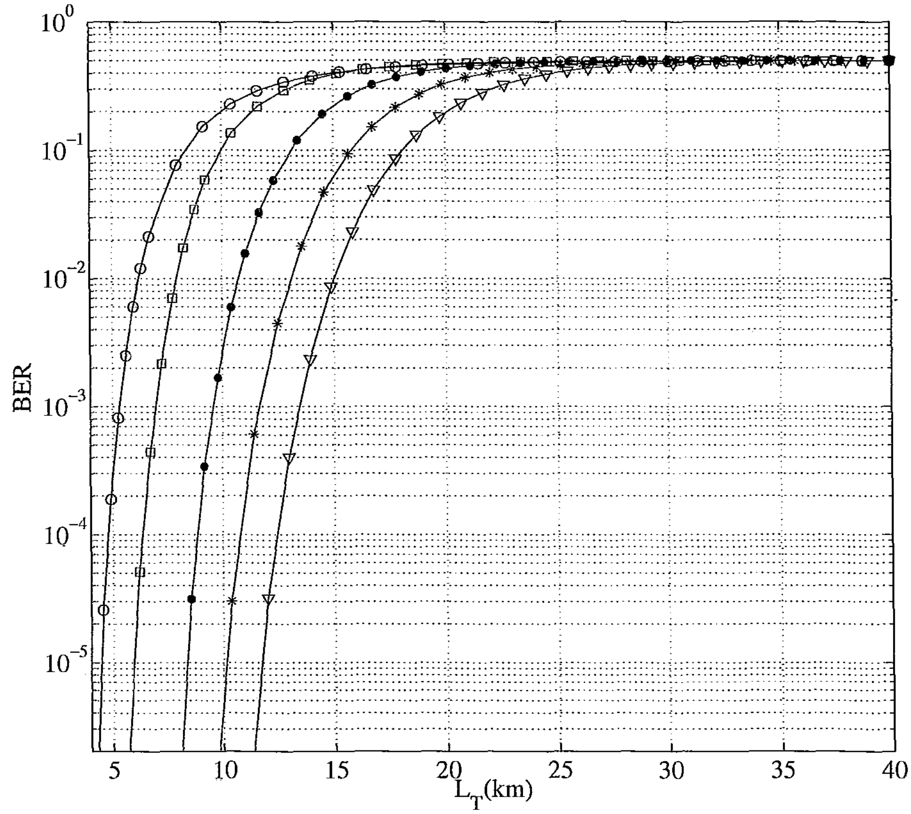

Figure 3.18: BER versus the total communicating distance, L_T (km), for different number of relays M, $P_t = 500$ mW, $N_0 = 2 \times 10^{-15}$ W/Hz, BR= 1.25 Gbps, without fading effects. (The plot descriptions are given in Table 3.5)

3.3.2 Maximum Accessible Communicating Distance

As mentioned in section 3.3.1, by increasing the number of relays during a fixed-length link, error performance of FSO systems improves and more power gain is achieved. However, the gain improvement reduces as the number of relays increases because the total accumulated background noise grows by the number of relays. For example, for a 3 km link, by increasing the number of relays from $M = 4$ to $M = 5$, at BER= 10^{-5}, the system performance gains only 0.74 dB improvement which from

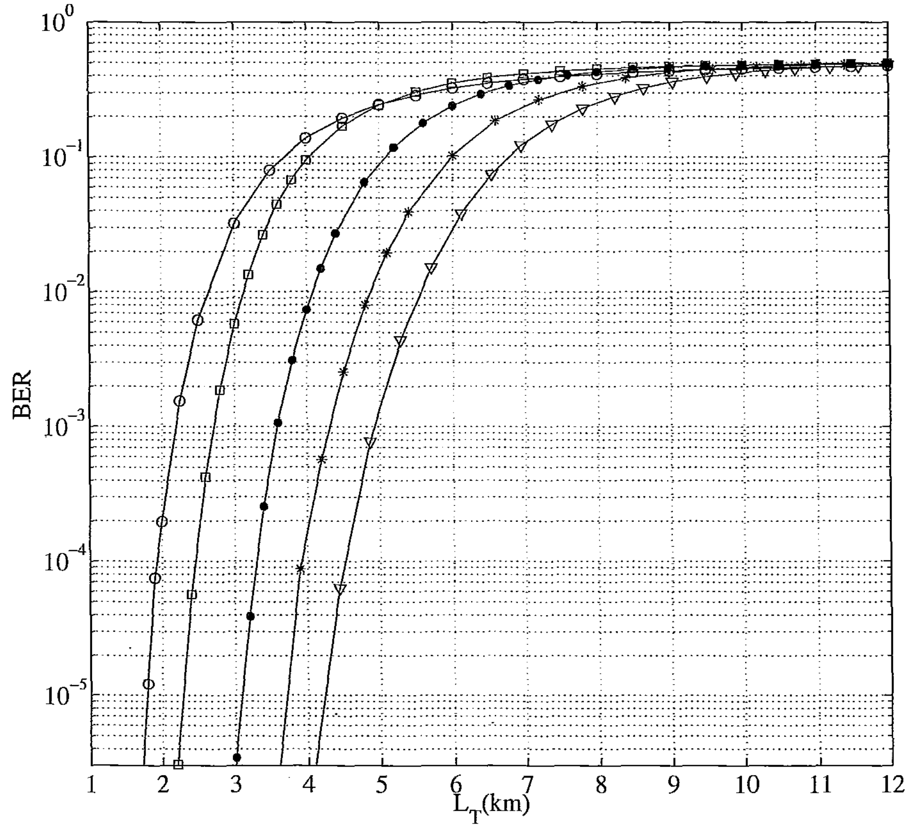

Figure 3.19: BER versus the total communicating distance, L_T (km), for different number of relays M, $P_t = 500$ mW, $N_0 = 2 \times 10^{-15}$ W/Hz, BR= 10 Gbps, without fading effects. (The plot descriptions are given in Table 3.5)

commercial point of view is not satisfactory. Therefore, there exists a compromise between the number of relays and average transmit power to achieve a particular BER. Since average transmit power is restricted to the eye-safe region, the number of relays determine the maximum total communicating distance at a given BER and average transmit power. Figs. 3.18 and 3.19 show the BER of different relaying systems with different number of relays, M, which are arranged in an equally-spaced relaying configuration. The average transmit power is assumed $P_t = 500$ mW which

Table 3.5: Maximum achievable communicating distance L_T(km) without fading effects

Marker	Number of Relays M	BR= 1.25Gbps L_T(km)	BR= 10Gbps L_T(km)
—⊖—	0	4.46	1.71
—⊟—	1	5.95	2.28
—●—	3	8.34	3.09
—✳—	5	10.15	3.71
—▽—	7	11.72	4.23

is inside the accessible power region. For each M, BER is simulated for different hop distances, i.e. for different total communicating lengths. The effects of atmospheric turbulence are not considered in these plots.

Table 3.5 provides the maximum achievable communicating distances at two bit rates BR= 1.25 Gbps and BR= 10 Gbps for different number of relays M so that BER= 10^{-5} is obtained at the receiver. As indicated in this table, the maximum accessible distance for a direct FSO system operating at BR= 1.25 Gbps is 4.46 km when the atmospheric fading is not considered. This distance for the system operating at BR= 10 Gbps is 1.71 km. The huge difference between these two systems is referred to the wider bandwidth of optical elements operating at higher bit rates and consequently collection of more additive white noise at the receiving apertures. By employing relaying technique ($M = 7$) FSO systems can access to 11.72 km and 4.23 km distances at BR= 1.25 Gbps and BR= 10 Gbps respectively which is a considerable accomplishment for short-range high-rate FSO communication systems. By increasing the number of relays (more than $M = 7$) even longer distances are accessible.

As demonstrated before, due to additive background noise, the performance of

Table 3.6: Distance improvements (ΔL_T) by increasing the number of relays.

Increasing the number of relays	BR= 1.25 Gbps		BR= 10 Gbps	
$M \rightarrow M+2$	ΔL_T(km)	ΔL_T^M(%)	ΔL_T(km)	ΔL_T^M(%)
$1 \rightarrow 3$	2.39	40.01	0.81	35.53
$3 \rightarrow 5$	1.81	21.71	0.62	20.06
$5 \rightarrow 7$	1.57	15.46	0.52	14.01

multihop FSO systems improves nonlinearly by increasing the number of relays. Table 3.6 shows the distance improvements (ΔL_T) by increasing the number of relays at a particular BER$= 10^{-5}$. ΔL_T^M is the percentage change in L_T and is defined as

$$\Delta L_T^M = \frac{\Delta L_T}{L_T^M} \times 100,$$

where L_T^M is the maximum accessible communicating distance when M relays are employed. ΔL_T^M represents the relative improvement in L_T and can be used as a metric to compare the system performance at two different bit rates.

From Table 3.6, by increasing the number of relays, ΔL_T decreases gradually. Qualitatively at BR= 1.25 Gbps, by increasing $M = 1$ to $M = 3$ the total communicating distance extends 2.39 km while by changing $M = 3$ to $M = 5$, it increases only by 1.81 km. This deficiency is due to background noise. By increasing the number of relays, more background noise is added to the signal. High noise power not only confines the amplifier gain at each relay but also degrades the signal-to-noise ratio and system performance at the receiver. The degrading effects of background noise are more dominant at higher bit rates. By comparing the relative distance improvements ΔL_T^M at two bit rates, it turns out that OAF relaying technique has better performance at lower bit rates.

Table 3.7: Maximum achievable communicating distance in the presence of fading at BER$= 10^{-5}$, $P_t = 500$ mW, and $N_0 = 2 \times 10^{-15}$ W/Hz .

Number of Relays	BR= 1.25 Gbps			BR= 10 Gbps		
M	L_T^F (km)	L_k^F(km)	$\Delta L_T^F(\%)$	L_T^F (km)	L_k^F (km)	$\Delta L_T^F(\%)$
0	2.32	2.32	47.98	1.33	1.33	22.22
1	3.48	1.74	41.51	1.87	0.94	17.98
3	5.12	1.28	38.61	2.59	0.65	16.18
5	6.32	1.05	37.78	3.16	0.53	14.82
7	7.29	0.91	37.73	3.63	0.45	14.18

To evaluates the effects of atmospheric turbulence on the maximum communicating distance, Figs. 3.20 and 3.21 are provided. In these figures, the BER of the system in the presence of log-normal fading versus the total communicating distance L_T is plotted. As mentioned before, atmospheric fading deteriorates system performance. The log-normal atmospheric fading decreases the maximum communicating distance of a direct FSO system operating at BR= 1.25 Gbps by 2.14 km when BER$= 10^{-5}$ and $P_t = 500$ mW. This value for the system working at BR= 10 Gbps is 380 m. Table 3.7 provides the maximum communicating distances for various OAF FSO systems with different number of relays for both bit rates. Also the relative distance reductions due to atmospheric fading, $\Delta L_T^F(\%)$, are presented for different systems. ΔL_T^F is defined as

$$\Delta L_T^F = \frac{|L_T - L_T^F|}{L_T} \times 100,$$

where L_T^F and L_T are respectively the maximum achievable distances over the FSO channels with and without fading effects. The length L_k^F in Table 3.7 indicates the hop distance when atmospheric fading is considered.

By comparing L_T^F and L_T given in Tables 3.5 and 3.7, it is obvious that atmospheric

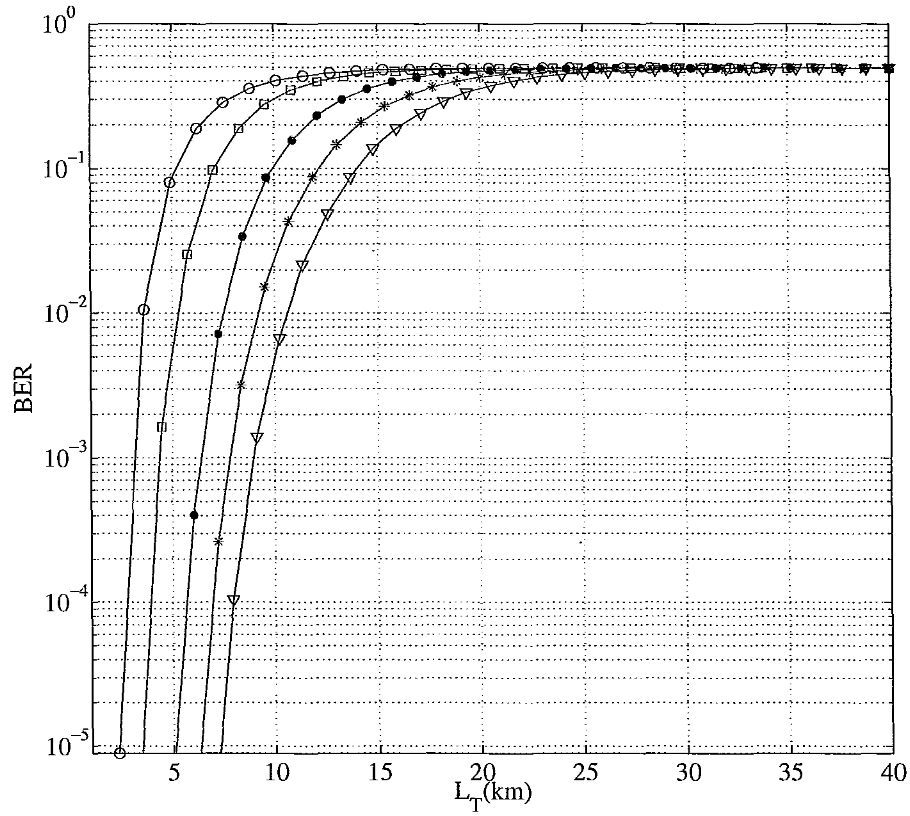

Figure 3.20: BER versus the total communicating distance, L_T (km), for different number of relays M, P_t = 500 mW, $N_0 = 2 \times 10^{-15}$ W/Hz, BR= 1.25 Gbps, with fading effects. (The plot descriptions are given in Table 3.5)

fading decreases the maximum accessible distance. By employing relaying technique the degrading effects of atmospheric fading are mitigated. In Table 3.7, the parameter ΔL_T^F expresses the relative decrement in the total communicating distance when atmospheric fading is considered and is introduced as a metric to readily analyze the fading effects on the BER of various systems with different number of relays and bit rates. From Table 3.7, by increasing the number of relays, the relative distance reduction ΔL_T^F decreases which means fading effects are compensated by using more

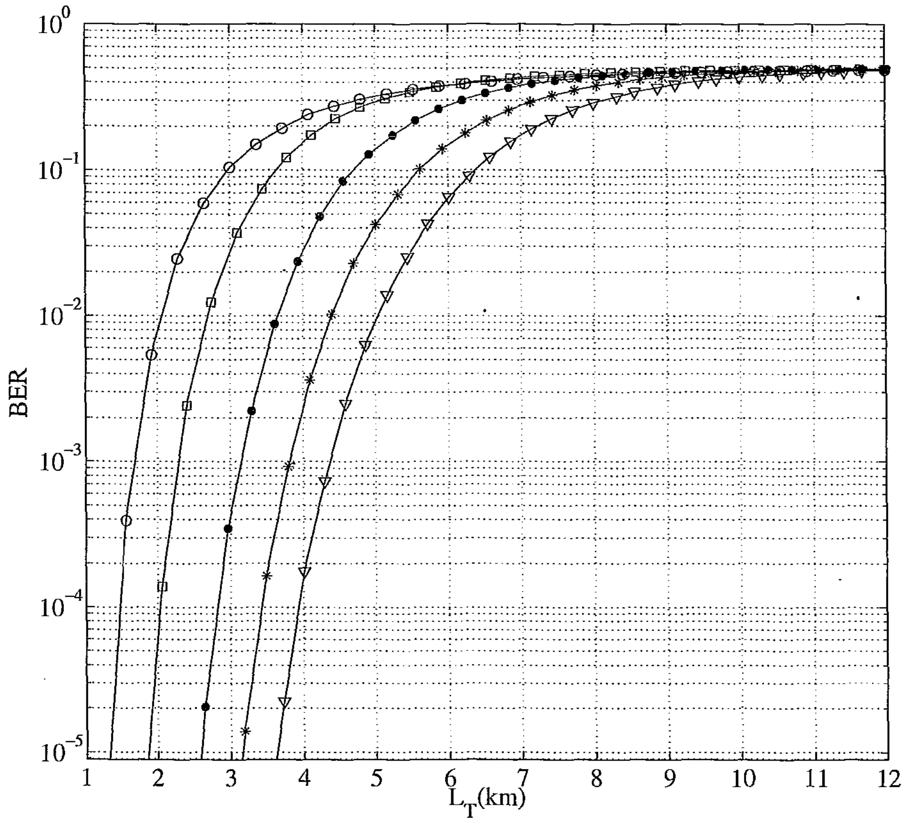

Figure 3.21: BER versus the total communicating distance, L_T (km), for different number of relays M, P_t = 500 mW, $N_0 = 2 \times 10^{-15}$ W/Hz, BR= 10 Gbps, with fading effects. (The plot descriptions are given in Table 3.5)

relays in multihop FSO systems. The reason is simply realized by considering hop distances (L_k^F). By increasing the number of relays, BER= 10^{-5} is obtained at shorter hop distances because the system needs to compensate the effects of more additive background noise by reducing the atmospheric fading and channel loss. At short hop distances (shorter than 1km) fading effects are negligible and therefore the relative distance reduction due to atmospheric fading decreases slightly. From Table 3.7, BER= 10^{-5} is achieved at shorter L_k^F in the systems working at BR= 10 Gbps

Table 3.8: Different system configurations for Figs.3.22 to 3.25 ($L_k = 1$ km)

Marker	Number of Relays M	Total Communicating Distance L_T
—○—	0	1 km
—×—	1	2 km
—□—	2	3 km
—●—	3	4 km
—∗—	4	5 km
—▽—	5	6 km

compared with BR= 1.25 Gbps. Therefore, atmospheric fading has less contribution in reducing the maximum accessible distance at higher bit rates and background noise is more dominant.

Distance-dependent atmospheric fading limits FSO systems to operate over short distances. Employing relaying techniques makes FSO communication possible over longer distances by shortening the hop distances and mitigating the effects of atmospheric fading. However, additive background noise still remains as a powerful factor in degrading the performance of multihop FSO systems. In the next section, the effects of background noise on BER of different systems are investigated at two bit rates.

3.3.3 Fixed hop Lengths

Optical AF multihop FSO systems strongly suffer from background noise. As demonstrated in sections 3.3.1 and 3.3.2, by increasing the number of relays more background noise is received at the receiver. On the other hand, to guarantee an eye-safe average output power at each relay, the amplification process does not completely compensate

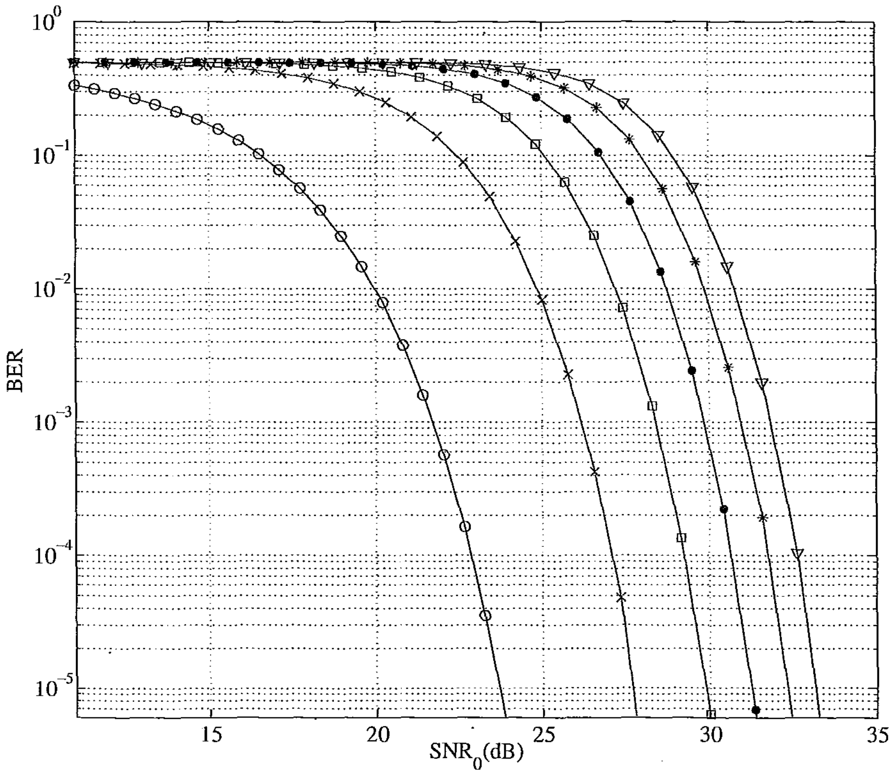

Figure 3.22: BER versus SNR_0 for the constant hop distance $L_k = 1$ km, bit rate BR= 1.25 Gbps, and different number of relays M without fading effects. (The plot descriptions are given in Table 3.8)

the attenuation of the previous channel. In Chapter 2, Equation (3.15) simply summarizes the amplification process and mathematically formulates the average optical SNR at the receiver.

From (3.15), by increasing the number of relays while the hop distance is fixed, i.e. constant g_k, the multiplication term in the denominator increases and totally the average received SNR decreases. By analyzing the system performance in terms of average received SNR, it is readily realized that because of background noise, extending the total communicating distance by consecutively adding more relays degrades the

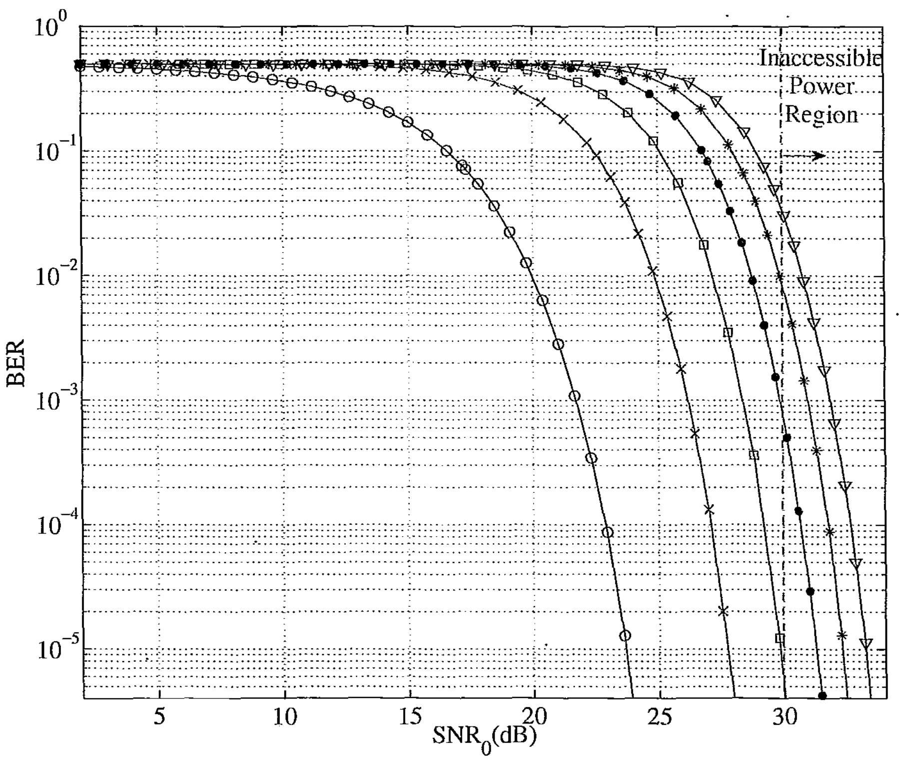

Figure 3.23: BER versus SNR_0 for the constant hop distance $L_k = 1$ km, bit rate BR= 10 Gbps, and different number of relays M without fading effects. (The plot descriptions are given in Table 3.8)

error performance. In order to analyze the degrading effects of background noise, an OAF FSO system with a fixed hop distance of $L_k = 1$ km is considered. The BER of the system for different number of relays and therefore different total communicating distances are plotted in Figs. 3.22 and 3.23. The effects of atmospheric turbulence are not considered in these plots. Table 3.8 summarizes the configuration of the systems considered in these figures.

At a given SNR_0, both systems have similar performance at BER= 10^{-5}. A 2 km link with an OAF relay in the mid-way consists of two 1 km DT links. From (3.12),

Table 3.9: Average transmit SNR_0(dB) to obtain BER= 10^{-5}.

Number of relays	BR= 1.25 Gbps		BR= 10 Gbps	
M	W/O Fading	With Fading	W/O Fading	With Fading
0	14.68	16.47	23.67	25.48
1	18.64	20.84	27.75	29.90
2	20.85	23.11	29.85	32.17
3	22.21	25.32	31.29	34.36
4	23.27	26.86	32.32	35.91
5	24.12	27.96	33.23	37.01

the background power at the receiver of the 2 km link is nearly twice the background power at the receiver of the 1 km DT link. At BER= 10^{-5}, the transmitter needs to send 3.97 dB more power to guarantee the particular BER= 10^{-5} at the receiver. By increasing the average transmit power, the FSO system overcomes the degrading effects of accumulated background noise and provides longer-range FSO links. However, the total communicating distance in OAF FSO systems is restricted because the average transmit power is limited. From Fig. 3.23, the maximum communicating distance for the system operating at BR= 10 Gbps is 3 km when fading effects are not considered. To reach longer distances, the system needs to send more power which lays inside the inaccessible power region.

Figures 3.24 and 3.25 are provided to show the degrading effects of atmospheric fading on the system performance. To mitigate the effects of atmospheric turbulence, the transmitter must launch additional power. Table 3.9 summarizes the required average transmit SNR_0 (dB) so as to obtain BER= 10^{-5} at the receiver.

In order to compare the atmospheric fading effects on the BER of various systems, the amount of increase in the average transmit signal-to-noise ratio, ΔSNR_0, is defined

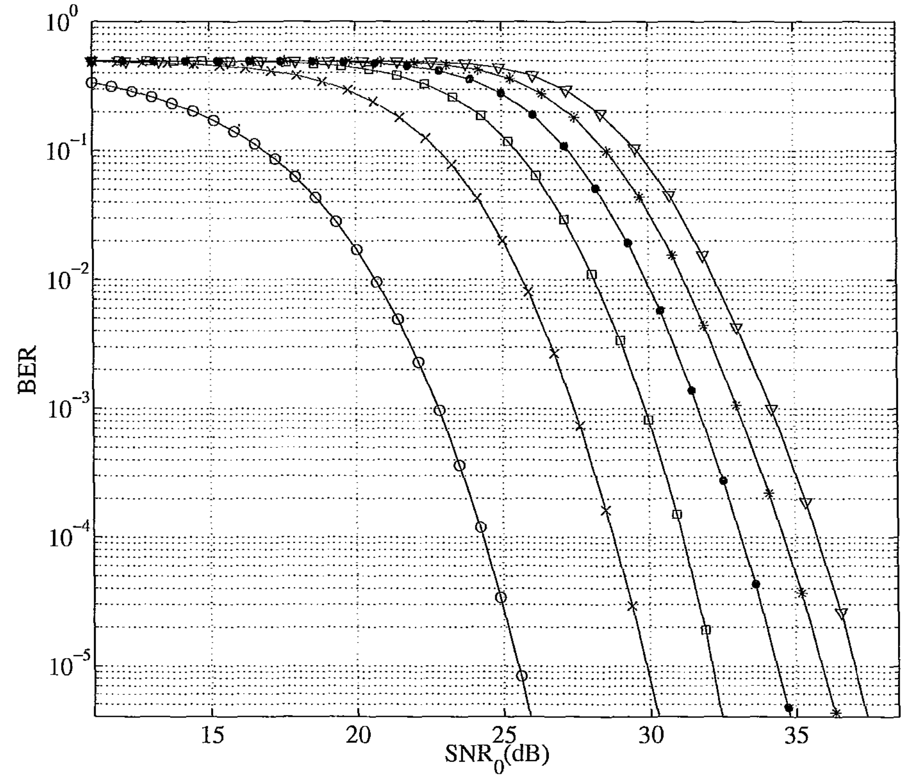

Figure 3.24: BER versus SNR_0 for the constant hop distance $L_k = 1$ km, bit rate BR= 1.25 Gbps, and different number of relays M considering fading effects. (The plot descriptions are given in Table 3.8)

as

$$\Delta SNR_0 = SNR_0^F - SNR_0,$$

where SNR_0^F and SNR_0 are respectively the average transmit signal-to-noise ratio sent over the channels with and without fading effects to hit the target BER= 10^{-5}. The variable ΔSNR_0 for two bit rates and different number of relays are given in Table 3.10. From this table, atmospheric fading imposes almost equal additional transmit power to the system at both bit rates. By increasing the number of relays, the required

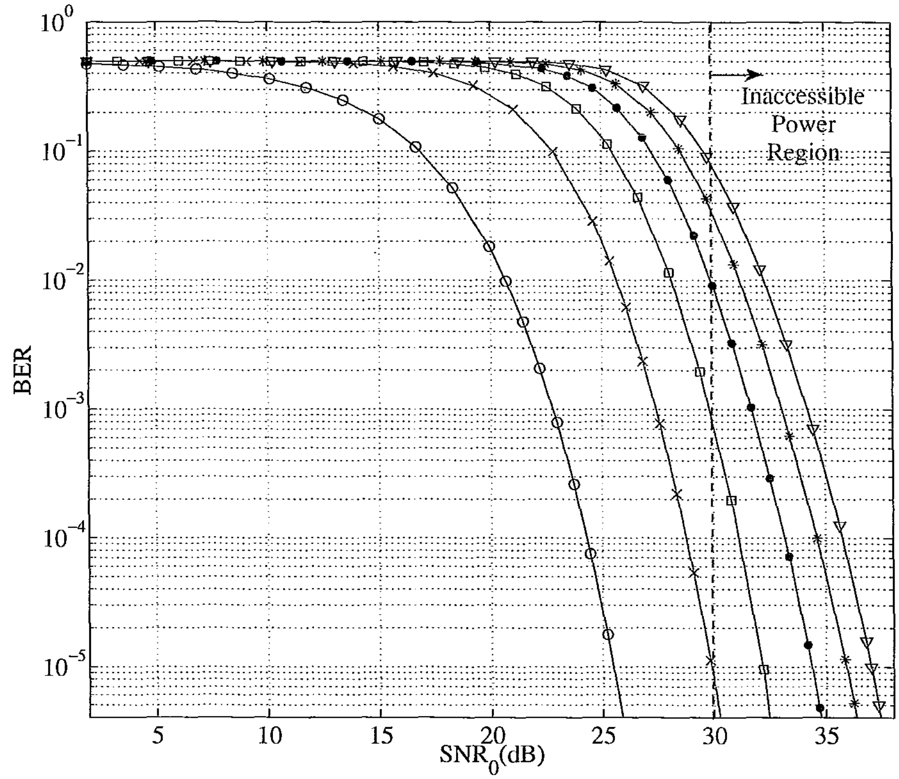

Figure 3.25: BER versus SNR_0 for the constant hop distance $L_k = 1$ km, bit rate BR= 10 Gbps, and different number of relays M considering fading effects. (The plot descriptions are given in Table 3.8)

additional transmit power increases because the overall channel fading is the result of multiplication of $M + 1$ fading coefficients defined over $M + 1$ different 1 km DT links. Therefore the overall fading variance and consequently its degrading effects increase. By increasing the average transmit power, the system compensates the effects of background noise and atmospheric turbulence and extends the link distance coverage. However the maximum average transmit power is restricted because of eye-safty issues and can not increase arbitrarily. This restriction on the average transmit power along with background noise and atmospheric effects confines OAF

Table 3.10: The relative SNR_0 increase $\Delta\mathrm{SNR}_0$(dB)

Number of Relays(M)	BR= 1.25 Gbps	BR= 10 Gbps
0	1.79	1.81
1	2.20	2.15
2	2.26	2.32
3	3.11	3.07
4	3.59	3.59
5	3.84	3.78

FSO transmissions to short distances.

3.4 Conclusion

FSO communication systems suffer extensively from atmospheric turbulence and background noise. A serial amplify-and-forward relaying technique has been introduced as a powerful technique to mitigate the atmospheric turbulence effects at long haul FSO systems. By deploying more relays and decreasing the hop distances, fading effects are reduced and FSO systems access to long distances at a lower average transmit SNR_0. Illustratively, by inserting only one relay at the middle of an FSO link with length $L_T = 3$ km, about 6.6 dB improvement is achieved in the transmit SNR_0 at BER= 10^{-5}. It has been numerically shown that for a given SNR_0, performance of the system is similar at both bit rates. However, the maximum distance coverage of the system operating at BR= 1.25 Gbps is more than the system working at BR= 10 Gbps to obtain a similar BER. Qualitatively, for a given $\mathrm{P}_t = 500$ mW and BER= 10^{-5}, the 1.25 Gbps system with $M = 7$ relays provides a 7.29 km long link, however this value for the similar 10 Gbps system is 3.63 km. Because the FSO system working at higher bit rates (wider bandwidths) collects more background noise at the receiving lens, therefore, for a given transmit power, the 10 Gbps system affords less SNR_0 and hence shorter communicating distance.

Increasing the number of relays is accompanied by collecting more additive background noise at relays that degrades the system performance. Therefore, to reach a specific communicating distance at a given BER, a trade off is compromised between the average transmit power and the number of relays. Since the average transmit power is limited due to eye-safety regulations, the number of relays determines the maximum communicating distance. By increasing the number of relays, besides the total communicating distance, the background noise also increases so that the distance improvement reduces. Although the OAF relaying technique reduces the effects of atmospheric fading, background noise still remains as a limiting factor in FSO communication systems. In Chapter 4, an optical regenerative relaying method using non-linear optics is developed to reduce the background noise effects and increase the communication distance coverage.

Chapter 4

Optical Regenerate-and-Forward Relaying Technique

FSO communication systems are strongly affected by the atmospheric turbulence fading and background illumination. In Chapter 3, the OAF relaying technique has been introduced as a powerful method to mitigate the degrading effects of atmospheric turbulence. But growing background noise remains as the major drawback of free-space optical relaying systems. In electrical Amplify-and-Forward relaying technique at each relay the optical signal along with the background noise is converted to an electrical signal which is amplified by an electrical amplifier. After amplification, the electrical signal is modulated by a photodiode and retransmitted to the next relay.

In an FSO system, the optical intensity the field distribution of the signal is analyzed. By employing an optical band pass filter (BPF) at the beginning of each optical relay, the out-of-band frequency components of the accumulated background noise are eliminated, however, the in-band noise components still remain in the system. In this chapter the *Optical Regenerate-and-Forward (ORF)* relaying technique is proposed to eliminate the background noise at each relay. In ORF, the quality of the received noisy signal is optically restored by a regenerator. In the next section, the internal structure of an ORF relay is described in detail.

4.1 ORF Relay Structure

The internal structure of an ORF relay is shown in Fig. 4.1. When a regenerator is used in an FSO system where broadband white noise is accumulated, an optical BPF centered at the signal frequency ω_0 is required. This filter is placed at the input of the regenerator so as to reject the noise outside the signal spectrum [63]. The bandwidth of the filter is assumed to be equal to the bandwidth of the photodetector. The photodetector bandwidth is dependent on the transmission bit rate and is found so that the best BER is achieved at the receiver. Here it is assumed that the optical filter does not attenuate the optical signal. The filtered signal is amplified with gain G_1 so as to adjust the average power of the signal to a level suitable for the regeneration process. The optimum gain G_1 depends on the average received SNR at each relay and for a given average transmit power and background illumination irradiance is constant. The regeneration process is performed by a regenerator. The regenerator suppresses the noise in zeros and the amplitude fluctuations in ones of optical data streams. The regeneration process will be analyzed in detail in Section 4.2. The regenerated pulses are amplified by another amplifier with gain G_2 and transmitted through the next relay. The gain G_2 is adjusted so that the average transmitted power at the output of each relay is equal to the average transmitted power at the source, P_t.

A sample of Gaussian pulses propagating through an ORF relay are shown in

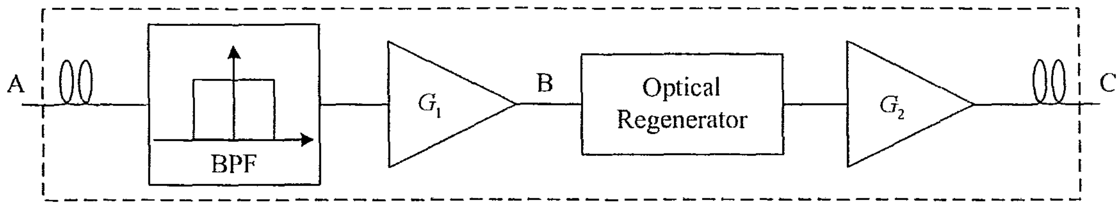

Figure 4.1: The typical structure of an ORF relay.

Fig. 4.2 shows at different points. As shown, the regenerator refines the signal by removing the noise at zeros and amplitude fluctuations in ones. The regenerated Gaussian pulses carry less noise and have a small displacement compared with the original pulses. The regeneration process and internal structure of a regenerator are described in the next section.

4.2 Optical Regenerator

To analyze the regeneration process for suppressing the signal background, the typical structure of a regenerator is shown in Fig. 4.3. The regeneration process is performed by utilizing the effects of *self-phase modulation* (SPM) on the signal in a nonlinear (NL) medium followed by an optical filtering at a frequency of ω_f which is shifted with respect to the carrier frequency of the input data ω_0. The optical fiber with high nonlinearity coefficient γ is employed as the nonlinear medium used in the regenerator. $\gamma(\mathrm{m}^{-1}\mathrm{W}^{-1})$ is defined as [64]

$$\gamma = \frac{n_2 \omega_0}{c A_{\text{eff}}}, \tag{4.1}$$

where n_2 (m^2/W) is the nonlinear-index coefficient, c (m/s) is light velocity, and A_{eff} (m^2) is the effective core area.

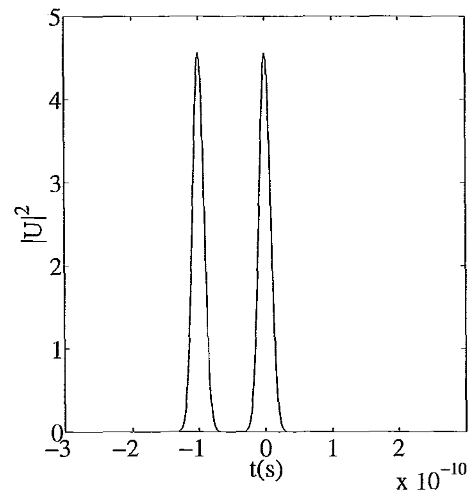

(a) Transmitted Pulses

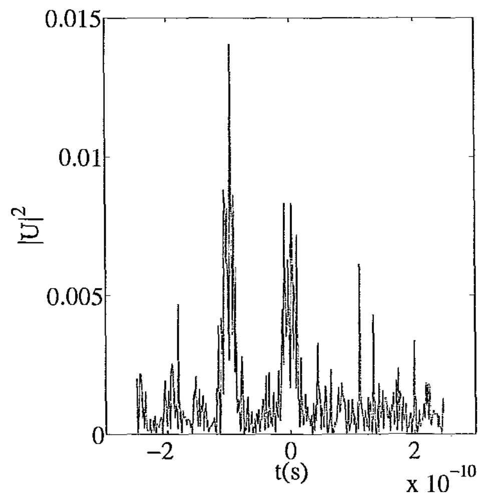

(b) The ORF Relay Input (Point A)

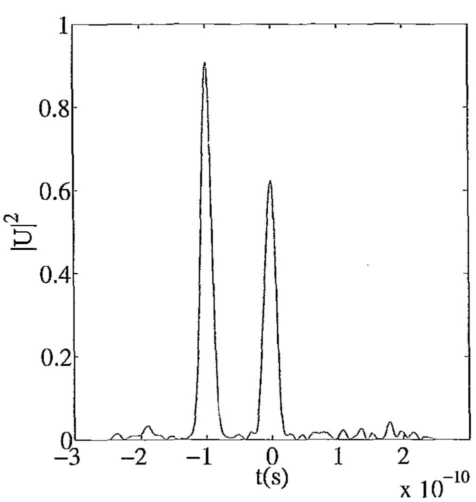

(c) The Regenerator Input (Point B)

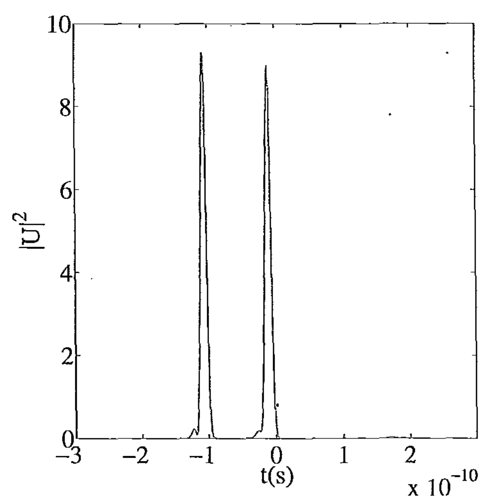

(d) The ORF Relay Output (Point C)

Figure 4.2: Gaussian Pulses propagating through an ORF relay at different points.

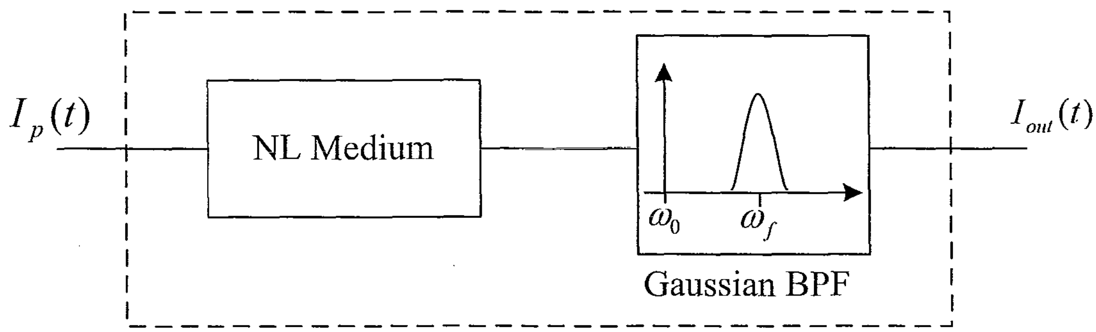

Figure 4.3: The internal structure of a regenerator.

The dependence of the refractive index in nonlinear media, e.g optical fiber, on the signal intensity causes self-phase modulation (SPM) which governs spectral broadening of optical pulses. The propagation of optical pulses inside a single-mode fiber in terms of normalized amplitude $S(z, \tau)$ is quantified by the nonlinear Schrödinger equation as [64]

$$\frac{\partial S}{\partial z} = \frac{i\beta_2}{2L_D}\frac{\partial^2 S}{\partial \tau^2} + \frac{i}{L_{NL}} \exp\left(-\sigma_F z\right)|S|^2 S, \tag{4.2}$$

where z is the propagation distance, $\tau = t/T_0$ is normalized time scale and T_0 is the pulse width. The parameters β_2 and $\sigma_F(\mathrm{m}^{-1})$ account for the fiber dispersion and fiber loss respectively. The dispersion length L_D and nonlinear length L_{NL} are given as

$$L_D = -\frac{T_0^2}{\beta_2} \quad , \quad L_{NL} = (\gamma P_M)^{-1}, \tag{4.3}$$

where P_M is the peak power of optical signal given by (2.5).

To analyze the effects of fiber nonlinearity on the self-phase modulation, fiber dispersion is ignored and the dispersion coefficient is set to zero. By substituting

$\beta_2 = 0$ in (4.2), the nonlinear Schrödinger equation can be solved as

$$U_t(z,t) = U_t(0,t)\exp\left(i\phi_{\mathrm{NL}}(z,t)\right), \tag{4.4}$$

where $U_t(0,t)$ is the field envelope at $z = 0$ and is defined from (2.4) for a single Gaussian pulse as

$$U_t(0,t) = \exp\left(-\frac{t^2}{2T_0^2}\right) \tag{4.5}$$

and

$$\phi_{\mathrm{NL}}(z,t)) = |U_t(0,t)|^2 \frac{z_{\mathrm{eff}}}{L_{\mathrm{NL}}} \tag{4.6}$$

with

$$z_{\mathrm{eff}} = \frac{1-\exp\left(-\alpha z\right)}{\alpha} \tag{4.7}.$$

As indicated in (4.4), the phase shift $\phi_{\mathrm{NL}}(z,t)$ induced by SPM is intensity-dependent while the squared field envelope governed by $|U_t(z,t)|^2$ remains unchanged ($\beta_2 = 0$) . From (4.6), the nonlinear phase shift $\phi_{\mathrm{NL}}(z,t)$ increases with the propagated distance z. The parameter z_{eff} is an effective distance that because of fiber loss is less than z (in the absence of fiber loss, $\alpha = 0$, $z_{\mathrm{eff}} = z$). Moreover, the time dependence of $U_t(0,t)$ and consequently $\phi_{\mathrm{NL}}(z,t)$ induces SPM spectral broadening. In general, temporally varying phase shift induces temporally varying frequency shift, therefore in NL medium the amount of spectral broadening differs across the pulse. By taking the time derivative of phase shift, the instantaneous frequency shift $\Delta\omega_{\mathrm{SPM}}(t)$ with respect to the central frequency ω_0 is obtained as

$$\Delta\omega_{\mathrm{SPM}}(t) = \left|\frac{\partial\phi_{\mathrm{NL}}(z,t)}{\partial t}\right| = \left|\frac{\partial}{\partial t}\left(|U_t(0,t)|^2\right)\right| \frac{z_{\mathrm{eff}}}{L_{\mathrm{NL}}} \tag{4.8}$$

This difference is induced by SPM and increases with the propagated distance, z. In other words, new frequency components are continuously generated as the pulse propagates through the fiber. These SPM-induced frequency components broaden the pulse spectrum. Figure 4.4 shows the spectrums of the data stream presented in Fig. 4.2 for different propagated distances z inside a NL optical fiber.

As shown, the signal power is distributed over more frequency components as the pulses propagate down the fiber. Clearly, the length of the fiber is a main factor in determining the desired spectrum bandwidth at the output of the NL medium.

By substituting (4.5) into (4.8), the spectrum broadening of a Gaussian pulse propagating inside a lossless optical fiber ($z_{\text{eff}} = z$) is obtained as

$$\Delta\omega_{\text{SPM}}(t) = \frac{2t}{T_0^2} \exp\left(-\frac{t^2}{T_0^2}\right) \frac{z}{L_{\text{NL}}} \tag{4.9}$$

By plugging the value of L_{NL} from (4.3) into (4.9) and taking the time average over one bit interval T_b, the average spectrum broadening for one Gaussian pulse is calculated as [63]

$$\overline{\Delta\omega_{\text{SPM}}} = \Delta\omega_0(2\pi/\lambda)n_2 I_P z \tag{4.10}$$

where $\Delta\omega_0/2\pi = 1/T_{\text{FWHM}}$ is the -3 dB spectral bandwidth (T_{FWHM} is the full width at half maximum) and $I_P = P_t/A_{\text{eff}}$ is the average pulse intensity which varies for different pulses. It is clear that the spectrum broadening increases by the initial bandwidth $\Delta\omega_0$, the nonlinear refractive index n_2, the average pulse intensity I_p and the propagated distance z.

After the nonlinear medium, thc pulses pass through a Gaussian optical filter [65] whose center frequency ω_f is shifted with respect to the input signal carrier frequency

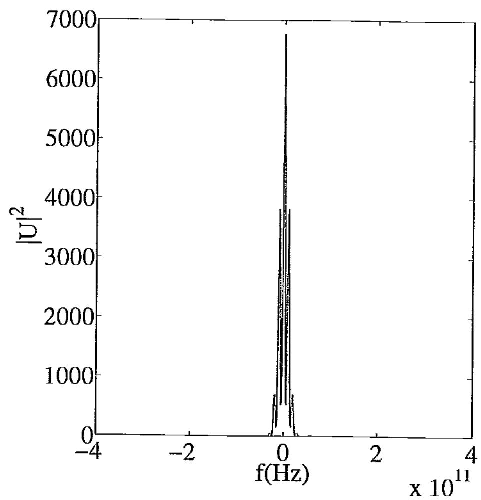

(a) Transmitted Pulses ($z = 0$)

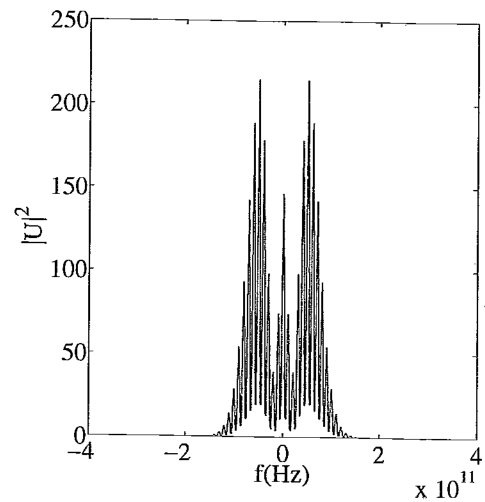

(b) $z = 2$ km

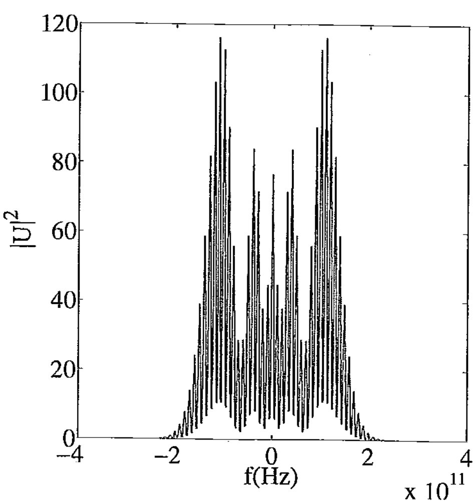

(c) $z = 4$ km

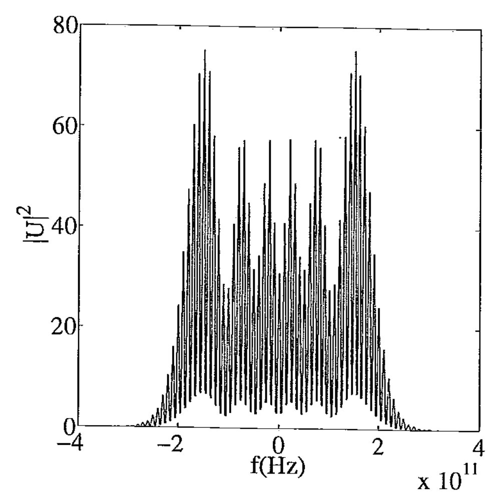

(d) $z = 6$ km

Figure 4.4: The Gaussian pulse spectrums for different propagated distances, z.

ω_0 by a certain value $\Delta\omega_{\text{shift}}$:

$$\omega_f = \omega_0 + \Delta\omega_{\text{shift}} \tag{4.11}$$

As mentioned before, there exists a displacement between the regenerator input pulses and the filtered ones. This misalignment originates from the shifted center frequency of the Gaussian filter.

When the pulse spectral broadening is small so that the spectral bandwidth of the self-phase modulated signal at the output of the NL medium, $\omega_{\text{SPM}} = \Delta\omega_0 + \overline{\Delta\omega}_{\text{SPM}}$, satisfies the following equation

$$\frac{\omega_{\text{SPM}}}{2} < \Delta\omega_{\text{shift}}, \tag{4.12}$$

the pulse is rejected by the filter. In the regenerator, this occurs when the pulse intensity is small, e.g. noise in zeros. If the pulse intensity is high, e.g. at ones, so that the new spectral bandwidth satisfies

$$\frac{\omega_{\text{SPM}}}{2} \geq \Delta\omega_{\text{shift}}, \tag{4.13}$$

depending on the amount of pulse broadening, the filter center frequency, and the filter bandwidth $\Delta\omega_f$, a part of the SPM-broadened spectrum passes through the filter and the rest of them are rejected. The spectral width of the filtered pulse is determined by the filter spectral bandwidth. By changing the filter spectral bandwidth, the bandwidth of the SPM-broadened spectrum changes. If $\Delta\omega_f = \Delta\omega_0$, the output pulsewidth is the same as the input pulsewidth.

In the case where the input pulse intensity I_P is very high, $I_P >> I_{\text{cr}}$, so that the pulse spectrum broadens extensively, $\omega_{\text{SPM}} >> \Delta\omega_{\text{shift}}$, the intensity of the output pulse is independent of the input pulse intensity. Therefore, a pulse transfer function for regenerator in terms of output pulse intensity versus input pulse intensity can be established as

$$I_{\text{out}} = \begin{cases} 0 & \text{if } \mathrm{I_P} < \mathrm{I_{cr}} \\ I_c & \text{if } \mathrm{I_P} > \mathrm{I_{cr}} \end{cases} \tag{4.14}$$

where I_c is the constant output pulse intensity and I_{cr} is the critical pulse intensity which is adjusted to a level so that compromise a trade off between removing the noise at zeros and suppressing the amplitude fluctuations at ones. If I_{cr} is chosen to be very small, the regenerator can not completely remove the noise at zeros. Otherwise, if the critical intensity is selected too big, the pulse spectrum broadens excessively so that the signal is distorted by generation of new out-of-band frequency components. On the other hand, by extensively broadening the pulse spectrum, the more parts of the signal are rejected by the filter that imposes more power loss to the system. The transfer function expressed by (4.14) is an ideal transfer function. Fig. 4.5 shows a typical transfer function of an ideal regenerator and its perfect performance in removing noise at zeros and suppressing the amplitude fluctuations at ones.

As expressed earlier, the regeneration process imposes a considerable power loss to the signal by rejecting a major portion of the pulse spectrum. Therefore, an amplifier is required after the regenerator to boost up the signal and retrieve its average power to the average transmitted power at the source, P_t. As shown in Table 4.2, the ORF relay receives the noisy signal and refines it via regeneration process, then amplifies and retransmits it through the next channel. Section 4.3 provides the

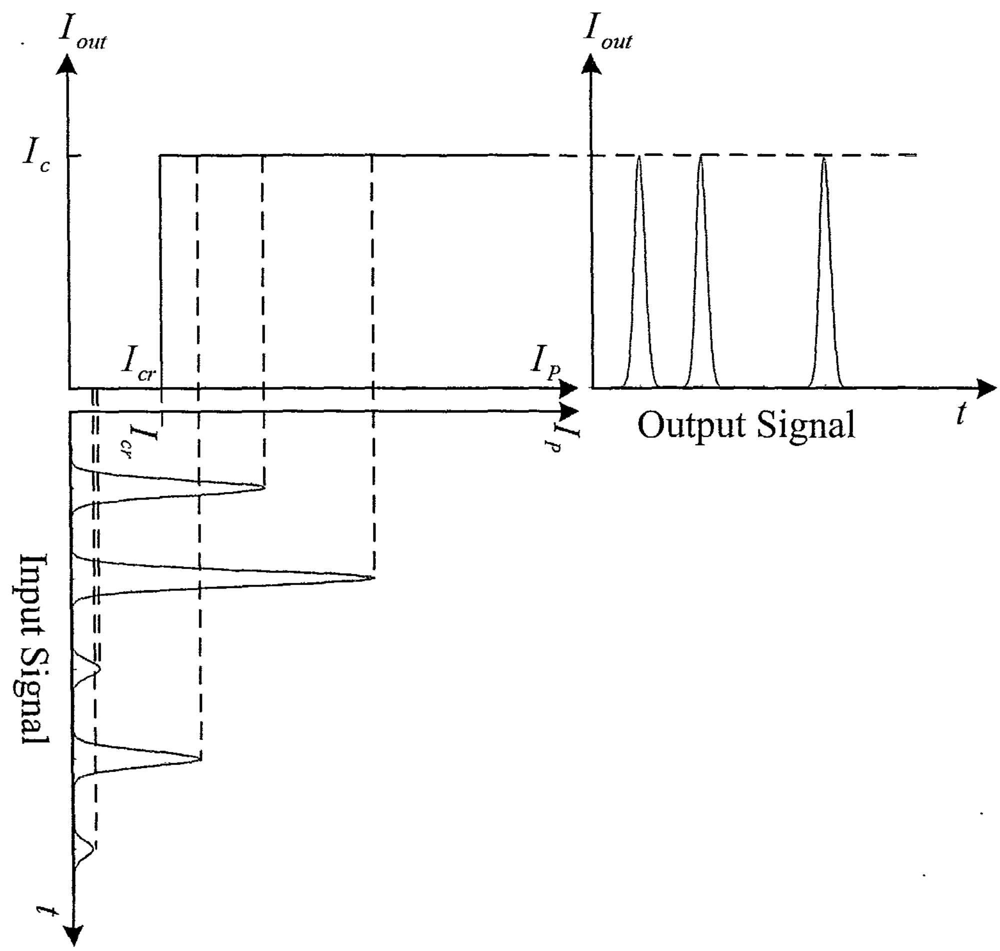

Figure 4.5: Typical transfer function of an ideal regenerator.

numerical simulations on ORF relaying technique and compares its performance with OAF multihop systems.

4.3 Numerical Results and System Performance

In this section, the performance of various ORF multihop FSO communication systems is investigated. Because of the long simulation time of MATLAB , a Q-factor estimation method is utilized to calculate the BER of FSO systems. When the additive noise has a Gaussian distribution, the Q-factor approximation is widely used instead of Monte-Carlo method for BER simulations. As demonstrated in Chapter 3, wideband FSO systems suffer from background noise and their maximum accessible distances are limited due to accumulated background noise. On the other hand, electrical processing limits the bandwidth of high rate optical systems, therefore all-optical relaying techniques are attractive. In this thesis, ORF relaying technique is proposed as a powerful method for optically suppressing the effects of background noise at high bit-rates. Here, the performance of ORF multihop systems are investigated at 10 Gbps and compared with the performance of OAF multihop systems. The degrading effects of atmospheric turbulence are not considered in ORF systems.

The considered FSO system has the same specifications as the OAF FSO system that are previously introduced in Chapter 3. The NL medium specifications are chosen as what Mamyshev considered in [63] for experimental simulations. At BR= 10Gbps, a fiber of length $z = 8$ km with effective core area $A_{\text{eff}} = 45\ \mu m^2$ at $\lambda = 1550$ nm is used. The Gaussian filter inside the regenerator has the -3 dB bandwidth of $\Delta\omega_f/2\pi = 29$ GHz, and the filter frequency offset with respect to the input signal carrier frequency is $\Delta\omega_{\text{shift}}/2\pi = 100$ GHz. The gain of the first amplifier G_1 is adjusted for each launch power and hop distance so that the best performance at the receiver is obtained.

4.3.1 Q-Factor Estimation

Simulating the BER of an ORF multihop system takes an extremely long time. Q factor is frequently utilized to evaluate the performance of optically amplified systems

[66]. In ORF relaying systems due to fiber nonlinearity, the accumulated noise at the receiver is not exactly Gaussian-distributed. However, it can be shown that a Gaussian approximation is a reasonable estimation for the noise distribution. The BER of an OOK modulated signal at the receiver is related to the Q factor as [66]

$$\mathrm{BER} = \frac{1}{2}\mathrm{erfc}\left(\frac{\mathrm{Q}}{\sqrt{2}}\right), \tag{4.15}$$

where the complementary error function erfc(x) is defined as

$$\mathrm{erfc(x)} = \frac{2}{\sqrt{\pi}}\int_{\mathrm{x}}^{\infty} \mathrm{e}^{-\mathrm{t}^2}\mathrm{dt}. \tag{4.16}$$

The Q factor is also expressed as

$$Q = \frac{\mu_1 - \mu_0}{\sigma_1 + \sigma_0}, \tag{4.17}$$

where μ_0 (μ_1) and σ_0 (σ_1) are the means and the standard deviations of zeros (ones) respectively. In numerical simulations, the mean μ_0 (μ_1) of a pulse stream is simply found by getting average over the values obtained by sampling pulses at the middle of the bit intervals, $t = kT_b/2, k = 0, 1, 2, ...$ By squaring the sampled values and taking average, the variance σ_0 (σ_1) of the pulse stream is also obtained.

Fig. 4.6 shows the BER of an ORF multihop system with the total communicating distance of 3 km where one ORF relay is placed at the middle of the link. BER of the system is simulated using both Monte-Carlo (MC) and Q-factor estimation (QF) methods. The total number of transmitted bits is $N = 2^{14}$. In the all MC analyses considered in this work, at least 100 errors in the received bit streams are required

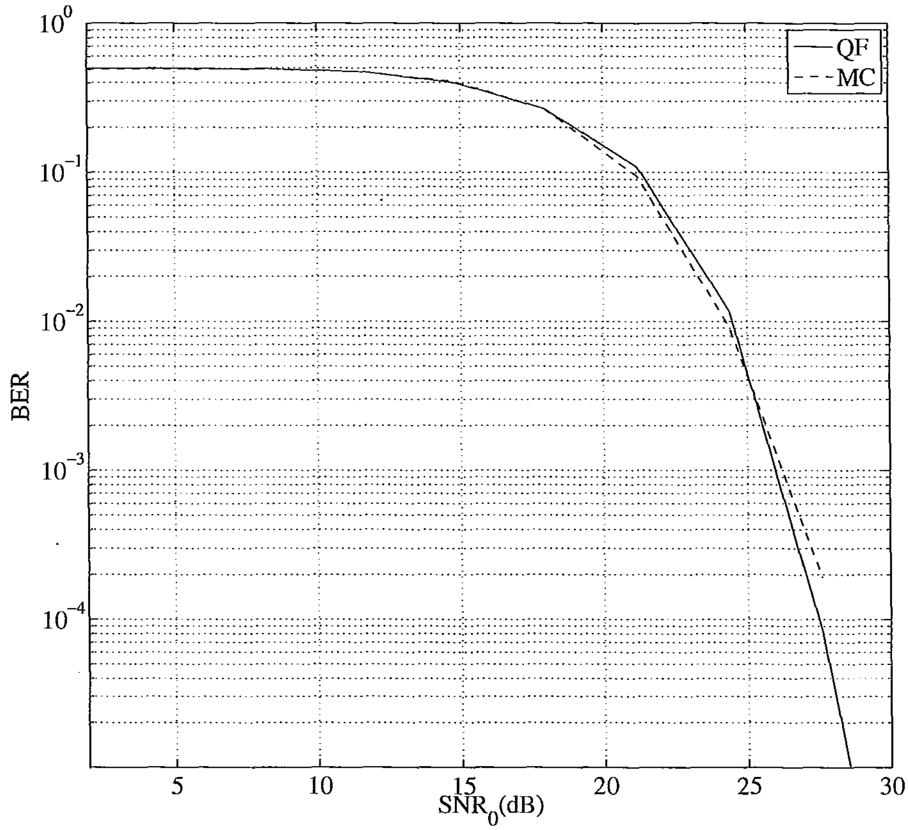

Figure 4.6: BER of an ORF FSO system with $M = 1$ and $L_T = 3$ km, obtained by MC and QF methods.

to be able to rely on the received BER. By sending $N = 2^{14}$ bits and taking average on about 20 different iterations, the smallest reliable BER obtained by MC method will be around BER=10^{-3}. However, simulation results indicate that 2^{14} sent bits are enough to rely on BER as low as 10^{-5} when QF method is employed. As seen from the figure, the performance of the system driven by Q-factor estimation is very close to the Monte-Carlo simulation result (less than 1 dB offset). Therefore, in the rest of this section, QF is considered as a reliable method used to calculate BER of different

Table 4.1: Different system configurations for Fig.4.7 ($L_T = 3$ km)

Marker	L_1(km)	L_2 (km)
−⊟−	1	2
−⊖−	1.5	1.5
−●−	2	1

ORF FSO systems.

4.3.2 Optimal Relaying Configuration

As proved in Chapter 3, the equally-spaced relaying configuration provides the best performance at the receiver of OAF systems. For ORF systems, there exists no explicit mathematical relations between the hop lengths and the average received SNR at the receiver. Therefore, numerical simulations is utilized to found the best configurations. Fig. 4.7 corresponds to the BER of three different ORF systems. In all systems, the total communicating distance is $L_T = 3$ km and one relay is placed between the source and destination nodes. The distance between the source and ORF relay is denoted by L_1 and the distance between the ORF relay and the destination is L_2. Table 4.1 summarizes the configurations of the systems considered in this figure.

From Fig. 4.7, the lowest BER corresponds to the system where the ORF relay is placed at the middle of the link ($L_1 = L_2 = 1.5$ km). Hence, it can be assumed that equally-space relaying may also provide one of the optimal configurations for ORF multihop systems, although enough evidences do not exist for its proof. In the following simulations, ORF relays are arranged in serial equally-space relaying configurations.

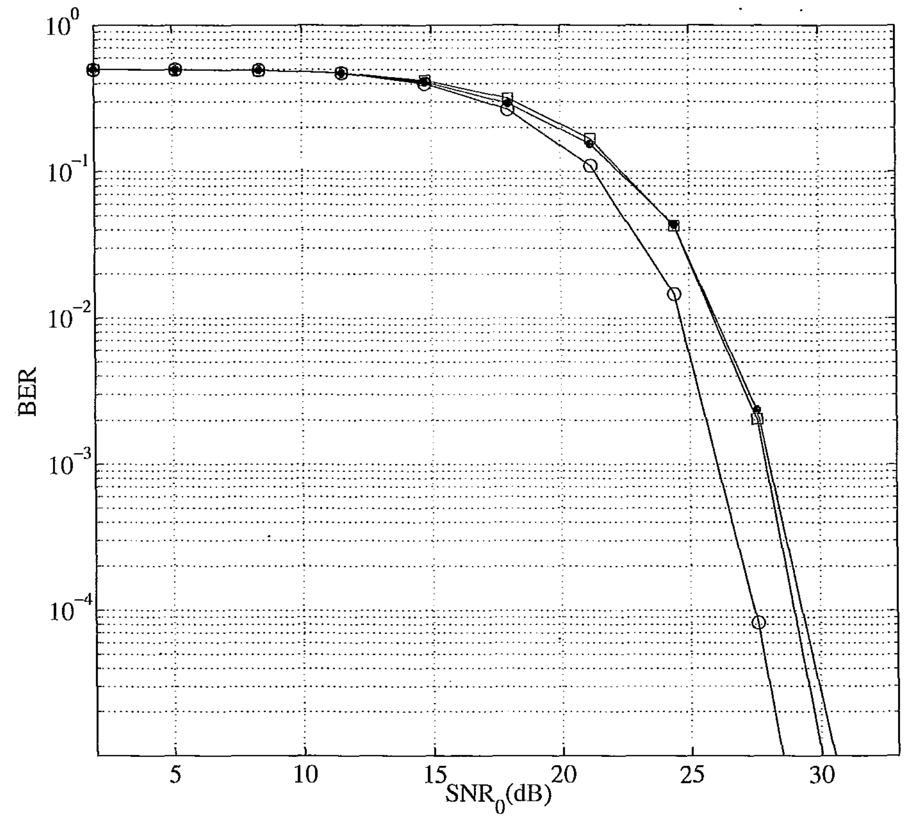

Figure 4.7: BER of different ORF multihop FSO systems with $M = 1$, $L_T = 3$ km, and BR= 10 Gbps. (The plot descriptions are provided in Table 4.1)

4.3.3 Fixed Total Communicating Distance

In Chapter 3, it was shown via numerical simulations that increasing the number of relays between the source and destination nodes while keeping the total communicating distance fixed, improves the system performance (Fig. 3.13). Fig. 4.8 compares the performance of ORF multihop systems with OAF systems. In this plot, the BER of ORF FSO systems for $M = 1$ and $M = 2$ relays are illustrated while the total communicating distance is fixed ($L_T = 3$ km). Table 4.2 summarizes the configurations

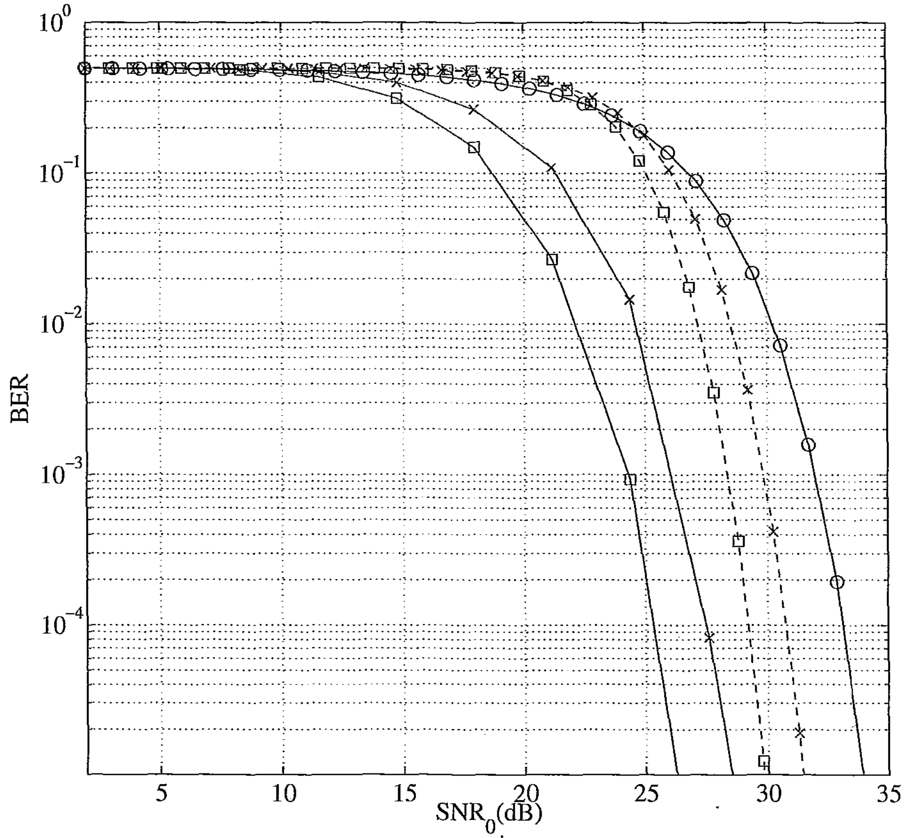

Figure 4.8: BER of different ORF multihop FSO systems with $M = 1$ and $M = 2$ for a fixed total communicating distance of $L_T = 3$ km and, BR= 10 Gbps. (The plot descriptions are provided in Table 4.2)

of the systems considered in this figure.

From Table 4.2, at a given BER= 10^{-5}, by replacing OAF relays with ORF relays, the system gains 2.93 dB ($M = 1$) and 3.51 dB ($M = 2$) improvement in SNR_0 with respect to OAF relaying technique. It is expected that by increasing the number of relays, ORF systems outperform OAF systems more rapidly. As mentioned in Chapter 3, in OAF systems, utilizing more relays injects more accumulated background noise to the system. Thus by increasing the number of relays, BER improvement decreases

Table 4.2: Different system configurations for Fig.4.8 ($L_T = 3$ km)

Marker	M	L_k (km)	Relaying Technique	SNR_0 (dB)
–⊖–	0	3	DT (no relay)	33.93
- -×- -	1	1.5	OAF	31.46
- -⊟- -	2	1	OAF	29.84
—×—	1	1.5	ORF	28.53
—⊟—	2	1	ORF	26.33

(Table 3.4). In ORF systems, background noise is ideally eliminated at each relay, hence background noise does not propagates through the channel and its average power is almost constant at all relays. On the other hand, increasing the number of relays is equivalent to decreasing hop distances and channel loss and therefore the average received SNR increases by the number of relays. In summary, in ORF systems, it is expected that in a fixed-length link, BER improves by increasing the number of relays and its improvement increases rapidly.

4.3.4 Combination of OAF and ORF Relays

In this section, the performance of various multihop systems composed of both OAF and ORF relays is investigated. Consider a 3 km FSO link with two equally-spaced relays placed between the source and destination nodes (the hop distances are 1 km). Fig. 4.9 provides the BER of various relaying schemes whose configurations are summarized in Table 4.3.

As illustrated in Fig. 4.9, by replacing one OAF relay by an ORF relay, i.e. System 2 $\rightarrow$ System 3 (4) in Table 4.3, 1.01 dB (1.33 dB) gain is achieved in SNR_0 at BER$= 10^{-5}$. Surprisingly, if the signal is first amplified by the first relay and then

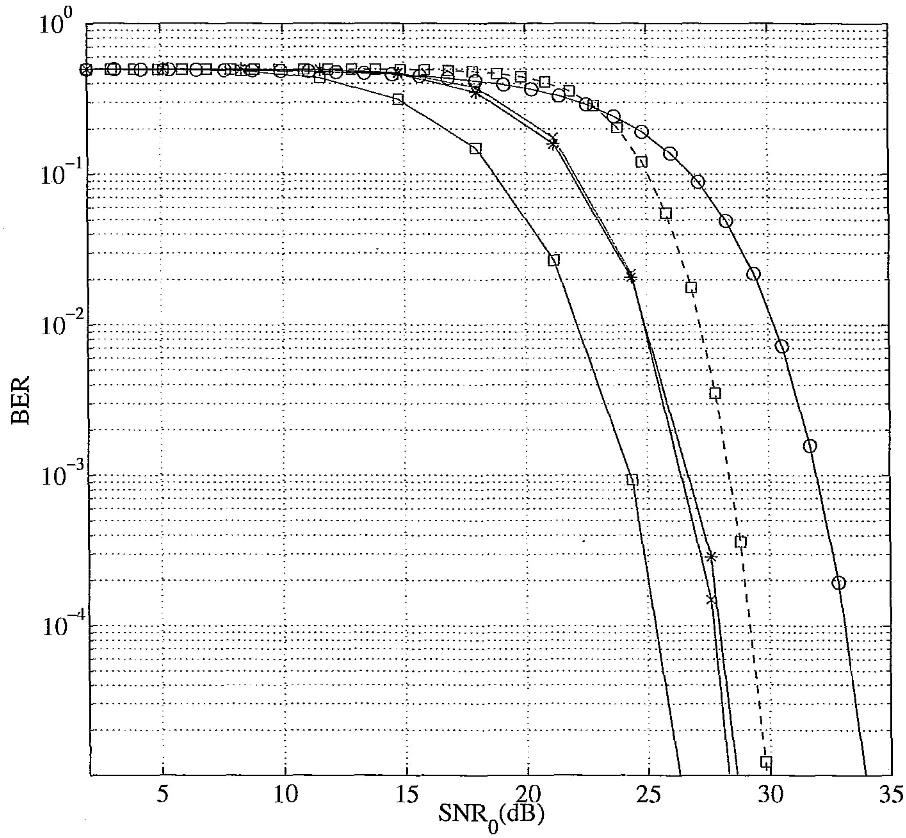

Figure 4.9: BER of different multihop FSO systems with $M = 2$ for a fixed total communicating distance of $L_T = 3$ km and, BR= 10 Gbps. (The plot descriptions are provided in Table 4.3)

regenerated at the second one (System 3) or it is first regenerated and then amplified (System 4), the performance of both systems is nearly the same. At high SNR_0s, System 4 has slightly better performance. Because the received SNR is higher and the regenerator suppresses the amplitude fluctuations at ones more evenly, in other words, regenerator has better performance at high SNR_0.

By replacing both OAF relays by ORF relays, i.e. System 2 (3) $\rightarrow$ System 5, the system performance improves by an additional 2.50 dB (2.18 dB). This value is

Table 4.3: Different system configurations for Fig.4.9 ($L_T = 3$ km, $M = 2$)

System No.	Marker	First Relay	Second relay	SNR_0 (dB)
1	—⊖—	no relay	no relay	33.93
2	- -⊡- -	OAF	OAF	29.84
3	—✳—	OAF	ORF	28.83
4	—×—	ORF	OAF	28.51
5	—⊟—	ORF	ORF	26.33

almost twice the gain achieved by replacing only one OAF relay with an ORF relay (System 2 → System 3 or 4). The reason can be simply explained: the regenerator eliminates the background noise at each relay therefore by using all ORF relays, a negligible amount of background noise remains in the system. In general, regenerators have better performance at higher SNRs. In System 3, the signal is first amplified by an amplifier in the first relay, and then the noisy signal is regenerated at the second relay. Obviously, System 5 benefits from the regeneration process at the second relay more than System 3. In System 4, the noiseless signal regenerated at the first relay is amplified along with the collected background light at the second relay. This amplified background noise considerably deteriorates the performance of System 4. System 5 achieves totally 3.57 dB gain with respect to System 2 and 8.18 dB gain with respect to the direct transmission (System 0.)

4.3.5 Maximum Accessible Communicating Distance

The OAF relaying technique has been introduced as a powerful method in mitigating the effect of atmospheric fading and consequently increasing the maximum achievable distance in FSO communication systems. Although atmospheric fading is suppressed

Table 4.4: Different system configurations for Fig.4.10 ($P_t = 500$ mW, $N_0 = 2 \times 10^{-15}$ W/Hz, and BER= 10^{-5})

System No.	Marker	Number of Relays M	Relaying Technique	L_T (km)	Relaying Distance L_k (km)
0	—⊖—	0	DT	1.70	1.70
1	--×--	1	OAF	2.20	1.10
2	--⊟--	2	OAF+OAF	2.62	0.87
3	—×—	1	ORF	3.08	1.54
4	—⊟—	2	ORF+ORF	4.48	1.50
5	—▽—	2	ORF+OAF	3.40	1.13

by OAF relaying technique, amplify-and-forward FSO systems encounter an essential difficulty originating from accumulating background noise at each relay. The ORF relaying technique is proposed as an effective technique to reduce the background noise and increase the maximum accessible distance in FSO communication systems. Fig. 4.10 provides BER of various OAF, ORF and hybrid OAF/ORF multihop systems. The average transmit power is $P_t = 500$ mW for all schemes and atmospheric fading effects are neglected in this study. The number of relays at each system is either one or two and relays are arranged in an equally-spaced relaying configuration. Table 4.4 summarizes the configurations of the systems considered in this figure.

By comparing ORF and OAF relaying systems in Fig. 4.10, it is realized that ORF technique improves the maximum achievable distance several times more than OAF technique. By replacing OAF relays with ORF relays in System 1 and 2, i.e. System 1 $\rightarrow$ System 3 and System 2 $\rightarrow$ System 4 in Table 4.4, the maximum accessible distance increases respectively by 0.88 km and 1.86 km. Despite OAF technique, in ORF systems as the number of relays increases, maximum accessible distance

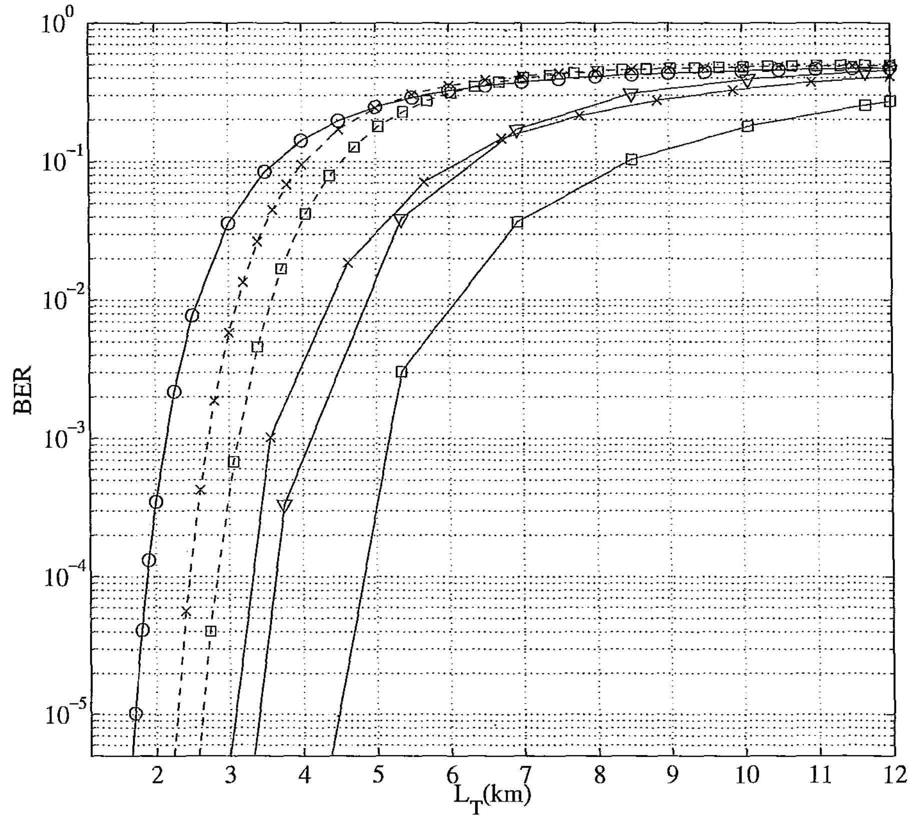

Figure 4.10: The maximum accessible communicating distance of different multihop FSO systems with $M = 1$ and $M = 2$ when $P_t = 500$ mW, $N_0 = 2 \times 10^{-15}$ W/Hz, and BR= 10 Gbps. (The plot descriptions are provided in Table 4.4)

improves more rapidly, e.g. by utilizing only one ORF relay (System 3), L_T increases by 1.38 km, by using another ORF relay (System 4), additional 1.4 km increment is obtained in L_T. As mentioned in Chapter 3, by increasing the number of relays, maximum L_T occurs at shorter hop distances so that the system overcomes the effects of accumulated background noise. By deploying ORF relaying technique, background noise is mostly eliminated at each relay and shortening hop distances no longer is required, e.g. from Table 4.4, the hop distances in the considered ORF systems are almost 1.5 km for both System 3 and System 4. Under this circumstance, in ORF systems, the maximum accessible distance extends linearly by the number of relays. Ideally, if atmospheric turbulence effects are neglected, *ORF relaying technique can greatly extend the total communicating distance L_T by desirably increasing the number of relays.*

The relaying system which consists of two equally-spaced ORF and OAF relays (System 5) has slightly better performance than the system with just one ORF relay (System 3). This small improvement corresponds to the shorter hop distances to compensate the effects of background noise. For long hop distances where the received SNR at relays is very small, employing OAF relays not only does not improve the system performance but it also deteriorates it (Fig. 3.13). As shown in Fig. 4.10, at very long hop distances ($L_k \geq 2.2$ km), the performance of System 3 is better than performance of System 5, because at very low received SNRs, using OAF relays is equivalent to injecting background noise to the system. Although System 5 takes advantage of one more OAF relay, totally, performance of System 3 and System 5 are very similar even at short hop distances. This similarity accentuates the superior performance of ORF technique to OAF method and its dominant role in hybrid systems for improving the system performance. Next section is spent to compare resistivity of both techniques in the presence of background noise.

4.3.6 Fixed hop Lengths

In order to compare ORF technique resistivity to background noise with OAF technique, Fig. 4.11 is provided. In the systems under consideration, hop lengths are fixed $L_k = 1$ km. The total communicating distance increases by subsequently adding a

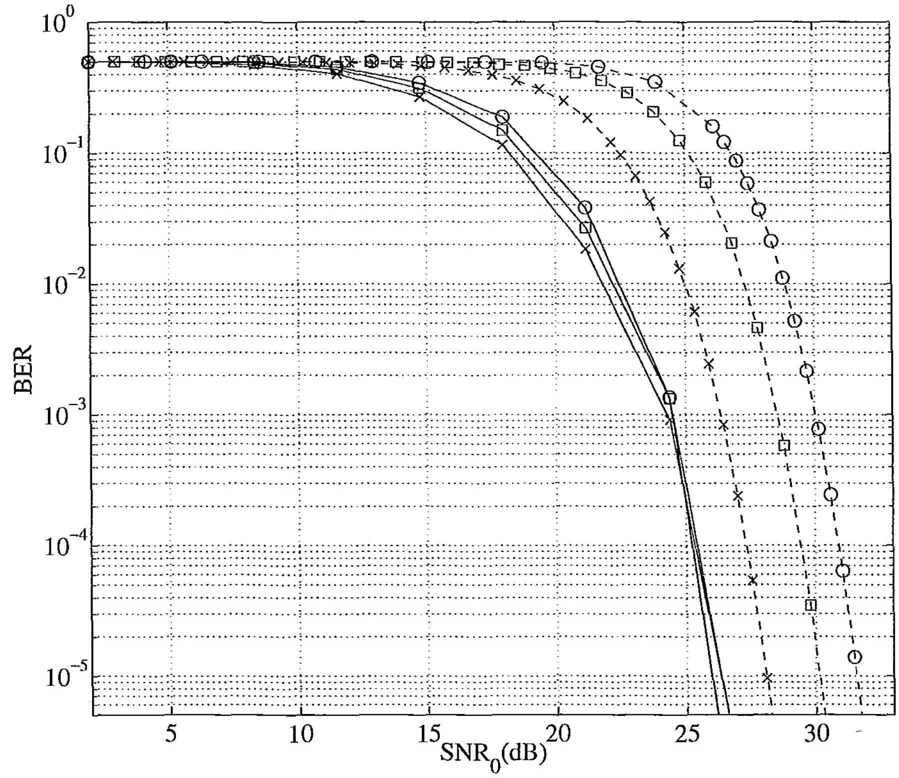

Figure 4.11: BER of different ORF FSO systems with different number of relays M for a fixed hop distance of $L_k = 1$ km and BR= 10 Gbps. (The plot descriptions are provided in Table 4.5)

new relay to the previous system. The amount of accumulated background noise increases by the number of relays. In the OAF relaying technique, it is shown that this increment in background power deteriorates the system BER and limits its maximum accessible distance. However Fig. 4.11 indicates that increasing the number of relays in ORF systems does not influence the system performance because the accumulated background noise is eliminated at each relay. Table 4.5 summarizes the configurations of the systems considered in this figure.

From Fig. 4.11, by replacing ORF relays with OAF relays, at a given BER= 10^{-5},

Table 4.5: Different system configurations for Fig.4.11 ($L_k = 1$ km)

Marker	M	L_T(km)	Relaying Technique	SNR_0 (dB)
--⊖-	3	4	OAF	31.29
--⊟-	2	3	OAF	29.84
--×--	1	2	OAF	27.75
—⊖—	3	4	ORF	25.96
—⊟—	2	3	ORF	26.31
—×—	1	2	ORF	26.33

the average transmit SNR_0 improves by 1.44 dB, 2.92 dB and 5.36 dB when the number of relays are $M = 1$, $M = 2$, and $M = 3$ respectively. In OAF systems, by increasing the number of relays (increasing the total communicating distance) more average transmit power is required to guarantee a specific BER at the receiver. However when ORF technique is used, by subsequently adding more relays, the system BER remains nearly unchanged. This feature makes the ORF relaying technique a distinguished method for removing the background noise in multihop FSO communication systems and leading to significantly extending the FSO communication distance coverage.

4.4 Conclusion

In Chapter 3, the OAF relaying technique has been developed to reduce the degrading effects of atmospheric turbulence. It has been shown that by mitigating atmospheric fading effects via reducing hop distances, the link coverage can be extended. But the magnitude of improvement is limited due to growing accumulated background noise during the channel. In this chapter, ORF relaying technique has been proposed as a powerful method to optically remove background noise at each relay. A very weak turbulence fading condition ($C_n^2 < 1 \times 10^{-17}$ m$^{-2/3}$ [52]) has been considered under which the atmospheric fading effects can be neglected over distances up to 1 km. Assuming this condition, BER performance of different ORF systems operating at BR= 10 Gbps are investigated and compared with the performance of OAF systems. The results indicate that the distance coverage of ORF FSO links can be significantly extended by increasing the number of relays because collected background light at each relay is mostly eliminated by a regenerator. Qualitatively, by employing only one ORF relay, the total communicating distance increases respectively by 1.38 km and 0.88 km with respect to direct transmission and a similar OAF multihop system.

In ORF systems, background noise is mainly eliminated by the relay and does not propagate through the channel, this feature which is also involved in the decode-and-forward relaying technique causes ORF systems to significantly outperform OAF systems, especially for large number of relays and longer distances. Although the ORF technique provides superior performance to OAF technique, it requires more sophisticated equipment such as an automatic gain controller, optical Gaussian filters, adjustable non-linear optical medium, two amplifier at each relay, etc, which increase the complexity and implementation costs of the system. The regeneration process is highly sensitive to the incident signal SNR, the pre-amplifier adjusted gain, and the Gaussian filter frequency offset and bandwidth. Also as mentioned, the regenerator output signal has a small displacement with respect to the original pulses that in some applications this delay might be undesired [63]. The error propagation is another performance limiting factor in ORF systems. In general, the amplitude of the regenerator output pulses are not completely equal and they have negligible fluctuations. If the regenerator is not well adjusted and does not work at its optimal operating condition, it can even add extra amplitude fluctuations to the output pulses. These fluctuations, e.g. at bit "1", propagate through the channel and by subsequent regeneration in the following relays lead to wrong detection of the pulse (completely rejecting the pulse). These challenges in the proposed ORF system provide motivation to finding methods to increase the system stability and reduce the implementation complexity.

Chapter 5

Conclusion and Future Work

5.1 Conclusion

This thesis presents new optical relaying techniques to mitigate atmospheric turbulence-induced fading effects and eliminate background noise in free space optical (FSO) communication systems. The main contributions of the thesis are proposing all-optical amplify-and-forward (OAF) and regenerate-and-forward (ORF) relaying techniques and applying them to relay assisted FSO systems.

In order to define an all optical relay-assisted FSO system, a new channel model is developed which characterizes the variations of intensity and phase of the optical signal during wave propagation. An additive AWGN channel is assumed in which background illumination is the dominant source of noise. Three primary factors have been considered to model the free space channel effects: 1) atmospheric attenuation which includes both absorption and scattering contributions; 2) log-normal fading under weak atmospheric turbulence conditions; and 3) propagation loss due to optical beam spreading through optical channel. The Beers-Lambert law is modified to find the atmospheric attenuation factor applied to the optical field envelope. Since the optical field envelope is analyzed, both amplitude and phase of atmospheric-induced fading are statistically modeled and new definition for propagation loss is defined. The numerical results show that the new model for propagation loss is close to the conventional model (geometric loss), however, the proposed model provides more accurate estimation of beam propagation loss especially over short ranges (a few hundred meters). The atmospheric channel effects are assumed as multiplicative complex terms which are multiplied by the field envelope and induce intensity and phase fluctuations at the receive aperture. These fluctuations degrade the overall system performance.

The OAF relaying technique is proposed as a powerful technique for mitigating the atmospheric turbulence-induced fading while all relaying processes, e.g. amplification, filtering (as needed), etc, are performed in optical domain. The all-optical AF relaying technique allows users to take advantage of high data rate (wide bandwidth) optical transmissions over longer distances. It also provides less delay and complexity in implementation rather than the previously considered AF communication systems which need OE and EO conversions at each relay. Performance of OAF systems has been considered for two bit rates BR= 1.25 Gbps and BR= 10 Gbps under no fading and weak fading effects. It is numerically shown that by increasing the number of relays between source and destination, hop distances decrease and consequently distance-dependent atmospheric-induced fading is mitigated. In fact by employing more OAF relays, longer communicating distances are accessible for a given average transmit power. However, distance improvements slow down by increasing the number of relays because the collected background light at each relay is accumulated during propagation and totally more noise is added to the signal. The accumulated background noise is the major limiting factor in improving the maximum accessible distance of OAF multihop systems.

The decode-and-forward (DF) relaying method has been widely used in RF systems to remove the effects of background noise at each relay. Due to its superior performance to AF relaying technique, DF method is recently applied to FSO systems as well. The considerable loss in data rate, complexity of encoding/decoding processes, and delay induced by electrical processors at each relay accentuate the need for an innovative technique to remove background noise completely in optical domain. In this thesis, the ORF relaying method is developed as a promising technique for removing background noise at each relay. The ORF systems operating at high bit rate BR= 10 Gbps are considered under a very weak atmospheric turbulence condition where atmospheric fading effects can be neglected over short distances (less than 1 km). Under this assumption, BER performance of ORF systems are analyzed. The simulation results indicate that by employing ORF technique, the background noise can be eliminated at each relay that results in accessing greatly longer communicating distances. Despite the OAF method, in ORF systems the communicating distance improves steadily as the number of relays. In other words, the ORF technique used in multihop FSO systems makes high data rate communications possible over a greatly extended communicating distance by employing reasonable number of relays. Although the ORF technique distinguishably outperforms the OAF method in terms of BER performance, it requires complex relay structures and adjustable gain amplifiers that imposes more complexity and implementation costs to the system.

5.2 Future Work

In this thesis, all-optical multihop FSO communication systems are studied and its BER performance is analyzed for the first time. Therefore many future directions still remain to be investigated in the future, some of which are described as follows.

- Although most FSO manufactures utilize the bit error rate (BER) as a standard performance metric to characterize their products, the BER is not itself a comprehensive metric to evaluate the performance of FSO systems. In multihop systems, the end-to-end outage occurs when a local outage happens during one of intermediate hops. The intensity fluctuations induced by atmospheric turbulence, blockage of the line-of-sight link due to temporary obstructions, e.g. birds, temporary disalignment between two consequent relays, etc, lead to an end-to-end outage in the whole system. Therefore, analyzing outage probability factor would be a critical step in performance analyses of all-optical multihop FSO systems.

- In Chapter 4, the error performance of ORF FSO systems has been investigated when the atmospheric turbulence-induced fading effects are neglected. This assumption holds for short hop-distances (less than 1 km) and under weak atmospheric turbulence conditions. In order to utilize ORF technique to support long-haul applications, atmospheric turbulence effects must been taken into account. The ORF FSO system performance has been analyzed in the presence of background noise and it has been shown that in the absence of fading, ORF technique greatly extends the total communicating distance. The next work can be devoted on investigating the limitations that atmospheric turbulence imposes to the maximum achievable distance of ORF FSO systems.

- The performance of multihop FSO systems has been analyzed in the absence/presence of weak atmospheric turbulence-induced fading. The performance of FSO links is very dependent upon weather conditions therefore investigating the performance of multihop FSO systems under different turbulence conditions is another interesting approach for the future work. On the other hand, the system performance can be analyzed for different amounts of collected background power at the receive apertures when the ambient illumination varies during the day and for different locations.

- The cooperative diversity scheme is another future approach for increasing both the reliability and distance coverage of FSO systems. The information redundancy at the receiver of such systems can improve the error performance. On the other hand, since each path experiences a different atmospheric condition, it is expected that the end-to-end outage probability decreases.

Appendix A

Optimum relaying configuration

A.1 Dual-hop relaying system

Recall the expression for $f_1(x)$ given in Eq. (3.26):

$$f_1(x) = \left[e^{\alpha x}x^2 + e^{\alpha(L_T - x)}(L_T - x)^2 + (\kappa \mathrm{SNR}_0)^{-1} e^{\alpha L_T} x^2 (L_T - x)^2\right]. \tag{A.1}$$

It will be shown that

$$\begin{aligned} f_1'(x) &\Big|_{x=\frac{L_T}{2}} = 0 \\ f_1''(x) &> 0, \quad \text{for} \quad 0 < x < L_T. \end{aligned} \tag{A.2}$$

A.1.1 $f_1'(\frac{L_T}{2}) = 0$

$$\begin{aligned} f_1'(x) &= \frac{\partial f_1(x)}{\partial x} = \alpha x^2 e^{\alpha x} + 2x e^{\alpha x} - \alpha (L_T - x)^2 e^{\alpha(L_T - x)} - 2(L_T - x) e^{\alpha(L_T - x)} \\ &+ (\kappa \mathrm{SNR}_0)^{-1} e^{\alpha L_T} (2x(L_T - x)^2 - 2(L_T - x)x^2), \end{aligned} \tag{A.3}$$

$$\begin{aligned} \Rightarrow f_1'(x) &= \alpha \left[e^{\alpha x} x^2 - e^{\alpha(L_T - x)} (L_T - x)^2 \right] + 2 \left[e^{\alpha x} x - e^{\alpha(L_T - x)} (L_T - x) \right] \\ &+ 2(\kappa \mathrm{SNR}_0)^{-1} e^{\alpha L_T} x (L_T - x)(L_T - 2x). \end{aligned} \tag{A.4}$$

From (A.4), it is clear that at $x = \frac{L_T}{2}$ the first derivative of $f_1(x)$ is zero: $f_1'(\frac{L_T}{2}) = 0$.

A.1.2 $f_1''(\frac{L_T}{2}) > 0$

First it will be shown that the second derivative is nonnegative at $x = \frac{L_T}{2}$. From (A.4)

$$\begin{aligned} f_1''(x) &= \frac{\partial f_1'(x)}{\partial x} = \alpha \left[\alpha e^{\alpha x} x^2 + 2x e^{\alpha x} + \alpha e^{\alpha(L_T - x)} (L_T - x)^2 + 2(L_T - x) e^{\alpha(L_T - x)} \right] \\ &+ 2 \left[e^{\alpha x} + \alpha x e^{\alpha x} + e^{\alpha(L_T - x)} + \alpha (L_T - x) e^{\alpha(L_T - x)} \right] \\ &+ 2(\kappa \mathrm{SNR}_0)^{-1} e^{\alpha L_T} \left[(L_T - 2x)^2 - 2x(L_T - x) \right]. \end{aligned} \tag{A.5}$$

By substituting $x = \frac{L_T}{2}$ in (A.5)

$$\begin{aligned} f_1''\left(\frac{L_T}{2}\right) &= 2\alpha\left[\frac{L_T}{2}e^{\alpha L_T/2}(\frac{L_T}{2}+2)\right] + 4\left[e^{\alpha L_T/2}(\frac{\alpha L_T}{2}+1)\right] - 2(\kappa\mathrm{SNR}_0)^{-1}e^{\alpha L_T}\frac{L_T^2}{2} \\ &= e^{\alpha L_T/2}\left[\underbrace{(\frac{\alpha}{2} - (\kappa\mathrm{SNR}_0)^{-1}e^{\alpha L_T/2})}_{c} L_T^2 + 4\alpha L_T + 4\right]. \end{aligned} \tag{A.6}$$

In the FSO systems which are considered in this work, the atmospheric attenuation coefficient is $\alpha = 0.43$ dB/km which in the linear system is equivalent to $\alpha = 10^{-4}(\mathrm{m}^{-1})$. In typical FSO systems, $\kappa \approx 10^5$ and the average transmit SNR_0 varies between 0 dB and 40 dB in our simulations or equivalently $1 < \mathrm{SNR}_0 < 10^4$ in the linear system. The term c in (A.6) is the coefficient of the dominant factor (L_T^2) and is described as $c = (\alpha/2 - (\kappa\mathrm{SNR}_0)^{-1}e^{\alpha L_T/2})$. Since the two other terms in (A.6) are positive, if $c > 0$, therefore $f_1''(L_T/2) > 0$ and the proof is complete. For $0 \leq L_T \leq 40$ km, the exponential term changes between $1 \leq e^{\alpha L_T/2} \leq 7.39$, in other words $e^{\alpha L_T/2} < 10$ for a long range of L_T. On the other hand, for the above mentioned range of SNR_0, $10^{-5} \leq (\kappa\mathrm{SNR}_0)^{-1} \leq 10^{-9}$. At the worst case where $\mathrm{SNR}_0 = 0$ dB ($(\kappa\mathrm{SNR}_0)^{-1} = 10^{-5}$), the maximum L_T over which $f_1''(L_T/2)$ is nonnegative can be obtained as

$$c = (\frac{\alpha}{2} - (\kappa\mathrm{SNR}_0)^{-1}e^{\alpha L_T/2}) > 0 \xRightarrow{\mathrm{SNR}_0=0} \frac{10^{-4}}{2} - 10^{-5}e^{\frac{10^{-4}\times L_T}{2}} > 0 \Rightarrow L_T < 35 \text{ km}. \tag{A.7}$$

For higher SNR_0, $f_1''(L_T/2)$ is nonnegative over longer distances. Since, in this work, shorter distances and higher SNR_0 are considered in the simulations, it can be assumed that $f_1''(L_T/2)$ is nonnegative in the desired range of L_T.

A.1.3 $f_1''(x) > 0$ for $x \in [0, L_T]$

Now it will be shown that $f_1''(x) > 0$ is also nonnegative over the range of typical L_T values where $f_1''(L_T/2)$ is nonnegative. In (A.5), the first two terms are nonnegative for every arbitrary value of $0 < x < L_T$. However the third term depends on the value of α, L_T, κ, and SNR_0. In A.1.2, the range of L_T over which $f_1''(L_T/2)$ is nonnegative has been discussed. In this section, it will be shown that $f_1''(L_T/2)$ is less than $f_1''(x)$ for every $x \neq \frac{L_T}{2}$ and $0 < x < L_T$, and therefore, $f_1''(x)$ is nonnegative over the region where $f_1''(L_T/2) > 0$. Consider the third term in (A.5).

$$g(x) = \left[(L_T - 2x)^2 - 2x(L_T - x)\right], \tag{A.8}$$

the first and second order derivatives of $g(x)$ are easily obtained as

$$\begin{aligned} g'(x) &= \frac{\partial g(x)}{\partial x} = -4(L_T - 2x) - 2(L_T - 2x)\Big|_{x=\frac{L_T}{2}} = 0 \\ g''(x) &= \frac{\partial g'(x)}{\partial x} = 8 + 8 = 16 > 0. \end{aligned} \tag{A.9}$$

From (A.9), $g(x)$ is convex over all possible values of x and $x = \frac{L_T}{2}$ is a global minimum point for $g(x)$. That is, $g(x) > g(L_T/2)$ or equivalently $f_1''(x) > f_1''(L_T/2)$ for every x inside the region $(0 < x < L_T)$. Since, $f_1''(L_T/2)$ is nonnegative for the desired range of L_T, therefore $f_1''(x)$ is also nonnegative for every $0 < x < L_T$, and $x = \frac{L_T}{2}$ is a global minimum point for $f_1(x)$ over the desired range of L_T.

A.2 $(p+1)$-hop relaying system

From (3.36)

$$f_{p+1}(x) = \left[1 + (\kappa\text{SNR}_0)^{-1} e^{\alpha\left(\frac{x}{p+1}\right)} \left(\frac{x}{p+1}\right)^2\right]^{p+1} \left[1 + (\kappa\text{SNR}_0)^{-1} e^{\alpha(L_T - x)} (L_T - x)^2\right] \tag{A.10}$$

A.2.1 $f'_{p+1}(x)$

$$\begin{aligned} f'_{p+1}(x) &= \frac{\partial f_{p+1}(x)}{\partial x} = (p+1)\left[1 + (\kappa\text{SNR}_0)^{-1} e^{\alpha\left(\frac{x}{p+1}\right)} \left(\frac{x}{p+1}\right)^2\right]^p \\ &\times \left[(\kappa\text{SNR}_0)^{-1} e^{\alpha\left(\frac{x}{p+1}\right)} \left(\frac{\alpha}{p+1}(\frac{x}{p+1})^2 + \frac{2}{p+1}(\frac{x}{p+1})\right)\right] \\ &\times \left[1 + (\kappa\text{SNR}_0)^{-1} e^{\alpha(L_T - x)} (L_T - x)^2\right] \\ &- \left[1 + (\kappa\text{SNR}_0)^{-1} e^{\alpha\left(\frac{x}{p+1}\right)} \left(\frac{x}{p+1}\right)^2\right]^{p+1} \\ &\times \left[(\kappa\text{SNR}_0)^{-1} e^{\alpha(L_T - x)} \left(\alpha(L_T - x)^2 + 2(L_T - x)\right)\right]. \end{aligned} \tag{A.11}$$

Define $x_M = L_T/p + 2$. For $x = (p+1)x_M$, the first order derivative is zero

$$\begin{aligned} f'_{p+1}((p+1)x_M) &= \left[1 + (\kappa\text{SNR}_0)^{-1} e^{\alpha x_M} x_M^2\right]^p (\kappa\text{SNR}_0)^{-1} e^{\alpha x_M} \\ &\times \left[\alpha(x_M^2 + 2x_M) - \alpha(x_M^2 + 2x_M)\right] = 0 \end{aligned} \tag{A.12}$$

A.2.2 $f''_{p+1}(x)$

From (A.11), the second order derivative is derived as

$$
\begin{aligned}
f''_{p+1}(x) &= \frac{\partial f'_{p+1}(x)}{\partial x} = p\left[1+(\kappa\mathrm{SNR}_0)^{-1}e^{\alpha(\frac{x}{p+1})}\left(\frac{x}{p+1}\right)^2\right]^{p-1} \\
&\times \left[(\kappa\mathrm{SNR}_0)^{-1}e^{\alpha(\frac{x}{p+1})}\left(\frac{\alpha}{p+1}(\frac{x}{p+1})^2+\frac{2}{p+1}(\frac{x}{p+1})\right)\right] \\
&\times \left[1+(\kappa\mathrm{SNR}_0)^{-1}e^{\alpha(L_T-x)}(L_T-x)^2\right] \\
&\times \left[e^{\alpha(\frac{x}{p+1})}\left(\frac{\alpha}{p+1}(\frac{x}{p+1})^2+\frac{2}{p+1}(\frac{x}{p+1})\right)\right] \\
&- \left[1+(\kappa\mathrm{SNR}_0)^{-1}e^{\alpha(\frac{x}{p+1})}\left(\frac{x}{p+1}\right)^2\right]^{p} \\
&\times \left[(\kappa\mathrm{SNR}_0)^{-1}e^{\alpha(L_T-x)}\left(\alpha(L_T-x)^2+2(L_T-x)\right)\right] \\
&\times \left[e^{\alpha(\frac{x}{p+1})}\left(\frac{\alpha}{p+1}(\frac{x}{p+1})^2+\frac{2}{p+1}(\frac{x}{p+1})\right)\right] \\
&+ \left[1+(\kappa\mathrm{SNR}_0)^{-1}e^{\alpha(\frac{x}{p+1})}\left(\frac{x}{p+1}\right)^2\right]^{p} \\
&\times \left[1+(\kappa\mathrm{SNR}_0)^{-1}e^{\alpha(L_T-x)}(L_T-x)^2\right] \\
&\times \left[e^{\alpha(\frac{x}{p+1})}\left[\frac{\alpha}{p+1}\left(\alpha(\frac{x}{p+1})^2+2(\frac{x}{p+1})\right)+\left(\frac{2\alpha}{p+1}(\frac{x}{p+1})+\frac{2}{p+1}\right)\right]\right] \\
&- (p+1)\left[1+(\kappa\mathrm{SNR}_0)^{-1}e^{\alpha(\frac{x}{p+1})}\left(\frac{x}{p+1}\right)^2\right]^{p} \\
&\times \left[(\kappa\mathrm{SNR}_0)^{-1}e^{\alpha(\frac{x}{p+1})}\left(\frac{\alpha}{p+1}(\frac{x}{p+1})^2+\frac{2}{p+1}(\frac{x}{p+1})\right)\right] \\
&\times \left[e^{\alpha(L_T-x)}\left(\alpha(L_T-x)^2+2(L_T-x)\right)\right] \\
&+ \left[1+(\kappa\mathrm{SNR}_0)^{-1}e^{\alpha(\frac{x}{p+1})}\left(\frac{x}{p+1}\right)^2\right]^{p+1} \\
&\times \left[e^{\alpha(L_T-x)}\left[\alpha\left(\alpha(L_T-x)^2+2(L_T-x)\right)+\left(2\alpha(L_T-x)+2\right)\right]\right]. \qquad \text{(A.13)}
\end{aligned}
$$

By substituting $(p+1)x_M$ into (A.13), a similar equation to (A.6) is found

$$f''_{p+1}((p+1)x_M) = \frac{p+2}{p+1}e^{\alpha x_M}\left[(\alpha - 2(\kappa\mathrm{SNR}_0)^{-1}e^{\alpha x_M})x_M^2 + 4\alpha x_M + 2\right]. \quad \text{(A.14)}$$

For $p = 0$, (A.14) results in (A.6). Here, x_M depends on the number of relays $M = p+1$

$$\begin{aligned} f''_{p+1}\left(\tfrac{L_T}{p+2}\right) \\ &= \frac{p+2}{p+1}e^{\alpha\left(\frac{L_T}{p+2}\right)}\left[(\alpha - 2(\kappa\mathrm{SNR}_0)^{-1}e^{\alpha\left(\frac{L_T}{p+2}\right)})\left(\frac{L_T}{p+2}\right)^2 + 4\alpha\left(\frac{L_T}{p+2}\right) + 2\right] \\ &= \frac{1}{p+1}e^{\left(\frac{\alpha}{p+2}\right)L_T}\left[\left(\alpha - 2(\kappa\mathrm{SNR}_0)^{-1}e^{\left(\frac{\alpha}{p+2}\right)L_T}\right)\frac{L_T^2}{p+2} + 4\alpha L_T + 2(p+2)\right]. \end{aligned} \quad \text{(A.15)}$$

By comparing (A.6) and (A.15), it is evident that by increasing the number of relays at a given SNR_0, a new acceptable region for L_T is obtained which is larger than what obtained in (A.7). In this region, equally spaced relaying provides maximum received SNR at point x_M. Using the same approach expressed in Section A.1.3, it is possible to show that $f_{p+1}(x)$ is also convex over all $0 < x < L_T$ for typical values of system parameters and x_M is the global optimum point over the acceptable region of L_T.

Bibliography

[1] J. R. Barry, *Wireless Infrared Communications.* Kluwer Academic Publisher, 1994.

[2] M. R. Pakravan and M. Kavehrad, "Indoor wireless infrared channel characterization by measurements," *IEEE Transaction on Vehicular Technology,* vol. 50, 2001.

[3] T. Komine and M. Nakagawa, "Fundamental analysis for visible-light communication systems using LED lights," *IEEE Transaction on Consumer Electronics,* vol. 50, pp. 100–107, February 2004.

[4] S. S. Muhammad, P. kohldorfer, and E. Leitgeb, "Channel modeling for terrestrial free space optical channels," in *Proceedings of the International Conference on Transparent Optical Networks,* vol. 1, pp. 407–410, july 2005.

[5] A. Harris, J. J. Sluss, H. H. Refai, and P. G. LoPresti, "Alignment and tracking of a free space optical communications link to a UAV," in *Proceeding of the 24th Digital Avionics Systems Conference (DASC),* pp. 1.C.2-1 to 1.C.2–9, 2005.

[6] E. Leitgeb, K. Zettl, S. Muhammad, N. Schmitt, and W. Rehm, "Investigation in free space optical communication links between unmanned aerial vehicles

(UAVs)," in *Proceeding of the 9th International Conference on Transparent Optical Networks* (152-155, ed.), July 2007.

[7] D. Giggenbach, J. Horwath, and B. Epple, "Optical satellite downlinks to optical ground stations and high-altitude platforms," in *The 16th IST Mobile and Wireless Communications Summit*, pp. 1–4, 2007.

[8] C. G. C.-C. Chen, "Impact of random pointing and tracking errors on the design of coherent and incoherent optical intersatellite communication links," *IEEE Transactions on Communications*, vol. 37, pp. 252–260, March 1989.

[9] A. Polishuk and S. Arnon, "Optimization of laser satellite communication system with an optical preamplifier," *Journal of Optical Society America*, vol. 21, pp. 1307–1315, July 2004.

[10] R. M. Gagliardi and S. Karp, *Optical Communications.* John Wiley and Sons Inc., second ed., 1995.

[11] fSONA Optical Wireless. [Online]. Available: http://www.fsona.com.

[12] MRV Optical Communication Systems™. [Online]. Available: http://www.mrv.com.

[13] Proxim Wireless. [Online]. Available: http://www.proxim.com.

[14] GigaBeam Corporation. [Online]. Available: http://www.gigabeam.com.

[15] A. A. Youssef, *Capacity and Signaling for Free-Space Optical Channels.* PhD thesis, McMaster University, October 2009.

[16] G. P. Agrawal, *Fiber Optic Communication Systems.* John Wiley and Sons Inc., third ed., 2002.

[17] D. Kedar and S. Arnon, "Urban optical wireless communication networks: the main challenges and possible solutions," *IEEE Communications Magazine*, vol. 42, pp. S2–S7, May 2004.

[18] F. Nadeem, V. Kvicera, M. Awan, E. Leitgeb, S. Muhammad, and G. Kandus, "Weather effects on hybrid FSO/RF communication link," *IEEE Journal on Selected Areas in Communications*, vol. 27, pp. 1687–1697, December 2009.

[19] D. A. Rockwell and G. S. Mecherle, "Optical wireless: low-cost, broadband, optical access," in *fSONA white paper*, 2001.

[20] LightPointe^{TM}, "Lightpointe unveils performance enhanced Flightlite^{TM}G FSO wireless bridging solution.," in *http: //www.lightpointe.com*, April 2009.

[21] I. I. Kim, B. McArthur, and E. J. Korevaar, "Comparison of laser beam propagation at 785 nm and 1550 nm in fog and haze for optical wireless communications," *Proceedings SPIE*, vol. 4214, pp. 26–37, February 2001.

[22] International Electrotechnical Commission. (2010). [Online]. Available: http://www.iec.ch.

[23] X. Zhu, "Free-space optical communication through atmospheric turbulence channels," in *IEEE Transactions on Communications*, vol. 50, August 2002.

[24] E. Biglieri, J. Proakis, and S. Shamai, "Fading channels: information-theoretic and communications aspects," *IEEE Transaction on Information Theory*, vol. 44, pp. 2619–2692, 1998.

[25] G. R. Osche, *Optical Detection Theory for Laser Applications.* New York, NY, USA: John Wiley and Sons, 2002.

[26] J. W. Goodman, *Statistical Optics.* A Wiley-Interscience Publication, 2000.

[27] T. Tsiftsis, H. Sandalidis, G. Karagiannidis, and N. Sagias, "Multihop free space optical communications over strong turbulence channels," in *IEEE International Conference on Communications ICC*, pp. 2755–2759, June 2006.

[28] M. Uysal, S. Navidpour, and L. Jing, "Error rate performance of coded free-space optical links over strong turbulence channels," *IEEE Communications Letters*, vol. 8, pp. 635–637, October 2004.

[29] X. Zhu and J. Kahn, "Performance bounds for coded free-space optical communications through atmospheric turbulence channels," *IEEE Transactions on Communications*, vol. 51, pp. 1233–1239, August 2003.

[30] X. Zhu and J. Kahn, "Markov chain model in maximum-likelihood sequence detection for free-space optical communication through atmospheric turbulence channels," *IEEE Transactions on Communications*, vol. 51, pp. 509–516, March 2003.

[31] E. Lee and V. Chan, "Part 1: Optical communication over the clear turbulent atmospheric channel using diversity," *IEEE Journal on selected areas in communications*, vol. 22, pp. 1896–1906, November 2004.

[32] M. Safari and M. Uysal, "Relay-assisted free-space optical communication," in *IEEE Transactions on Wireless Communications*, vol. 7, pp. 5441–5449, 12 2008.

[33] K. Kiasaleh, "Turbo-coded optical PPM communication systems," *Journal of Lightwave Technology*, vol. 16, pp. 18–26, January 1998.

[34] E. Forestieri, *Optical communication theory and techniques.* Springer, 2004.

[35] I. Djordjevic, B. Vasic, and M. Neifeld, "Power efficient LDPC-coded modulation for free-space optical communication over the atmospheric turbulence channel," in *Conference on Optical Fiber Communication and the National Fiber Optic Engineers Conference (OFC/NFOEC)*, pp. 1–3, March 2007.

[36] B. Vasic, I. Djordjevic, and R. Kostuk, "Low-density parity check codes and iterative decoding for long-haul optical communication systems," *Journal of Lightwave Technology*, vol. 21, pp. 438–446, February 2003.

[37] A. Paulraj, R. Nabar, and D. Gore, *Introduction to Space-Time Wireless Communications.* Cambridge University Press, 2003.

[38] E. Shin and V. Chan, "Optical communication over the turbulent atmospheric channel using spatial diversity," in *IEEE Global Telecommunications Conference (GLOBECOM)*, vol. 3, pp. 2055–2060, March 2002.

[39] S. Hass and J. Shapiro, "Capacity of wireless optical communications," *IEEE Journal on selected areas in communications*, vol. 21, pp. 1346–1357, October 2003.

[40] J. Akella, M. Yuksel, and S. Kalyanaraman, "Error analysis of multi-hop free-space optical communication," in *IEEE International Conference on Communications ICC*, vol. 3, pp. 1777–1781, May 2005.

[41] M. Hasna and M.-S. Alouini, "Outage probability of multihop transmission over Nakagami fading channels," *IEEE Communications Letters*, vol. 7, pp. 216–218, May 2003.

[42] J. Laneman and G. Wornell, "Energy-efficient antenna sharing and relaying for wireless networks," in *IEEE Wireless Communications and Networking Conference (WCNC)*, vol. 1, pp. 7–12, 2000.

[43] J. Laneman, D. Tse, and G. Wornell, "Cooperative diversity in wireless networks: Efficient protocols and outage behavior," *IEEE Transactions on Information Theory*, vol. 50, pp. 3062–3080, December 2004.

[44] G. Karagiannidis, T. Tsiftsis, and H. Sandalidis, "Outage probability of relayed free space optical communication systems," *Electronics Letters*, vol. 42, pp. 994–995, August 2006.

[45] C. Datsikas, K. Peppas, N. Sagias, and G. Tombras, "Serial free space optical relaying communications over gamma-gamma atmospheric turbulence channels," *IEEE/OSA Journal of Optical Communications and Networking*, vol. 2, pp. 576–586, August 2010.

[46] G. Karagiannidis, A. Tsiftsis, and R. Mallik, "Bounds for multihop relayed communications in nakagami-m fading," *IEEE Transactions on Communications*, vol. 54, pp. 18–22, January 2006.

[47] M. Hasna and M.-S. Alouini, "A performance study of dual-hop transmissions with fixed gain relays," *IEEE Transactions on Wireless Communications*, vol. 3, pp. 1963–1968, November 2004.

[48] M. Karimi and M. Nasiri-Kenari, "BER analysis of cooperative systems in free-space optical networks," *Journal of Lightwave Technology*, vol. 27, pp. 5639–5647, December 2009.

[49] A. Acampora and S. Krishnamurthy, "A broadband wireless access network based on mesh-connected free-space optical links," *IEEE Personal Communications*, vol. 6, pp. 1070–9916, October 1999.

[50] PMC-Sierra. [Online]. Available: http://www.pmc-sierra.com.

[51] U. Adar, T. Kuzniz, I. Haber, and M. Tur, "An all-optical multi-hop (cascaded) high bit rate wireless communication field trial," in *Optical Fiber Communication Conference and Exhibit (OFC)*, pp. 446–448, March 2002.

[52] L. C. Andrews and R. L. Philips, *Laser Beam Propagation through Random Media.* SPIE-The International Society for Optical Engineering, second ed., 2005.

[53] I. Kim, B. McArthur, and E. Korevaar, "Comparison of laser beam propagation at 785 nm and 1550 nm in fog and haze for optical wireless communications," in *Proceeding SPIE*, vol. 4214, pp. 26–27, February 2001.

[54] D. Bushuev and S. Arnon, "Analysis of the performance of a wireless optical multi-input to multi-output communication system," *Journal of Optical Society of America A*, vol. 23, pp. 1722–1730, July 2006.

[55] D. L. Fried, "Optical heterodyne detection of an atmospherically distorted signal wave front," *Proceeding of IEEE*, vol. 55, January 1967.

[56] B. E. A. Saleh and M. C. Teich, *Fundamentals of Photonics.* John Wiley and Sons Inc., 1991.

[57] V. P. Lukin and V. V. Pokasov, "Phase fluctuations of an optical wave which propagates in a turbulent atmosphere," *Institute of Atmospheric Optics, Translated from Izvestiya Vysshikh Uchebnykh Zavedenii, Radiofizika*, vol. 16, pp. 1726–1729, November 1973.

[58] V. I. Tatraski, *Wave Propagation in a Turbulent Medium.* The McGraw-Hill Book Company, Inc., 1961.

[59] H. Willebrand and B. S. Ghuman, *Free-Space Optics: Enabling Optical Connectivity in Today's Networks.* Sams Publishing, 2002.

[60] J. W. Goodman, *Introduction to Fourier Optics.* The McGraw-Hill Companies,INC, second ed., 1988.

[61] Y. Dikmelik and F. M. Davidson, "Fiber-coupling efficiency for free-space optical communication through atmosphere turbulence," *Applied Optics*, vol. 44, pp. 4946–4952, August 2005.

[62] S. B. Alexander, *Optical Communication Receiver Design.* SPIE-The International Society for Optical Engineering, 1997.

[63] P. Mamyshev, "All-optical data regeneration based on self-phase modulation effect," in *24th European Conference on Optical Communication*, vol. 1, pp. 475–476, 20-24 September 1998.

[64] G. P. Agrawal, *Nonlinear Fiber Optics.* Academic Press, Inc., second ed., 1995.

[65] J. Berger, F. Ilkov, D. King, and A. Tselikov, "Widely tunable, narrow optical bandpass Gaussian filter using a silicon microactuator," in *Optical Fiber Communication Conference*, vol. 1, pp. 252–253, March 2003.

[66] S. Norimatsu and M. Maruoka, "Accurate Q-factor estimation of optically amplified systems in the presence of waveform distortion," *Journal of Lightwave Technology*, vol. 20, pp. 19–27, January 2002.